NEUROMECHANICAL CONSTRAINTS AND OPTIMALITY FOR BALANCE

A Dissertation
Presented to
The Academic Faculty

by

Johnathan Lucas McKay

In Partial Fulfillment
of the Requirements for the Degree
Doctor of Philosophy in the
Department of Electrical Engineering

Georgia Institute of Technology

August 2010

NEUROMECHANICAL CONSTRAINTS AND OPTIMALITY FOR BALANCE

Approved by:

Dr. Lena H. Ting
Biomedical Engineering
Georgia Institute of Technology
Emory University

Dr. Christopher J. Rozell
Electrical and Computer Engineering
Georgia Institute of Technology

Dr. Steven P. DeWeerth
Biomedical Engineering
Georgia Institute of Technology
Emory University

Dr. Thomas J. Burkholder
Applied Physiology
Georgia Institute of Technology

Dr. Robert H. Lee
Biomedical Engineering
Georgia Institute of Technology
Emory University

Date Approved: July 2, 2010

To KEL

ACKNOWLEDGEMENTS

In the study of neuromechanics, we watch people make movements – or not make movements, in the case of balance control – and we try and figure out just how they did it. “Out of all of the myriad ways that that movement could have happened,” we ask, “what underlying mechanisms caused that particular one to happen at that particular time?” This turns out to be a tough question, because although the number of possible movements may be infinite, the number of possible mechanisms might just be more so. Luckily for the reader (and even more so for the writer), the primary mechanisms underlying the production of this thesis will be enumerated here.

My very significant other, Ms. Katie Lafond, never waivered in her belief in me. She gave me strength, support, and made our life together wonderful. For these things I will always be grateful, and I could have never done it without her.

My advisor, Dr. Lena H. Ting, taught me how to see the essence of problems, and not just the details. She taught me how to be a scientist when all of my tendencies were to be an engineer. She was the type of mentor that I hope to be.

My family, especially my Mother and Father, inspired me with their strength, humor, and kindness. I aspire to make them as proud of me as I am of them.

Friends in the Neuromechanics Laboratory and elsewhere at Georgia Tech and Emory helped me to develop and refine my ideas. In particular, Dr. Gelsy Torres-Oviedo, Dr. Kyla Ross, Stacie Chvatal, Dr. Kartik Sundar, Dr. Torrence Welch, and Seyed Safavynia helped me to make my research make sense. Dr. Julia Choi, especially, helped me to put all of it together at the end. Keith van Antwerp, Dr. Nate Bunderson, Jeff Bingham, and Hongchul Sohn helped me to make my research make a more rigorously defined kind of sense. My committee members provided a great deal of useful input – in particular, Dr. Tom Burkholder and Dr. Christopher Rozell met with me to provide much-appreciated technical expertise.

My extended Atlanta family – Travis, Steve, Paul, Sarah, Deon, and all of the rock kids – made Georgia feel like home.

Thank you all. I am thankful for and humbled by all of your support.

TABLE OF CONTENTS

LIST OF TABLES

LIST OF FIGURES

SUMMARY

Although people can typically maintain balance on moving trains, or press the appropriate button on an elevator with little conscious effort, the apparent ease of these sensorimotor tasks is courtesy of neural mechanisms that continuously interpret many sensory input signals to activate muscles throughout the body. The overall hypothesis of this work is that motor behaviors emerge from the interacting constraints and features of the nervous and musculoskeletal systems. The nervous system may simplify the control problem by recruiting muscles in groups called muscle synergies rather than individually. Because muscles cannot be recruited individually, muscle synergies may represent a neural constraint on behavior. However, the constraints of the musculoskeletal system and environment may also contribute to determining motor behaviors, and so must be considered in order to identify and interpret muscle synergies.

Here, I integrated techniques from musculoskeletal modeling, control systems engineering, and data analysis to identify neural and biomechanical constraints that determine the muscle activity and ground reaction forces during the automatic postural response (APR) in cats. First, I quantified the musculoskeletal constraints on force production during postural tasks in a detailed, 3D musculoskeletal model of the cat hindlimb. I demonstrated that biomechanical constraints on force production in the isolated hindlimb do not uniquely determine the characteristic patterns of force activity observed during the APR. However, when I constrained the muscles in the model to activate in a few muscle synergies based on experimental data, the force production capability drastically changed, exhibiting a characteristic rotation with the limb axis as the limb posture was varied that closely matched experimental data. Finally, after extending the musculoskeletal model to be quadrupedal, I simulated the optimal feedforward control of individual muscles or muscle synergies to regulate the center of mass (CoM) during the postural task. I demonstrated that both muscle synergy control and optimal muscle control reproduced the characteristic force patterns observed during postural tasks. These results are consistent with the hypothesis that the nervous system may use a low-dimension control scheme based on muscle synergies to approximate the

optimal motor solution for the postural task given the constraints of the musculoskeletal system.

One primary contribution of this work was to demonstrate that the influences of biomechanical mechanisms in determining motor behaviors may be unclear in reduced models, a factor that may need to be considered in other studies of motor control. The biomechanical constraints on force production in the isolated hindlimb did not predict the stereotypical forces observed during the APR unless a muscle synergy organization was imposed, suggesting that neural constraints were critical in resolving musculoskeletal redundancy during the postural task. However, when the model was extended to represent the quadrupedal system in the context of the task, the optimal control of the musculoskeletal system predicted experimental force patterns in the absence of neural constraints.

A second primary contribution of this work was to test predictions concerning muscle synergies developed in theoretical neuromechanical models in the context of a natural behavior, suggesting that these concepts may be generally useful for understanding motor control. It has previously been shown in abstract neuromechanical models that low-dimension motor solutions such as muscle synergies can emerge from the optimal control of individual muscles. This work demonstrates for the first time that low-dimension motor solutions can emerge from optimal muscle control in the context of a natural behavior and a realistic musculoskeletal model. This work also represents the first explicit comparison of muscle synergy control and optimal muscle control during a natural behavior. It demonstrates that an explicit low-dimension control scheme based on muscle synergies is competent for performance of the postural task across biomechanical conditions, and in fact, may approximate the motor solution predicted by optimal muscle control.

This work advances our understanding how the constraints and features of the nervous and musculoskeletal systems interact to produce motor behaviors. In the future, this understanding may inform improved clinical interventions, prosthetic applications, and the general design of distributed, hierarchal systems.

CHAPTER 1
INTRODUCTION

Although people can typically maintain standing balance on moving trains, or press the appropriate button on an elevator with little conscious effort, the apparent ease of these sensorimotor tasks is courtesy of neural mechanisms that continuously interpret many sensory input signals to activate muscles throughout the body. One question that is central to understanding how the nervous system accomplishes this sensorimotor transformation is known as the "degrees of freedom problem" (Bernstein 1967). In most natural behaviors, task-level goals can be equivalently achieved with different kinetic or kinematic strategies (Kuo 2005; Todorov 2004; Yang et al. 2007), which can themselves be equivalently achieved with different spatial and temporal patterns of muscle activation (Gottlieb 1998; Lockhart and Ting 2007; van Bolhuis and Gielen 1999). Despite this redundancy, appropriate patterns of torques and muscle activity emerge easily during most motor tasks. How does this selection happen in the nervous system, and by what underlying mechanisms?

Bernstein hypothesized that to address the degrees of freedom problem, the nervous system might be organized to control multiple degrees of freedom as modules, rather than individually (Bernstein 1967). An advantage of modular organization is that higher motor centers could then operate on increasingly conceptual variables related to task-level motor performance, enabling sparser and more rapid computations (Ting and McKay 2007). This idea is supported by observations that task-level variables, such as the trajectory of the endpoint in reaching or targeting tasks (Adamovich et al. 2001; Bernstein 1967; Tseng et al. 2002; Tseng and Scholz 2005) and center of mass position during postural control (Gollhofer et al. 1989; Scholz et al. 2007) are more rigidly controlled during motor tasks than lower level variables such as individual joint angles. Neurophysiological studies also suggest that task-level variables are preferentially encoded within the nervous system. For example, in primates, the direction, velocity, and force of the hand are encoded in motor cortex during reaching movements (Georgopoulos et al. 1982; Georgopoulos et al. 1986; Scott and Kalaska 1997). Similarly, in cats, the length, orientation, and velocity of the foot, rather than the angles of individual joints, are

encoded at the level of dorsal roots during locomotion (Weber et al. 2007) and in the dorso-spinal-cerebellar tract during passive limb manipulation (Bosco et al. 2000). Above the level of the spinal cord in cats, in the mesencephalic locomotor region of the midbrain, simple pulse train stimulation is sufficient to induce locomotion, including gait transitions, when combined with treadmill movement (Grillner and Shik 1973), suggesting that at this high level, the relevant task-level variable may be, simply, "go."

MUSCLE SYNERGIES

We hypothesize that the nervous system resolves redundancy at the level of muscle activation by recruiting muscles in groups called muscle synergies, rather than individually, reducing the number of degrees of freedom that must be controlled and limiting the complexity of the resulting muscle activity (Ting and McKay 2007). We define muscle synergies as invariant patterns of activation across multiple muscles that serve as building blocks for the production of sophisticated muscle activation patterns. Neuroanatomically, muscle synergies may represent the connection strengths of polysynaptic neuronal networks within the CNS that impinge on the motor pools of multiple muscles. Our muscle synergy hypothesis assumes that 1) any given muscle can belong to more than one muscle synergy, 2) that the muscles within any given muscle synergy are activated in fixed proportion within the muscle synergy, and that 3) when a given muscle synergy is recruited during a motor task, all of the participating muscles are recruited by a common scaling coefficient according to their proportion. As an algebraic example, the net activation of a single muscle e_1 resulting from the activation of two synergies w_1 and w_2, recruited according to scaling coefficients c_1 and c_2, respectively, can be expressed as the sum of the contribution of each muscle synergy: $e_1 = c_1 \cdot w_{11} + c_2 \cdot w_{21}$, where the coefficients w_{11} and w_{12} are the proportion of the recruitment of muscle 1 by the first and the second muscle synergy respectively. If the activation levels of all of the muscles e_i are assembled into a column vector $\bar{e}$, and the scaling factors of all of the muscle synergies c_i are assembled into a column vector $\bar{c}$, then the net activation levels of all of the muscles can be expressed as the matrix equation $\bar{e} = W \cdot \bar{c}$, where each muscle synergy $\overline{w_i}$ comprises a column of the matrix W.

Consistent with the muscle synergy hypothesis, low dimension muscle activity has been observed in many motor behaviors during studies of humans and animals (Cheung et al. 2009; Krishnamoorthy et al. 2003; Krouchev et al. 2006; Muceli et al. 2010; Torres-Oviedo et al. 2006; Torres-Oviedo and Ting 2007; Tresch et al. 1999). In these studies, patterns of electromyographic (EMG) activity are subjected to components analysis techniques. Universally, the number of underlying components required to adequately represent the EMG data is fewer than the number of sampled muscles, consistent with the hypothesis that the muscles are recruited by a smaller number of underlying muscle synergies. Although the essential evidence for the muscle synergy hypothesis is the small number of components required to describe the spatial recruitment of muscles, various extensions of the muscle synergy hypothesis exist that attempt to describe the temporal recruitment of muscles in the context of muscle synergies, including unit bursts (Kargo et al. 2010) and time varying-synergies (d'Avella et al. 2006).

Muscle synergy recruitment has also been correlated with task-level biomechanical variables, consistent with their proposed role as the final output of the motor hierarchy. Muscle synergy recruitment has been correlated to center of mass (CoM) shifts in standing (Krishnamoorthy et al. 2003), foot and limb kinematics in walking (Ivanenko et al. 2003), foot acceleration in pedaling (Ting et al. 1999), and postural force generation during balance tasks (Torres-Oviedo et al. 2006). Observations that common muscle synergies are used across behaviors with different biomechanical contexts, such as swimming, jumping, and walking (Cheung et al. 2005; d'Avella and Bizzi 2005), as well as in different loading conditions (Cheung et al. 2009) suggests that the task-level functions of muscle synergies may be preserved across biomechanical contexts. Finally, it has been demonstrated that muscle synergy structure can be largely unaffected by altering (Kargo and Giszter 2008) or totally eliminating (Cheung et al. 2005) sensory feedback during movements, although alterations in the recruitment of muscle synergies may be observed.

Although various components analysis techniques are used to identify muscle synergies, one method that is particularly useful is nonnegative matrix factorization, or NNMF (Lee and Seung 2001). Because muscles can only “pull,” the activation of each

muscle e_i is confined to the unit interval $(0,1)$. NNMF is well suited to this natural nonnegativity, and enforces the simple constraint that all of the elements of each muscle synergy are strictly positive. Despite the fact that NNMF does not enforce any higher-order structure on the identified muscle synergies – for example, orthogonality or assumptions of a particular population distribution – NNMF is often more successful than strictly orthogonal factorization techniques like principal components analysis (PCA) (Ivanenko et al. 2005; Ivanenko et al. 2004) at breaking complex patterns into meaningful parts. For example, when applied to a dataset of faces, the basis functions identified by NNMF resemble intuitive, spatially-localized physical features, like noses or mouths, whereas the bases identified by orthogonal decomposition techniques tend to represent more abstract, less spatially-localized features of the dataset, similar to the basis functions identified by Fourier decomposition (Lee and Seung 1999).

BIOMECHANICAL CONSTRAINTS

In considering experimental data only, it is difficult to determine whether identified muscle synergy patterns reflect modular structure within the nervous system, or simply serve as a compact basis with which to describe the muscle patterns that satisfy the biomechanical constraints of the musculoskeletal system and task. Consider a hypothetical motor task requiring maximal performance – for example, generating the maximum possible torque at a single joint. If the muscles were controlled individually in this hypothetical task, the constraints of the musculoskeletal system would determine a unique pattern of muscle activity corresponding to the maximum possible torque. If the muscle activity from repeated presentations of this task were subjected to components analysis, a dominant component corresponding to that unique pattern would likely be sufficient to describe the muscle activity during all of the presentations very well. Should that component be considered a muscle synergy as defined above? Likely not – although the putative muscle synergy does describe the way that muscles are recruited, its structure reflects the biomechanical constraints of the musculoskeletal system and task, rather than modular structure within the nervous system. Although this hypothetical example represents a degenerate case, it illustrates that before identified muscle synergy patterns

can be attributed to modular structure within the nervous system, it must therefore be determined whether they simply reflect biomechanical constraints.

In particular, it has been suggested that muscle synergy patterns may emerge as the optimal way to control the musculoskeletal system given the biomechanical constraints of the musculoskeletal system and task, rather than reflecting explicit modular organization within the nervous system. During motor tasks, it has been suggested the nervous system may optimally minimize effort or energy (Fagg et al. 2002; Hoyt and Taylor 1981; Todorov 2004), execution error associated with irreducible noise (Harris and Wolpert 1998; Müller and Sternad 2009; Scholz and Schöner 1999), or a balance of the two (O'Sullivan et al. 2009). Although each of these different criteria will predict slightly different particular solutions to any given motor control problem, each predicts muscle patterns that are characterized by coactivation across multiple muscles, similar to the dependencies between muscles observed in experimentally-identified muscle synergies (Todorov 2004). Although the underlying mechanisms by which the nervous system might perform optimal control remain unclear, except in very abstract representations (Denève et al. 2007), it is therefore possible that experimentally-identified muscle synergies may simply serve as a convenient basis with which to describe the optimal control of individual muscles during motor tasks, rather than reflecting explicit constraints on muscle activation within the nervous system.

Detailed musculoskeletal models are required in order to accurately quantify the biomechanical constraints of the musculoskeletal system and task, because the influence of the musculoskeletal system on task performance may be very sophisticated. Due to purely biomechanical mechanisms, the degrees of freedom of the musculoskeletal system may exhibit coordinated covariation in the absence of neural control. For example, during grasping movements in the human hand, joints in different fingers are coupled by the sophisticated tendon network, as well as by multi-slip extrinsic hand muscles (Schieber and Santello 2004; Valero-Cuevas et al. 2007). Purely biomechanical mechanisms within the musculoskeletal system of the cat hindlimb function to constrain the individual joint angles to a lower-dimension subspace, reducing the number of apparent degrees of freedom in a manner that could be attributed to active control (Bosco et al. 1996). Similarly, biomimetic mechanical systems can be appropriately designed so that the

dominant modes are very stable, and even sufficient to maintain complex behaviors like locomotion in a completely passive manner (McGeer 1990).

Finally, biomechanical constraints on maximal task performance may also inform strategy selection during submaximal motor tasks when these constraints are not active *per se.* For example, the forces produced during static and dynamic pedaling in the human lower limb reflect biomechanically favorable force directions. Although it may be possible to produce forces in other directions, a static musculoskeletal model demonstrated that the set of feasible forces ("feasible force set," or FFS) that can be produced by the limb is elongated, with the orientation of the maximal possible force coinciding with the stereotypical force directions observed experimentally (Gruben et al. 2003; Schmidt et al. 2003), suggesting that biomechanical factors influence self-selection of force directions when they are not explicitly specified by the task. Similarly, considering muscle activation, it has also been demonstrated that muscle activation patterns for submaximal force production are merely scaled versions of the patterns required for maximal force generation in both pedaling (Raasch and Zajac 1999) and finger pinch (Valero-Cuevas 2000), again suggesting that biomechanical constraints on maximal performance may inform motor performance in other regimes of the motor repertoire.

THE AUTOMATIC POSTURAL RESPONSE

The studies presented here consider how the nervous system addresses redundancy during the automatic postural response (APR) to postural perturbations in cats. When a perturbation is issued, either as a translation of the support-surface in the horizontal plane, or as a rotation in either the pitch or roll axes, stereotyped, directionally-specific patterns of muscle activity are evoked that begin at about 50 ms in a cat, and at about 100 ms in a human (Horak and Macpherson 1996). Although the muscle activity evoked during the APR was initially assumed to be – and was referred to as – a "reflex," analogous to the monosynaptic stretch reflex elicited by tendon tap, APR muscle activity occurs later than the time at which stretch reflexes occur, and in some cases acts in direct opposition to the mechanical action of stretch reflexes (Nashner 1976). The APR likely requires supraspinal influences, as cats with complete spinal transection exhibit disrupted flexor responses to perturbation (Macpherson and Fung 1999). In particular, neural

centers at level of the brainstem have been implicated as necessary for the shortest latency components of the APR (Honeycutt et al. 2009), although components with later latencies may elicit longer feedback loops with cortical involvement (Jacobs and Horak 2007). Consistent with this higher-level representation, APR muscle activity cannot be easily predicted from changes in local sensory variables, as would be expected with a stretch reflex; instead, the direction and magnitude of CoM destabilization is the only reliable predictor of the activity of muscles during the APR (Carpenter et al. 1999; Diener et al. 1988).

In addition to the sophisticated patterns of muscle activity associated with the APR, the patterns of ground reaction forces elicited during postural perturbation tasks are highly stereotyped. The forces observed during the force constraint strategy are as follows: during quiet standing, the ground reaction forces at each limb are directed downward and away from the center of mass (CoM), acting along diagonal axes when viewed in the horizontal plane. When a balance perturbation is issued, the muscle activity during the APR gives rise to corrective ground reaction forces at the limbs, which tend to be directed either towards or away from the CoM along the same diagonal axes as the quiet standing forces, with little dependence on the direction of the perturbation (Ting and Macpherson 2004). Macpherson (1988a) described this characteristic pattern of forces as the *force constraint strategy*, and suggested that it may represent a control strategy within the nervous system.

Many features of the APR are conserved across cats and humans, despite differences in morphology. For example, the patterning of muscles during postural responses in humans supported on their hands and feet is very similar to that in cats, characterized by reciprocal activation of antagonists in the lower limbs and co-activation or co-inhibition of antagonists in the upper limbs (Macpherson et al. 1989). Similarly, responses in cats change dramatically when standing bipedally on their hindlimbs, although they cannot completely assume plantigrade posture (Dunbar et al. 1986). Forces during human postural responses also exhibit a stereotyped force-constraint-like pattern that may be clinically relevant, as it is disrupted in patients with Parkinson's disease (Dimitrova et al. 2004).

The dependence of the APR on task-level, rather than local-level variables may be the reason that aspects of postural perturbation responses are common across cats and humans. Although CoM is an abstract task-variable that is not directly encoded by any particular sensory receptor, the displacement of the CoM is a reliable predictor of which muscles will be recruited during a given postural task (Gollhofer et al. 1989; Nashner 1977). Similarly, the kinematics of the CoM predict the timecourse of muscle activation during postural tasks in both cats and humans (Lockhart and Ting 2007; Welch and Ting 2009; 2008), suggesting that neural mechanisms of CoM state estimation may be shared across both species. CoM is likely estimated from multiple sensory modalities, the relative influences of which are likely reorganized during compensation to deficits. Vestibular loss, for example, increases the magnitude but does not alter the timing or pattern of muscle activation following postural disturbances in humans and cats (Inglis and Macpherson 1995; Runge et al. 1998); similarly, somatosensory loss delays the onset of the postural response but, again, does not change the pattern of muscle activation in humans or cats (Bloem et al. 2000; Inglis et al. 1994; Stapley et al. 2002).

In support of the hypothesis that the neural substrates of the APR in cats are organized hierarchically, both the muscle activity and ground reaction forces observed during the APR in cats can be described by a small set of five "functional" muscle synergies, which specify both a pattern of hindlimb muscle activation (a muscle synergy) and a correlated "synergy force vector" at the ground (Torres-Oviedo et al. 2006). When cats performed the task in various biomechanical conditions (anterior-posterior "stance distances," Macpherson 1994), identical synergies were observed as in a control biomechanical condition approximating the natural posture of the animal ("preferred" stance distance). This suggests that the muscle synergies recruited for postural control may be organized to provide task level-functions, in this case endpoint force. Further, this generalization was apparent only when synergy force vectors were expressed in a coordinate system that rotated with the hindlimb axis in the sagittal plane. The fact that synergy force vectors are invariant in the intrinsic coordinates of the limb, although the postural task itself – generating an appropriate net response force at the ground with all four limbs – is based in extrinsic coordinates suggests that synergy force vectors may be internally represented in the intrinsic coordinates of the hindlimb.

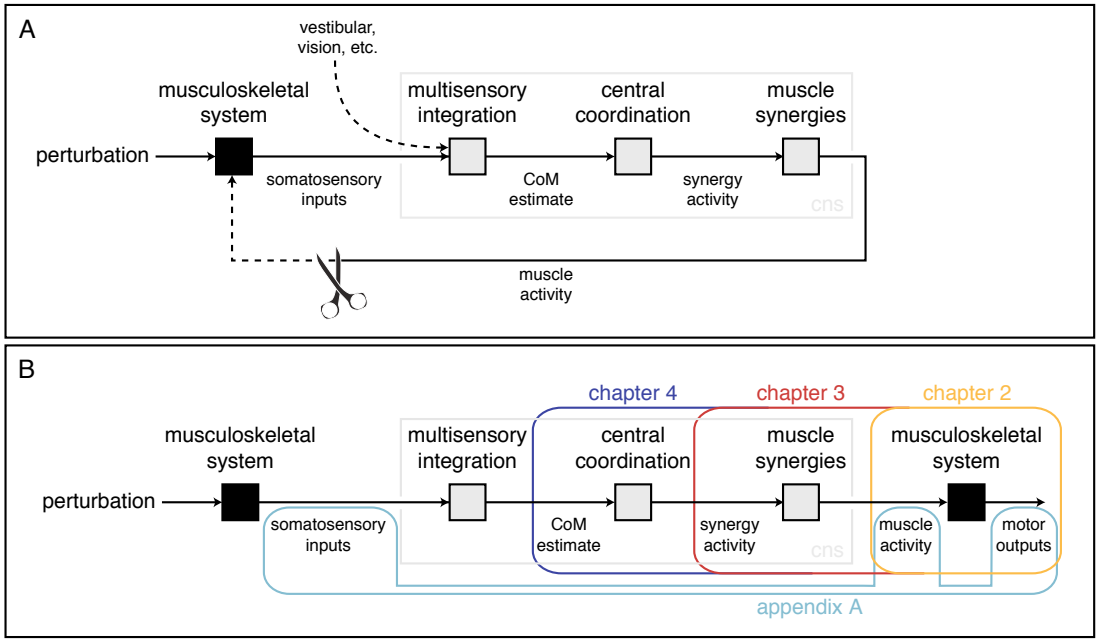

Figure 1.1. Hypothesized feedback and feedforward representations of the sensorimotor transformation postural control. *A*. Postural control as a feedback process. In this representation, postural perturbations excite the dynamics of the musculoskeletal system; the resulting disturbances in somatosensory information is aggregated with other sensory information in a multisensory integration process to form an estimate of the kinematics of the CoM. This CoM estimate is then used in a central coordination process to recruit muscle synergies and to stabilize the body. *B*. Postural control as a feedforward process. Because the APR has a characteristic long latency (≥60 ms), the elements of the feedforward pathway can be examined by considering the earliest phases of the response, before ongoing feedback can have significant effects. The studies here isolate individual blocks of the hypothesized sensorimotor transformation (see text).

NEUROMECHANICAL APPROACH

The overall objective of the studies presented here was to investigate the neural and biomechanical constraints that determine muscle activity and ground reaction forces during the APR in cats. I treated the sensorimotor transformation during the APR as a feedback process, and then used mathematical modeling and data analysis techniques to characterize hypothesized elements of the feedforward pathway. A representation of the hypothesized feedback process is depicted in Figure 1.1A. When a perturbation is issued, it excites the dynamics of the musculoskeletal system, creating a suite of somatosensory inflow that is aggregated with sensory estimates from other modalities (including vision and vestibular sources, Peterka 2002) into an overall estimate of the CoM kinematics. This CoM estimate is then used in a central coordination process to recruit muscles throughout the body (Lockhart and Ting 2007; Welch and Ting 2009) in a small number of functional muscle synergies (Torres-Oviedo et al. 2006). APR muscle activity is then conveyed back through the musculoskeletal system to respond to the perturbation with ground reaction forces and changes in kinematic and kinetic variables at the periphery. Because of the characteristic long latency of the APR ($\geq$ 60 ms), the elements of the feedforward pathway can be characterized by considering the initial phases of the APR, before ongoing feedback can have significant effects. Also, because postural perturbations introduce relatively small changes in joint angles throughout the body, static musculoskeletal models can be used, enabling a much wider range of analysis techniques than would be available if fully dynamic models were required.

In **Chapters 2 and 3**, I tested whether the forces associated with the force constraint strategy reflect biomechanical or neural constraints on the force production capability of the isolated cat hindlimb. Previous studies of musculoskeletal mechanics suggest that the diagonal axis is a primary torque direction for single muscles activated through direct nerve stimulation (Lawrence et al. 1993) or spinal reflexes (Nichols et al. 1993), and for ensembles of muscles activated through reflex mechanisms (Bonasera and Nichols 1996; Nichols 2002; Siegel et al. 1999). Therefore, it is possible that biomechanical constraints on hindlimb force production may determine the forces observed during posture. Alternatively, if the force production capability of the hindlimb is not limited to the forces observed during posture, the force production capability may

be reduced if muscles are constrained to act in a limited number of muscle synergies. To test this, I quantified the force production capability of an anatomically detailed musculoskeletal model of the cat hindlimb parameterized to match experimental data of three cats. I compared the directions of small and large feasible forces to the patterns of forces observed during balance tasks. Then, I further constrained the muscles in the model to activate in simulated muscle synergies derived from experimental data and examined changes in the force production capability.

In **Chapter 4**, I tested whether the forces associated with the force constraint strategy reflect the optimal strategy to control the quadrupedal musculoskeletal system in a given postural configuration rather than modularity in motor outputs. Optimal control theory predicts various motor behaviors (Todorov 2004), and control effort or energy minimization is a strong predictor of behavior (Hoyt and Taylor 1981; O'Sullivan et al. 2009). Therefore, it is possible that the muscle activity and forces observed during posture emerge from the optimal control of individual muscles during the postural task, without explicit neural constraints. To test this, I simulated the optimal feedforward control of individual muscles and muscle synergies in a quadrupedal neuromechanical model. I to simulate the balance task, I identified the optimal patterns of individual muscle or muscle synergy activation that could produce appropriate net forces and moments at the CoM during postural perturbations. I then compared the forces predicted by each control strategy to each other and to experimental data.

CHAPTER 2
BIOMECHANICAL CAPABILITIES INFLUENCE POSTURAL CONTROL STRATEGIES IN THE CAT HINDLIMB

This chapter was originally published as an article in the *Journal of Biomechanics*:

McKay JL, Burkholder TJ, and Ting LH. Biomechanical capabilities influence postural control strategies in the cat hindlimb. *J Biomech* 40: 2254-2260, 2007.

ABSTRACT

During postural responses to perturbations, horizontal plane forces generated by the cat hindlimb are stereotypically directed either towards or away from the animal's center of mass, independent of perturbation direction. We used a static, three-dimensional musculoskeletal model of the hindlimb to investigate possible biomechanical determinants of this "force constraint strategy" (Macpherson 1988a). We hypothesized that directions in which the hindlimb can produce large forces are preferentially used in postural control. We computed feasible force sets (FFS) based on hindlimb configurations of three cats during postural equilibrium tasks (Jacobs and Macpherson 1996) and compared them to horizontal plane postural force directions. The grand mean FFS was bimodal, with maxima near the posterior-anterior axis (-86 ± 8° and 71 ± 4°), and minima near the medial-lateral axis (177 ± 8° and 8 ± 8°). Postural force directions clustered near both maxima; there were no medial postural forces near the absolute minimum. However, the medians of the anterior and posterior postural force direction histograms in the right hindlimb were rotated counter-clockwise from the FFS maxima ($p < 0.05$; Wilcoxon signed-rank test). Because the posterior-anterior alignment of the FFS is consistent with a hindlimb structure optimized for locomotion, we conclude that the biomechanical capabilities of the hindlimb strongly influence, but do not uniquely determine the force directions observed in the force constraint strategy. Forces used in postural control may reflect a balance between a neural preference for using forces in the

directions of large feasible forces and other criteria, such as the stabilization of the center of mass, and muscular coordination strategies.

INTRODUCTION

Forces generated by each limb of the cat during postural equilibrium tasks are characterized by a "force constraint strategy" whereby the directions of forces produced by each limb are more constrained than the directions of net force produced together by all of the limbs (Macpherson 1988a). A similar force constraint strategy has also been identified during bipedal postural control (Fung and Macpherson 1995; Henry et al. 2001). It has been suggested by Macpherson (1988a) that such a strategy simplifies the coordination problem faced by the nervous system (i.e., the "degrees of freedom problem," Bernstein 1967), because an appropriate net postural response force is achieved by modulating the amplitudes of the individual limb forces without altering their directions. The stereotypical force directions observed in the force constraint strategy are as follows: during quiet standing, limb forces are directed downward and away from the center of mass, acting along diagonal axes when viewed in the horizontal plane. Following horizontal plane translation perturbations of the support surface, or rotation of the support surface about the pitch or roll axis, active postural response forces in each limb act along the same diagonal axes, regardless of the direction of the perturbation (Macpherson 1988a; Ting and Macpherson 2004).

We hypothesized that the limited directions of force produced by the cat hindlimb during postural responses are preferentially chosen because they are biomechanically favorable. Previously, acute studies have demonstrated the diagonal axis used in the force constraint strategy is also a primary torque direction for single muscles activated through direct nerve stimulation (Lawrence et al. 1993) or spinal reflexes (Nichols et al. 1993), and for ensembles of muscles activated through reflex mechanisms (Bonasera and Nichols 1996; Nichols 2002; Siegel et al. 1999). Similarly, forces produced during static and dynamic pedaling reflect biomechanically favorable force directions in the human lower limb. A static musculoskeletal model demonstrated the set of feasible forces ("feasible force set," or FFS) that can be produced by the limb is elongated, with the orientation of the maximal possible force coinciding with the stereotypical force directions observed experimentally (Gruben et al. 2003; Schmidt et al. 2003). Although it

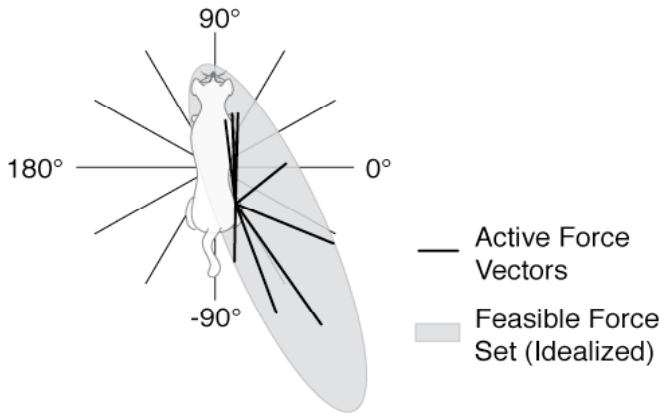

Figure 2.1. The force constraint strategy (Macpherson 1988a). Perturbations in 12 directions in the horizontal plane (thin lines) elicit postural response forces that are more constrained in direction (thick lines). Postural response forces exerted by the hindlimb act along a diagonal axis, regardless of perturbation direction. We hypothesized that this behavior reflects a neural preference for using directions of maximum feasible force, represented by the idealized feasible force set ("FFS," gray oval) (Gruben et al. 2003; Schmidt et al. 2003; Valero-Cuevas et al. 1998).

may be possible to produce forces in other directions, this study showed that biomechanical factors influence self-selection of force directions when they are not explicitly specified by the task.

We tested our hypothesis by quantifying the FFS of the cat hindlimb and comparing it to the directions of observed postural response forces in three cats performing postural equilibrium tasks (Jacobs and Macpherson 1996). The FFSs were based on experimentally measured kinematic configurations and constraints on individual muscle forces (Kuo and Zajac 1993; Schmidt et al. 2003; Valero-Cuevas et al. 1998). Because sagittal plane models (He et al. 1991; Hof 2001; Kaya et al. 2005; Prilutsky et al. 1997) were inadequate for investigating horizontal plane forces, we created a three-dimensional model based on the measurements of Burkholder and Nichols (2000; 2004). Our hypothesis that biomechanically favorable force directions are preferentially used during postural control would be supported if the FFS were elongated along the same axes as the force directions observed experimentally (e.g., Figure 2.1, solid oval).

METHODS

We constructed FFSs using a model of the cat hindlimb in postures based on kinematic data taken from 412 individual trials of three cats during translation perturbations of the support surface in 12 directions (Figure 2.1). We then compared active postural response force directions to the average FFS over all trials. Simulations and subsequent analyses were conducted in Matlab (The Mathworks, Natick, Mass., USA).

MODEL OF THE CAT HINDLIMB

A three-dimensional static model of the cat hindlimb was developed based on the measurements of Burkholder and Nichols (2000; 2004). The model consists of seven rotational degrees of freedom $(\vec{q})$ and 31 muscles (Figure 2.2). The hip joint was modeled as a ball joint, and the knee and ankle were each modeled using two non-intersecting, non-orthogonal axes. Muscles were modeled as straight lines between origin and insertion points, with via points. Muscle moment arm values were determined with SIMM software (Musculographics, Inc., Santa Rosa, CA).

The transformation between a 31-element input vector of muscle excitations $\vec{e}\ (0 \le e_i \le 1)$ and the (6 × 1) force and moment system $\vec{F}\left(\left[f_x\ f_y\ f_z\ m_x\ m_y\ m_z\right]^T\right)$ produced at the endpoint (approximated as the metatarsal-phalangeal joint, Jacobs and Macpherson 1996) is defined as:

$$\vec{F} = J\left(\vec{q}\right)^{-T} R\left(\vec{q}\right) F_O F_{AFL}\left(\vec{q}\right)\vec{e} \qquad (2.1)$$

All factors in Equation 2.1 except F_O vary with the limb posture $\vec{q}$; this dependence is omitted for clarity. The last four factors map muscle excitations $\vec{e}$ to a net joint torque

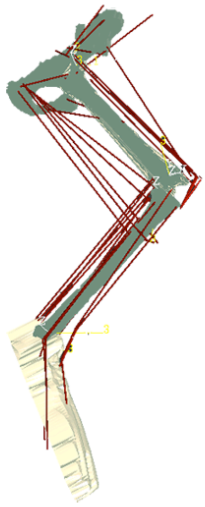

Figure 2.2. A three-dimensional model of the cat hindlimb. SIMM software (Musculographics, Inc., Santa Rosa, CA) was used to determine muscle moment arms for each of the 412 simulations. The model consists of seven rotational degrees of freedom and 31 muscles, based on the measurements of Burkholder and Nichols (2000; 2004).

vector through F_{AFL}, the (31×31) diagonal matrix of scaling factors based on active muscle force-length characteristics, F_O, the (31×31) diagonal matrix of maximal muscle forces, and R, the (6×31) moment arm matrix (Valero-Cuevas et al. 1998; Zajac 1989). All muscles were assumed to be at 95% optimum fiber length for the mean posture of each cat (Burkholder and Lieber 2001). The term J^{-T} maps the net joint torque vector to the endpoint force and moment system. A closed-form solution for the (6×7) system geometric Jacobian J was developed with Autolev software (Online Dynamics, Inc., Stanford, CA). All seven degrees of freedom were used to establish the limb postures. The degree of freedom corresponding to internal/external rotation of the femur was neglected ("locked") during endpoint force calculation so that J^T was (6×6) and directly invertible. This degree of freedom was chosen because it contributed primarily to the generation of moments rather than forces in the horizontal plane.

The complete model includes passive muscle forces $F_{PFL} \cdot \vec{1}$, where F_{PFL} is a (31×31) diagonal matrix of passive force-length scaling factors and $\vec{1}$ is a vector of ones:

$$\vec{F} = J^{-T} R F_O \left(F_{AFL} \vec{e} + F_{PFL} \vec{1} \right) \quad (2.2)$$

POSTURAL RESPONSE DATA

The kinematic and kinetic data used in this study have been presented previously (Jacobs and Macpherson 1996). Briefly, three cats (*Bi*, *Ni*, and *Ru*) were trained to stand on a moveable platform equipped with four triaxial force plates. Postural perturbations consisted of ramp-and-hold translations of the platform in one of 12 directions uniformly spaced in the horizontal plane (Figure 2.1). Although the perturbations were destabilizing, they resulted only in small changes in joint angles ($\leq 5°$), suggesting that a static musculoskeletal model is adequate to estimate feasible forces. The positions of the hip, knee, ankle, and metatarsal-phalangeal (MTP) joint centers were estimated from kinematic marker data (Fung and Macpherson 1995).

For the current analysis, we obtained the average kinematic configuration of the hindlimb in an 80 ms window before the onset of the perturbation in each trial (Figure 2.3, gray lines). We also obtained the active postural response force vector, which was computed as the difference in force direction between the active force response period during an 80 ms window 120 ms following perturbation onset, and the background period (Fung and Macpherson 1995).

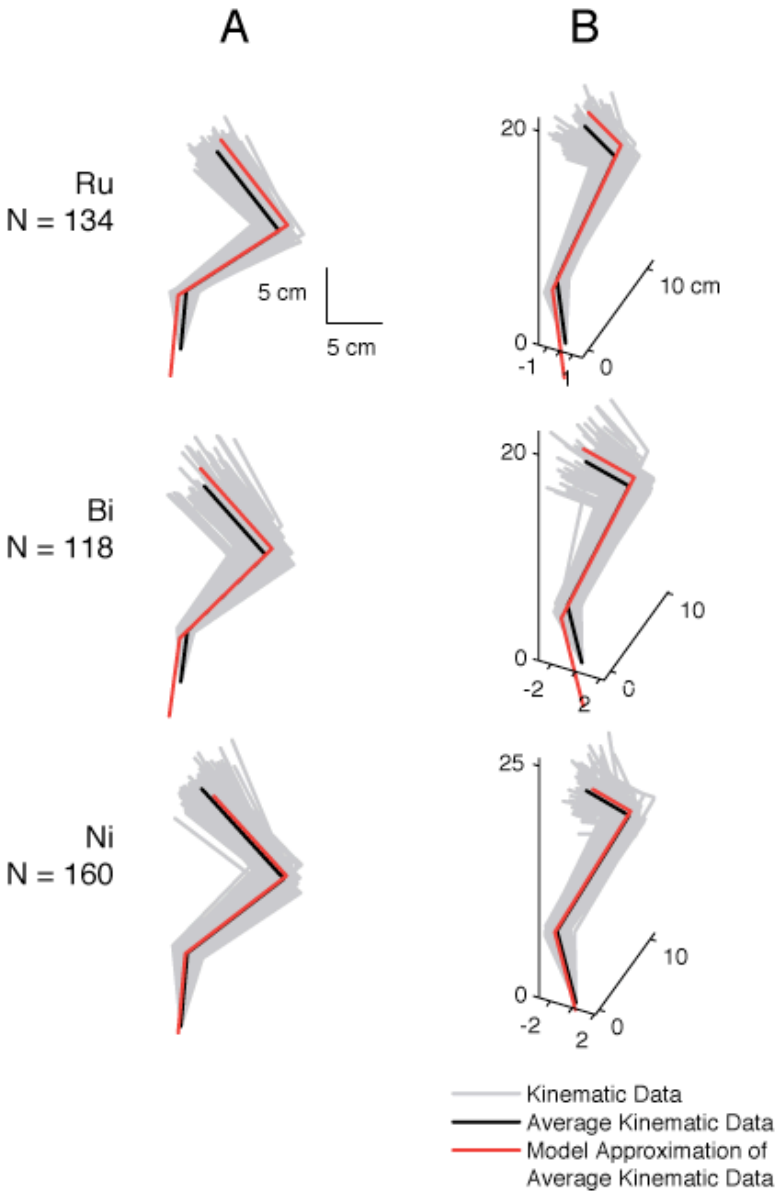

Figure 2.3. Model postures were based on kinematic data of three cats. Column A: sagittal view. Column B: posterior-lateral view. Light gray traces are kinematic data from each trial (*Ru:* N=134, *Bi:* N=118, *Ni:* N=160), used in the FFS computation. Black traces are the average kinematic data for each cat. Red traces illustrate the best fit of the model to the average segment angles in the frontal and sagittal planes for each cat.

FEASIBLE FORCE SETS

Feasible force sets were constructed for each of the 412 trials using linear programming. For each trial, numerical optimization was used to calculate the limb posture $\vec{q}$ that minimized the mean squared error between the sagittal and posterior plane femur, shank, and foot angles of the model and those of the kinematic data; all residual segment angle errors were $\leq 10^{-4}$ ° (Fig. 3).

After the best-match $\vec{q}$ was established, the muscle excitation vector $\vec{e}$ producing the maximal biomechanically feasible force projection in each of 520 directions on the unit sphere was calculated subject to the constraint that all muscle excitations varied between 0 and 1. The FFS was then defined as the smallest convex polygon in the dorsal plane that encompassed the projections of these 520 forces. The vertices of this polygon represent unique $\vec{e}$; the distance from each point on the boundary of the polygon to the origin is the maximal biomechanically feasible force magnitude in that direction (Kuo and Zajac 1993; Schmidt et al. 2003; Valero-Cuevas et al. 1998). We have found that this method produces results identical to exact solutions produced with computational geometry tools (Avis and Fukuda 1992) (e.g., *cdd*, K. Fukuda; *cddmex*, F. Torrisi and M. Baotic) when the dimension of $\vec{e}$ is ≤ 13 (data not shown). Exact solutions of this type are not feasible for larger numbers of muscles because computation time increases exponentially with the dimension of $\vec{e}$.

SENSITIVITY ANALYSIS

We tested the sensitivity of the FFS to morphological parameters and model architecture. A FFS was constructed based on the mean kinematic data of each cat. We then examined the changes in the maximal directions of these FFSs due to perturbations of ± 50% to all nonzero muscle moment arms, perturbations of ± 50% to the maximum force value for each muscle, and 1° perturbations to each joint angle (Lehman and Stark 1982; Scovil and Ronsky 2006). In addition, we tested the influence of an externally applied moment limit, the use of the pseudoinverse of the full seven degree of freedom system Jacobian $\left(J^T\right)^+$, and of scaling individual segment lengths to match the kinematic data.

RESULTS

All simulations exhibited strongly anisotropic FFS with maxima in both the posterior and anterior half-planes, (Figure 2.4A, solid red lines) consistent with stereotypical force directions observed in the force constraint strategy (Macpherson 1988a). Inter-trial variance of the FFS was minimal; maximum coefficients of variation for points on the FFS were 9.0%, 15.5%, and 15.3% for cats *Ru*, *Bi*, and *Ni* (Figure 2.4, upper row), respectively. Because of this small variability and the general similarity of FFS shape across cats, all FFSs were combined into a grand mean for subsequent analysis (Figure 2.4, lower row) except for the sensitivity analyses, which were performed about the mean posture of each cat. Sensitivity analysis results based on the mean posture of *Ru* are reported in detail here because they were the most sensitive.

The grand mean FFS was bimodal, with maxima nearly aligned with the posterior-anterior axis (-87 ± 8° and 71 ± 4°; mean ± SD); the anterior maxima had a small lateral component (Figure 2.4A, red dashed lines). The absolute minimum of the FFS was directed medially (177 ± 8°), and a second minimum was directed almost exactly laterally (8 ± 8°). The magnitude of the posterior maximum was 8.2 times the absolute minimum, while anterior magnitude was 2.8 times the absolute minimum (Figure 2.4B, solid red line).

The histogram of the active postural force directions was also bimodal (Figure 2.4B, gray bars), with peaks located near the FFS maxima (Figure 2.4B, compare red and black dashed lines), consistent with the hypothesis that biomechanically favorable force directions are preferentially used. The medians of the posterior and anterior postural force direction histograms were rotated counter-clockwise relative to FFS maxima by a moderate but statistically significant amount (-22° and –21°, respectively; Wilcoxon signed-rank test, $p < 0.05$). There were few directly lateral forces where FFS magnitude was small (Figure 2.4B, near 0°), and notably, no medial forces near the absolute minimum of the FFS (Figure 2.4B, near 180°).

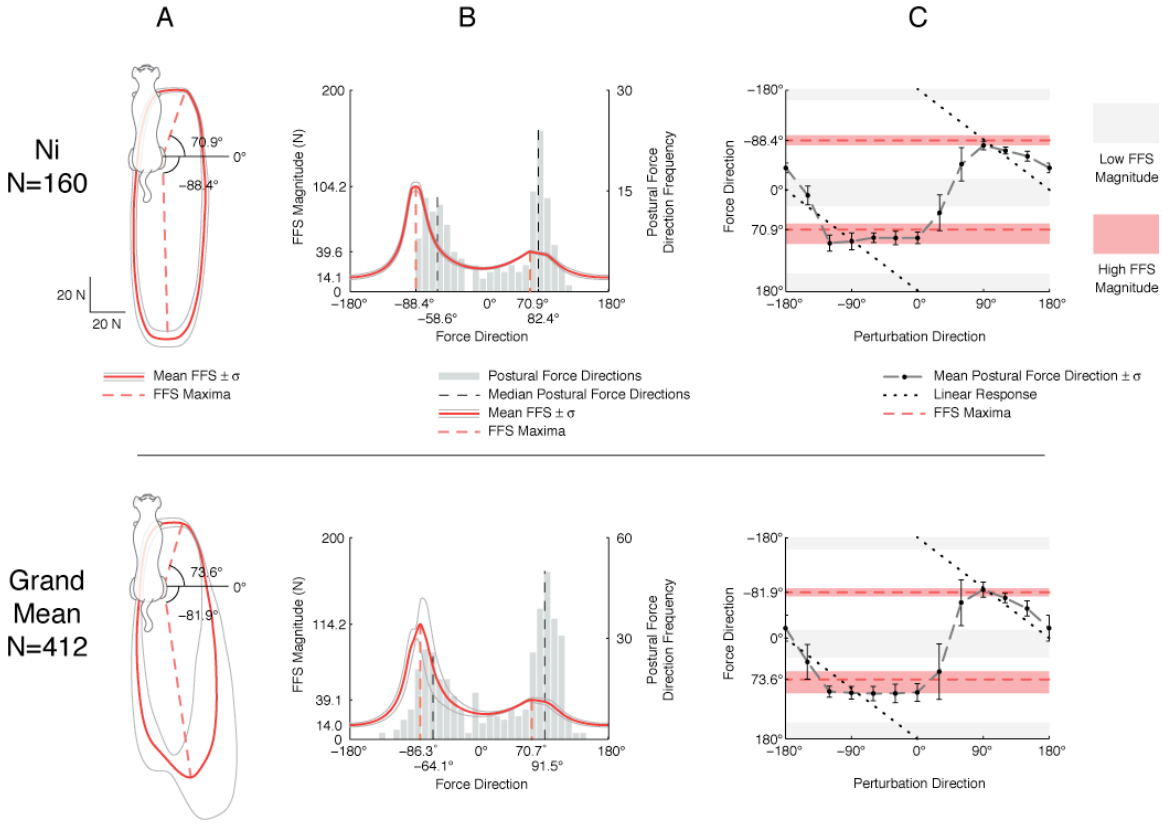

Figure 2.4. FFSs and active postural force directions for cat *Ni* (top row), and the grand mean across all cats (bottom row). Angle conventions are defined in Figure 2.1. A: Dorsal plane FFS mean ± SD (red thick and thin lines, respectively). FFS maxima (dashed lines) are directed either posteriorly or anteriorly with small lateral components. FFS minima are in the medio-lateral directions. The mean FFS of the individual animal and the grand mean are bimodal, similar to the two-vector force constraint strategy. B: FFS magnitude from A (solid red line, left hand scale), plotted against force direction and histogram of active postural response forces (gray bars, right hand scale). Postural force directions are bimodal with peaks (dashed gray lines) clustered near the maxima of the FFS (dashed red lines). No active forces were directed medially, near the FFS minima. C: Active postural forces generated by the hindlimb (black circles) are not directly opposite to the perturbation direction (dotted black line). Instead, forces tend towards directions of high feasible force magnitude (red shaded area) and away from regions of low feasible force magnitude (gray shaded area). The FFS maxima therefore act as attractors of force direction that have stronger influence on lateral perturbation directions (-90° to 90°) than medial perturbations (≤ -90° or ≥ 90°).

The anisotropic shape of the FFS qualitatively predicted the nonlinear relationship between perturbation direction and active postural force direction (Figure 2.4C) first reported by Macpherson (1988a, Figure 8B). Active force directions in response to a specific perturbation direction were not directly opposite to the perturbation direction (Figure 2.4C, dotted line). Instead, the active forces tended to gravitate towards directions where feasible forces were high (Figure 2.4C, red shaded area) and away from directions where feasible forces were low (Figure 2.4C, gray shaded area). Deviations from the linear response were more acute for perturbations directed laterally; postural forces either clustered around the anterior FFS maxima (-90° to 0°) or were dispersed (0° to 90°; notice the larger error bars in this region in Figure 2.4).

The FFS was robust to various perturbations to the model parameters. The results of the sensitivity analysis performed about the mean posture of *Ru* are summarized in Table 2.1; results for *Bi* and *Ni* were equally or less sensitive in general. The FFS maxima were insensitive to ± 50% perturbations to individual muscle moment arms and maximum muscle forces, eliciting maxima direction changes of ≤ 14° and magnitude changes of ≤ 27% across all cats. Sensitivity to individual joint angles was ≤ 3.5° for posterior maxima and ≤ 10.2° for anterior maxima; the increased sensitivity of anterior maxima is not critical because the anterior maxima were more broadly tuned in general. We found only small changes in FFS maximum directions (≤ 9.1°) when we scaled the model segment lengths to each cat, and comparably small changes (≤ 9.8°) when we recreated the analysis using the pseudoinverse $\left(J^T\right)^+$ of the full seven degree of freedom system Jacobian in Equation 2.2. The largest sensitivity values were associated with external limits placed on the endpoint moment. FFS maxima directions were moderately affected by moment limits ranging between 0.001 N-m and 10 N-m (≤ 17.6°), but the FFS magnitude was scaled considerably (≤ 85.3%). In all cases, however, FFSs retained their bimodal shape, and FFS magnitudes exceeded observed postural force magnitudes.

Table 2.1. Sensitivity of FFS maxima (cat *Ru*) to model architectural and morphological parameters. Sensitivity of posterior and anterior maxima directions and magnitudes are expressed separately; in general anterior maxima directions are more sensitive but are also less acutely tuned. This analysis was conducted about the mean limb posture for cat *Ru*; sensitivity values for *Bi* and *Ni* were similar or less sensitive in general.

	Direction		Magnitude	
	Posterior	*Anterior*	*Posterior*	*anterior*
Moment limit = 0.001 N-m	1.0°	-0.3°	-42.5%	-82.7%
Moment limit = 1 N-m	3.8	-17.6	-31.2	-64.9
Moment limit = 10 N-m	-3.4	9.6	3.6	-0.8
Pseudoinverse	-3.4	9.8	3.6	-0.1
Altered segment lengths	-3.3	9.1	14.1	8.0
1° perturbations to joint coordinates	≤ 3.5	≤ 10.2	≤ 3.8	≤ 1.7
± 50% perturbations to moment arms	≤ 5.1	≤ 13.6	≤ 23.9	≤ 6.8
± 50% perturbations to F_o values	≤ 4.9	≤ 13.5	≤ 15.8	≤ 12.0

DISCUSSION

We used a musculoskeletal model of the cat hindlimb to assess the possible biomechanical determinants of the stereotypical force directions observed during postural control. We hypothesized that postural forces are preferentially chosen in directions of biomechanically favorable force production. Experimental horizontal plane force directions were distributed bimodally, with peaks near the directions of maximum force predicted by the model. However, they were consistently rotated with respect to these maxima, which were almost directly anterior and posterior. Thus, the anisotropy of the FFS may influence, but does not completely determine the choice of force direction during postural control.

The elongated shape and orientation of the FFS was consistent between animals, across all trials, and was insensitive to variations in model parameters, including maximum muscle forces, moment arms, kinematic configuration, segment lengths, and endpoint moment constraints. Similarly, Kuo and Zajac (1993) reported minimal sensitivity of their feasible acceleration sets to morphological parameters and variations among standing postures in the human. The FFS shape is probably most strongly influenced by the kinematic description of the model (Valero-Cuevas et al. 1998), however, altering the number of kinematic degrees of freedom (via the use of the pseudoinverse of the full rank system Jacobian) did not significantly alter our results. Similarly, scaling the model segment lengths to match the morphology of each cat had little influence. Therefore, it is not likely that using a subject-specific model (Zajac 2002; Zajac et al. 2002), rather than our generic, unscaled model of the cat hindlimb would alter our results. Because endpoint moment data are unavailable, we could not estimate the exact effects of endpoint moment on the FFS (cf., Valero-Cuevas et al. 1998). However, the high sensitivity to limits on endpoint moment is not considered to be critical because the bimodal structure of the FFS was unchanged even for the most extreme limits on endpoint moment.

The external force and moment during a postural task could affect the peak force directions predicted by the FFS. The endpoint forces and moments during standing result from gravitational forces, muscular forces from the other limbs and trunk, and forces due to unmodeled muscles in the hindlimb. Adding the background force during standing

would effectively translate the origin of the FFS in a posterior and lateral direction, increasing the maximum force magnitude in the anterior direction. This could account for the relatively small anterior force peak (Figure 2.4B) in the FFS compared to the experimental force directions, which were measured during active unloading on a background of extensor activity (Macpherson 1988a). The addition of unmodeled pelvic muscles that contribute to flexion could also increase the anterior force magnitudes. As discussed above, maximum endpoint moment constraints affect FFS magnitude more than shape. The largest changes to force maximum directions were $\leq 17.6°$, when a moderate constraint was applied (≤ 1 N-m). Therefore, the addition of more realistic external forces and moments are not predicted to significantly alter force maximum directions, only magnitudes.

It is possible that the large number of muscles in our model decreased the sensitivity of the FFS to individual model parameters. For example, while single muscle forces predicted by optimization have been reported to be highly sensitive to parameter values (Kaya et al. 2005; Raikova and Prilutsky 2001), multiple muscle activation patterns have not (van Bolhuis and Gielen 1999). Similarly, in dynamic simulations of the human leg, Scovil and Ronsky (2006) report considerable sensitivity of single muscle forces to muscle model parameter perturbations, but reduced sensitivity of the overall model behavior (e.g., the ground reaction force during walking).

In contrast to maximal effort tasks (e.g., Pandy et al. 1990; Valero-Cuevas et al. 1998), the postural task presented here imposed no explicit biomechanical constraint on single limb force direction. While total force generated by all four limbs must oppose the perturbation direction, the nervous system is free to choose single limb force directions that may optimize arbitrary criteria (cf., Crowninshield and Brand 1981; Harris and Wolpert 1998; Kaya et al. 2005; Scott 2004; Todorov 2004).

Using a diagonal axis of force production may simplify the neural control mechanism required to coordinate force direction and amplitude during postural responses, but is not imposed by biomechanical limitations in hindlimb force production. The force of each limb could be controlled by modulating a limited number of muscle activation patterns (Ting and Macpherson 2005) that produce forces in an equally limited number of directions. Although postural force magnitudes ($\approx$ 1-2 N) are small, using a

biomechanically favorable force direction may also be energetically advantageous, and beneficial in an uncertain environment when the magnitude of the postural perturbation is unpredictable. Valero-Cuevas et al. (1998) has suggested that solutions to "maximal effort" tasks may represent functional units of neuromechanical organization applicable to tasks requiring submaximal effort. Scaled versions of the muscle excitation patterns determined by the maxima of the FFS of the human index finger are used over the entire voluntary range (Valero-Cuevas 2000).

Other factors not modeled here that could influence the choice of force directions used in postural control include interlimb coordination and stability criteria. The considerable anisotropy of the FFS may reflect hindlimb biomechanical capabilities tuned for locomotion, and not necessarily postural control. Large posterior forces are consistent with propulsion during locomotion, and anterior forces are used in the deceleration phase of gait. The maximal force directions of the FFS would have limited capacity to resist lateral perturbations. While the use of the diagonal force direction is not explicitly predicted by the FFS, the diagonal forces are still consistent with biomechanically favorable directions of force production, with the added benefit that lateral force components can also be generated. Moreover, rotation of the force vectors in each limb towards the center of mass is consistent with a self-stabilization strategy (Bauby and Kuo 2000; Holmes et al. 2006; Kubow and Full 1999), reducing torques about the center of mass.

CHAPTER 3

NEUROMECHANICAL MODELING OF FUNCTIONAL MUSCLE SYNERGIES FOR POSTURAL CONTROL IN THE CAT

This chapter was originally published as an article in the *Journal of Biomechanics*:

McKay JL, and Ting LH. Functional muscle synergies constrain force production during postural tasks. *J Biomech* 41: 299-306, 2008.

ABSTRACT

We recently demonstrated that five functional muscle synergies were sufficient to characterize both hindlimb muscle activity and active forces during automatic postural responses in cats. Notably, functional muscle synergies based on data from a biomechanical condition approximating the natural posture of the animal were sufficient to reproduce muscle activity and active forces when the hindlimb posture was varied in the sagittal plane. We predicted that as posture varies the forces produced by functional muscle synergies (synergy force vectors) rotate with the limb axis. Here, we first used a detailed, 3D static model of the hindlimb to confirm that this strategy is biomechanically plausible: as we varied the model posture, simulated synergy force vectors rotated monotonically with the limb axis in the parasagittal plane ($r^2 = 0.94 \pm 0.08$). We then tested whether five functional muscle synergies provide the same force-generating capability as 31 individuated muscles. We compared feasible force sets (FFS) of the model with and without a synergy organization. FFS volumes were significantly reduced with the synergy organization ($F = 1556.01$, $p << 0.01$), and as posture varied, the synergy-limited FFSs changed in shape, consistent with changes in experimentally-measured active forces. In contrast, nominal FFS shapes were invariant with posture, reinforcing prior findings that postural forces cannot be predicted by hindlimb biomechanics alone. We propose that an internal model for postural force generation may coordinate functional muscle synergies that are invariant in intrinsic limb

coordinates, and this reduced-dimension control scheme reduces the set of forces available for postural control.

INTRODUCTION

A common finding among studies of the neural control of movement is "dimensional collapse," whereby the behavior of neuromechanical systems that are in theory highly redundant (Bernstein 1967) and computationally formidable to control can be described with only a few degrees of freedom (Flash and Hochner 2005; Grasso et al. 1998; Sanger 2000; Zatsiorsky et al. 2003). Recent studies of muscle coordination, in particular, have demonstrated that the superposition of a few muscle activation patterns, defined as muscle synergies, is sufficient to describe muscular activity during many natural behaviors in humans and animals (Cheung et al. 2005; Krishnamoorthy et al. 2003; Poppele and Bosco 2003; Ting and Macpherson 2005), although due to motor abundance an infinite number of such patterns are theoretically possible.

The hierarchical structure suggested by these results has provided substantial new insight into the neural control of movement, however, comparably few studies have examined muscle synergies quantitatively from the perspective of biomechanical function (e.g., Loeb et al. 2000; Raasch and Zajac 1999; Valero-Cuevas 2006). Comparing muscle synergies across subjects or animals, for example, is difficult not only because of experimental limitations (e.g., electrode placement) but also, because muscle synergies that appear distinct may be functionally equivalent due to biomechanical redundancy. Similarly, because the number of synergies cannot be controlled in experiments, estimating the number of synergies that are sufficient for task performance is an open question, albeit an important one from the perspective of rehabilitation (Latash and Anson 2006).

In a recent study (Torres-Oviedo et al. 2006), we demonstrated that electromyographic and kinetic data from automatic postural responses in cats could be simultaneously decomposed into a small set of five "functional" muscle synergies, which specify both a pattern of hindlimb muscle activation (a muscle synergy) and a correlated "synergy force vector" at the ground. Significantly, cats performed the task in various biomechanical conditions (anterior-posterior "stance distances," Macpherson 1994) using the same synergies as in a control biomechanical condition approximating the natural

posture of the animal ("preferred" stance distance). However, the generalization was apparent only when the synergy force vectors were expressed in a coordinate system that rotated with the hindlimb axis in the sagittal plane. This result was compelling because it suggests that an internal model (Kawato 1999; Shadmehr and Mussa-Ivaldi 1994) for limb force production during postural control coordinates synergy force vectors that are invariant in the intrinsic coordinates of the limb, although the postural task itself - generating an appropriate net response force at the ground with all four limbs - is based in extrinsic coordinates.

The first aim of the present work was to verify whether the rotation of synergy force vectors we observed experimentally was feasible in the context of a detailed musculoskeletal model of the cat hindlimb (Burkholder and Nichols 2004; McKay et al. 2007). Although we demonstrated that the EMG and force components of the experimentally-identified functional muscle synergies were correlated, we could not demonstrate that this relationship was causal. Synergy force vectors identified in the control posture of each animal from our earlier study (Torres-Oviedo et al. 2006) were used as source data, and simulated muscle synergies corresponding to each synergy force vector were determined with numerical optimization (e.g., Crowninshield and Brand 1981; Harris and Wolpert 1998; Kurtzer et al. 2006; Valero-Cuevas et al. 1998). We then applied these muscle synergies to the model in other postures to test whether the resulting force vectors were oriented consistently with respect to the limb axis.

The second aim of the present work was to assess the impact of a muscle synergy organization on the functional capabilities of the model. In particular, we tested the hypothesis that constraining the muscles to coactivate in synergies would limit the model's total force-production capacity. We quantified the force-production capacity of the model with its feasible force set ("FFS," Valero-Cuevas et al. 1998). The FFS is a convex manifold in three-dimensional "force space;" the length of the vector from the origin to any point on the FFS is the maximum force that can generated by the model in that direction, subject to limits on individual muscle forces. The FFS is a useful descriptor because neural deficits reduce its volume and influence its shape (Kuxhaus et al. 2005). We computed FFSs across postures assuming 1) control of individuated muscles (nominal FFS), and 2) control only of the simulated muscle synergies

determined earlier (synergy-limited FFS). We then compared the FFSs from the two conditions (cf. Valero-Cuevas) to identify systematic changes; a reduction in FFS volume associated with the synergy constraint, for example, indicates the synergy organization limits force-production capacity, similar to a neuromuscular deficit (Kuxhaus et al. 2005). Finally, we investigated whether the stereotyped, posture-dependent changes observed in postural force production (the "force constraint strategy," Macpherson 1994) were predicted by posture-dependent changes in the nominal or synergy-limited FFS shape.

METHODS

We used a static musculoskeletal model of the cat hindlimb (McKay et al. 2007) and kinematic and kinetic data of three cats performing a horizontal translation balance task at four (cats *Bi* and *Ru*) or three (cat *Ni*) postural configurations to simulate functional muscle synergies based on those of Torres-Oviedo et al. (2006). Details of the laboratory experiment are presented in that work, and are omitted here for brevity. Model postures approximating the average background period kinematics of each animal in each postural configuration (11 in total) were calculated as in an earlier study (McKay et al. 2007). Due to practical limitations we could not use previously reported muscle synergies directly. Therefore, muscle activation patterns that could produce each of the five synergy force vectors reported from the control ("preferred") posture in each animal were determined using two optimization criteria drawn from the literature: "minimum-noise" optimization and "maximum-force" optimization.

We examined the endpoint force vectors of these simulated muscle synergies as hindlimb postural configuration varied to test the prediction (Torres-Oviedo et al. 2006) that changes in these vectors would be confined primarily to rotation in the sagittal plane. With this tested, we conducted an FFS analysis to assess whether a muscle synergy organization based on our simulated synergies would impact the force-production capability of the model by reducing FFS volume. A total of three FFSs were calculated for each of the 11 animal / posture combinations; first assuming individuated control of muscles (nominal FFS), then assuming only individuated control of the simulated synergies from the minimum-noise optimization (minimum-noise synergy-limited FFS), and last, assuming only control of the simulated synergies from the maximum-force optimization (maximum-force synergy-limited FFS). Finally, we compared the nominal

and synergy-limited FFSs with experimental postural force data to determine whether the stereotyped, posture-dependent changes observed in postural forces were qualitatively predicted by posture-dependent changes in the FFSs. Statistical tests were considered significant at $p < 0.05$.

HINDLIMB MODEL

The 3-dimensional hindlimb model is presented in detail in (McKay et al. 2007). Briefly, the model is a matrix equation relating 31-element muscle excitation vectors $\vec{e}$ to the six-element force and moment system $\vec{F}$ produced at the endpoint, approximated as the metatarsal-phalangeal joint:

$$\vec{F} = \left(J\left(\vec{q}\right)^T \right)^+ R\left(\vec{q}\right) F_O F_{AFL}\left(\vec{q}\right) \vec{e} \tag{3.1}$$

Where the vector $\vec{q}$ is comprised of the model's seven rotational degrees of freedom at the hip, knee, and ankle; $\left(J\left(\vec{q}\right)^T \right)^+$ is the pseudoinverse transpose of the geometric system Jacobian, $R\left(\vec{q}\right)$ is the moment-arm matrix, F_O is the diagonal matrix of maximal muscle forces, and $F_{AFL}\left(\vec{q}\right)$ is the diagonal matrix of scaling factors based on active muscle force-length characteristics. Muscle moment arm values and fiber lengths were determined with SIMM software (Musculographics, Inc., Santa Rosa, CA).

MUSCLE SYNERGIES

In our muscle synergy model (Torres-Oviedo et al. 2006; Tresch et al. 1999), muscle excitation vectors $\vec{e}$ are produced by the linear combination of a few non-negative muscle synergies $\vec{w}_1, \vec{w}_2, \ldots, \vec{w}_{NSYN}$, where the number of synergies N_{SYN} is fewer than the number of muscles N_{MUS}. Although the muscles within a synergy have a fixed proportional activation, the organization is somewhat flexible because any given muscle can belong to more than one synergy. Therefore, because several synergies may act on a given muscle, the net activation of that muscle is the sum of activations due to each synergy. In matrix form, this relationship is:

$$\vec{e} = W\vec{c} \tag{3.2}$$

Where $\vec{w}_1, \vec{w}_2, \ldots, \vec{w}_{NSYN}$ are the columns of W and $\vec{c}$ is a vector of synergy activation coefficients. Combining Equations 3.1 and 3.2 yields an expression for the force and moment system $\vec{F}_c$ due to synergy activation $\vec{c}$:

$$\vec{F}_c = \left(J(\vec{q})^T \right)^+ R(\vec{q}) F_O F_{AFL}(\vec{q}) W \vec{c} \tag{3.3}$$

OPTIMIZATION MODELS

Practical limitations necessitated that we could not use previously reported muscle synergies directly. In particular, as no absolute normalization data (e.g., maximum voluntary contraction Lloyd and Besier 2003) was available, EMG records in (Torres-Oviedo et al. 2006) were presented in arbitrary units which were unsuitable for use in the model. In addition, the model includes a superset of the muscles studied earlier, with the addition of *adductor femoris, adductor longus, flexor hallicis longus, gluteus maximus, gluteus minimus, peroneus brevis, peroneus longus, peroneus tertius, pectineus, pyrformis, quadratus femoris, tibialis posterior, vastus intermedius,* and the omission of *tensor fasciae latae*.

To resolve these issues, simulated muscle synergies based on experimentally measured synergy force vectors from the preferred posture of each animal were determined with two different optimization models. Given a synergy force vector $\vec{f}_{wi}$, the unique muscle synergy $\vec{w}_i$ that achieves $\vec{f}_{wi}$ while minimizing signal-dependent noise (equivalent to muscular stress, e.g., Crowninshield and Brand 1981; Harris and Wolpert 1998; Kurtzer et al. 2006) can be determined with quadratic programming. Notice that this formulation differs slightly from the "force-sharing problem" (e.g., van Bolhuis and Gielen 1999) because we consider endpoint forces as opposed to joint torques. First we partition Equation 3.1 to separately consider the rows corresponding to endpoint force (A_F) and moment (A_M):

$$\begin{bmatrix} A_F \\ A_M \end{bmatrix} \equiv \left(J(\vec{q})^T \right)^+ R(\vec{q}) F_O F_{AFL}(\vec{q}) \tag{3.4}$$

Then, $\vec{w}_i$ is given by

$$\text{minimum noise}: \begin{cases} \text{minimize}: & \vec{w}_i^{\,T}\,\vec{w}_i \\ \text{such that}: & \vec{f}_{wi} = A_F\,\vec{w}_i \end{cases} \tag{3.5}$$

Equivalently, the unique muscle synergy $\vec{w}_i$ that maximizes feasible force in the direction of $\vec{f}_{wi}$ subject to limits on individual muscle forces (Valero-Cuevas et al. 1998) is given by

$$\text{maximum force}: \begin{cases} \text{maximize}: & \vec{f}_i \cdot \left(A_F\,\vec{w}_i\right) \\ \text{such that}: & \left|\vec{f}_{wi} \times \left(A_F\,\vec{w}_i\right)\right| = 0 \\ & 0 \le w_{ij} \le 1, \quad j = 1, 2, \ldots, N_{MUS} \end{cases} \tag{3.6}$$

Where w_{ij} denotes the jth element of $\vec{w}_i$. For convenience, the cross-product constraint of Equation 3.6 was realized as the equivalent linear equality constraint $\vec{f}_{wi} \times \left(A_F\,\vec{w}_i\right) = \left[0\ 0\ 0\right]^T$. Solutions $\vec{w}_i$ were subsequently normalized by their maximum value.

Notice that because muscle synergies $\vec{w}_i$ are normalized to unit maximum value, enforcing the constraint (Equation 3.6) implicitly limits the elements c_k to the interval $[0,1]$ in the synergy-limited force set calculation; this is in contrast to our experimental studies (Ting and Macpherson 2005; Torres-Oviedo et al. 2006), where c_k are allowed to assume any non-negative value.

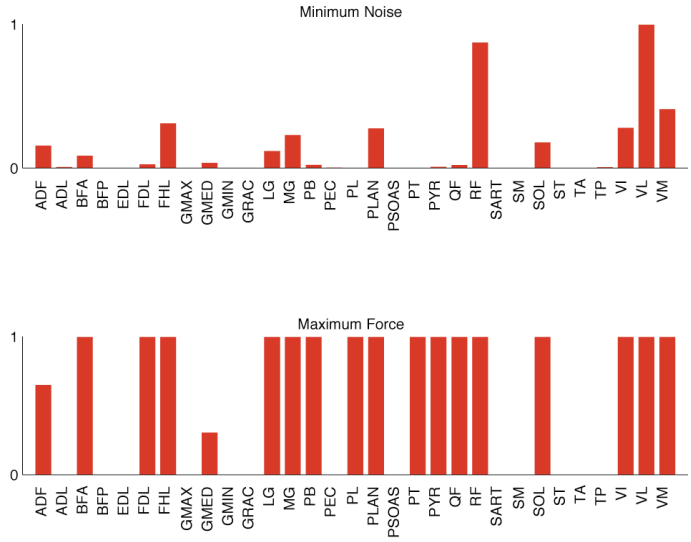

Figure 3.1. Drastically different muscle synergies producing identically-oriented synergy force vectors. The simulated muscle synergies shown were calculated to produce forces aligned with the synergy force vector shown in red for cat *Ru* in preferred posture (see Figure 2.1) using (A) minimum-noise and (B) maximum-force optimization criteria. The minimum-noise optimization, equivalent to muscle stress minimization (Crowninshield and Brand 1981), results in less coactivation than the maximum-force optimization.

NOMINAL AND SYNERGY-LIMITED FEASIBLE FORCE SETS

Nominal FFSs were constructed similarly to a previous study (McKay et al. 2007). Briefly, the muscle excitation $\vec{e}$ producing the largest possible force projection in each of 1000 directions distributed on the unit sphere was calculated using linear programming subject to the constraint that muscle activations varied between 0 and 1:

$$0 \le e_j \le 1, \quad j = 1, 2, \ldots, N_{MUS} \tag{3.7}$$

The FFS was then defined as the smallest three-dimensional convex polygon that encompassed these 1000 force projections. It was determined using the *convhull* package in Matlab.

Synergy-limited FFSs were constructed using an analogous procedure. For each synergy-limited FFS, the synergy activation vector $\vec{c}$ producing the maximal biomechanically feasible force in each of 1000 directions distributed on the unit sphere was calculated using linear programming subject to the constraint (Equation 3.7) and the additional non-negativity constraint

$$0 \le c_k, \quad k = 1, 2, \ldots, N_{SYN} \tag{3.8}$$

STATISTICAL TESTS

A series of linear regressions was performed to identify systematic variation in the orientation of synergy force vectors, nominal FFSs, and synergy-limited FFSs as the limb moved through the workspace. Sagittal and horizontal plane orientation data were treated separately. While angles of synergy force vectors in the sagittal and horizontal planes were calculated directly, orientation of the FFSs and synergy-limited FFSs was quantified by calculating the sagittal and horizontal plane angles of the 3D vector in $\left[f_x \; f_y \; f_z\right]^T$ from the origin to the FFS centroid (cf. Kuxhaus et al. 2005). Similarly, orientation of the limb itself was quantified with the sagittal and horizontal plane angles of the "limb axis," the 3D vector in $\left[x \; y \; z\right]^T$ from the hip center to the MTP.

Multiple ANOVA was applied to the pooled FFS and synergy-limited FFS volume data. Synergy organization, stance distance, and experimental animal were tested as independent variables.

RESULTS

Simulated synergy force vectors rotated monotonically with the limb axis in the sagittal plane as postural configuration varied, consistent with the predictions of Torres-Oviedo et al. (2006) (Figure 3.2). Synergy force vector angles were more highly correlated to limb axis angles in the sagittal plane ($r^2 = 0.94 \pm 0.08$, $\mu \pm \sigma$) than in the horizontal plane ($r^2 = 0.75 \pm 0.25$). The slopes of the regression lines were near unity in the sagittal plane (0.86 ± 0.44) and distributed about zero in the horizontal plane (0.28 ± 0.46); a slope of 1 would result if the synergy force vectors were fixed in the reference frame of the limb axis.

This monotonic rotation of synergy force vectors with the limb axis was independent of the optimization model used to derive the synergies. Minimum-noise and maximum-force synergy force vectors were aligned closely and differed primarily in magnitude, despite considerable differences in the muscle activation patterns from the two optimizations (Figure 3.1). Large variations in muscle activity across animals been previously demonstrated during quiet standing even though the forces produced were similar (Fung and Macpherson 1995).

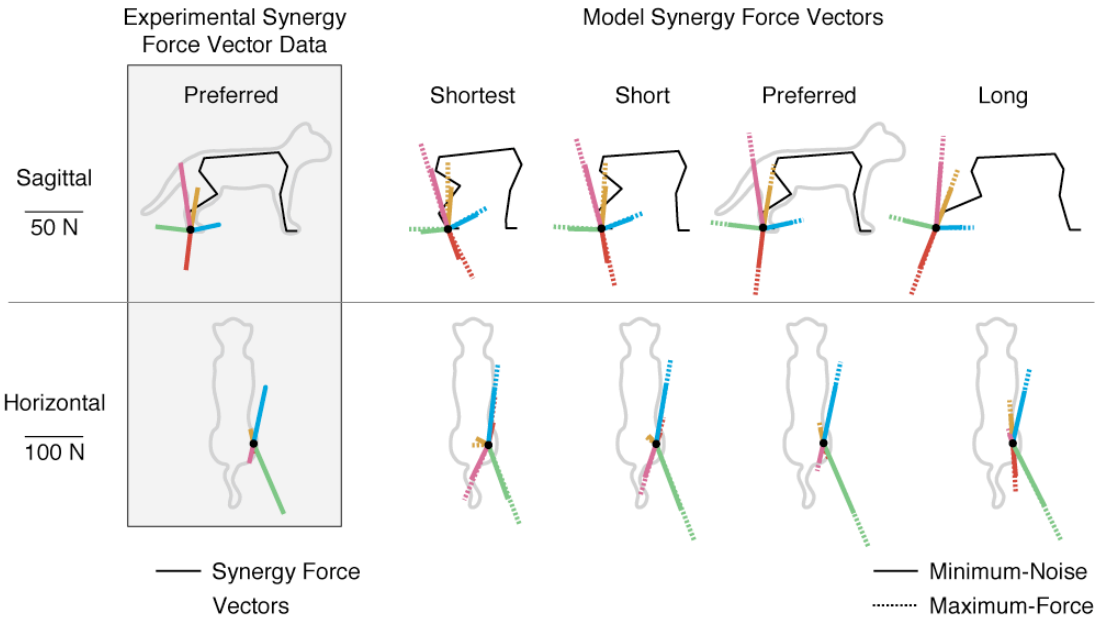

Figure 3.2. Synergy force vector rotation with postural configuration. Left: synergy force vectors from the control condition (preferred posture, P), as presented by Torres-Oviedo et al. (2006), used as source data. Average hindlimb kinematics are shown in black. Data shown are from cat *Ru*. Right: when simulated muscle synergies based on synergy force vectors at left are applied to the model in other postural configurations, the resulting synergy force vectors rotate monotonically with the sagittal-plane limb axis. Similar results are obtained whether minimum-noise (solid) and maximum-force (dashed) optimization is used to derive the simulated muscle synergies.

Nominal FFSs (Figure 3.3, gray polygons) were nearly isotropic in the sagittal plane, anisotropic and oriented along the anterior-posterior axis in the horizontal plane (cf. McKay et al. 2007). As posture varied, small changes were observed in the nominal FFS orientation, resulting in regression slopes that were near zero in both sagittal (0.06 ± 0.25; $r^2 = 0.77 \pm 0.15$) and horizontal planes (0.01 ± 0.03; $r^2 = 0.60 \pm 0.50$).

Synergy-limited FFSs were qualitatively very different from the nominal FFSs (Figure 3.3, Figure 3.4, white polygons) and were considerably more anisotropic in both the sagittal and horizontal planes, in particular with considerably reduced posterior force magnitude. From the standpoint of synergy-limited FFS shape, the only substantial difference between the two synergy optimization criteria was that FFSs based on maximum-force synergies encompassed some boundaries of the nominal FFSs, whereas minimum-noise FFSs did not. Synergy-limited FFSs rotated with the limb axis as posture

varied, primarily in the sagittal plane (slope = 1.41 ± 2.32; r^2 = 0.92 ± 0.05 (sagittal); slope = 0.33 ± 0.17; r^2 = 0.75 ± 0.14 (horizontal)).

Changes in the synergy-limited FFS as posture varied (Figure 3.4) were qualitatively similar to the changes in the distributions of active postural forces measured experimentally (Macpherson 1994). In the sagittal plane, active forces and synergy-limited FFSs both rotated closely with the limb axis. In the horizontal plane, active forces and synergy-limited FFSs were elongated along a posterior diagonal axis at "long" posture and more widely distributed, with increased anterior force magnitude at "short" and "shortest" postures; these stereotypical changes have been described previously as the "force constraint strategy" (Macpherson 1988a).

Multiple ANOVA (Figure 3.5) revealed that the synergy organization caused a highly significant reduction in FFS volume ($F = 1556.01$, $p << 0.005$). Tukey-Kramer pairwise comparisons applied post-hoc detected significant differences between the synergy-limited FFS volumes and nominal FFS volumes but no difference ($p > 0.05$) between the two optimization criteria. There was a significant main effect of stance distance ($F = 4.47$, $p < 0.012$); post-hoc tests revealed that FFS volume was highest in preferred posture. No effect of animal was detected ($F = 1.53$, $p > 0.22$). To increase statistical power, separate ANOVAs were performed to test the effect of posture on the three (nominal, minimum-noise, maximum-force) datasets; these results indicated significant effects of posture on the nominal FFS volumes ($F = 11.8$, $p < 0.004$) but not on the synergy-limited FFS volumes ($F = 0.31$, $p < 0.82$; $F = 0.25$, $p < 0.86$).

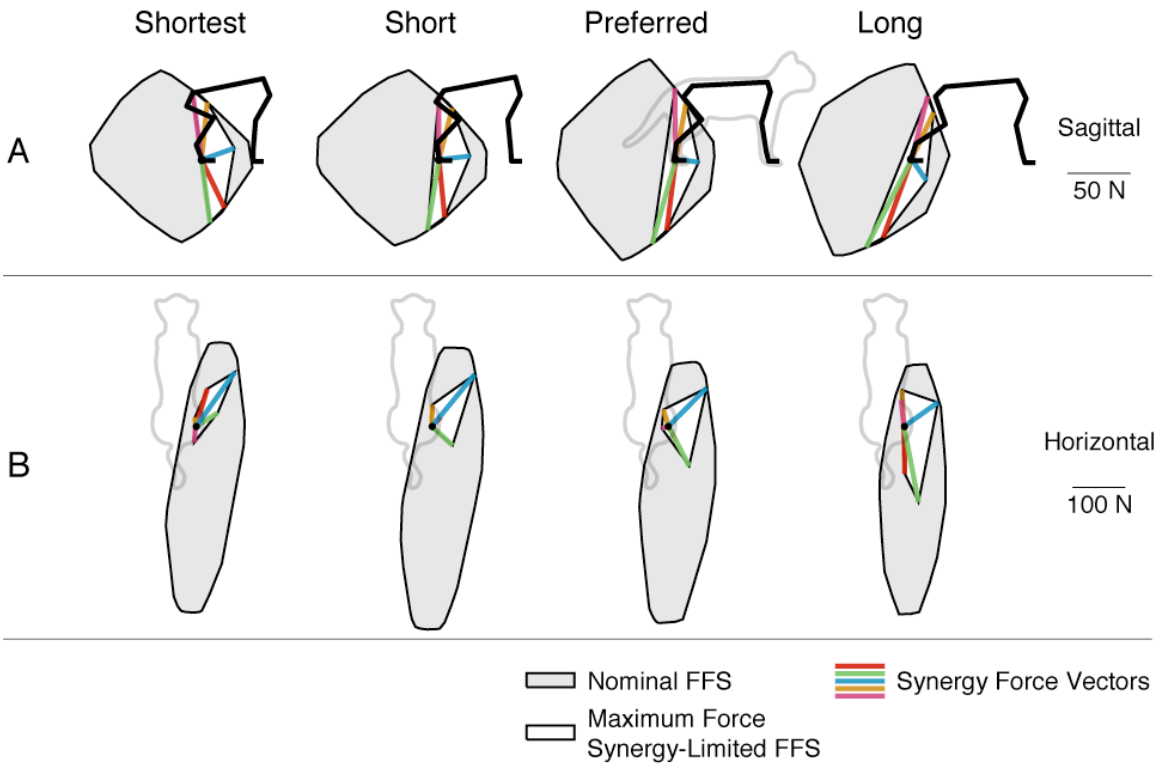

Figure 3.3. Nominal FFS (gray), maximum-force synergy-limited FFS (white), and simulated maximum-force synergy force vectors (colored lines) for cat *Bi* in all postures. A: sagittal projection. B: horizontal projection. Enforcing the muscle synergy organization dramatically reduces the volume of the FFS in all postures. The synergy force vectors span the synergy-limited FFS, so that any point on the synergy-limited FFS can be reached with a linear combination of the synergy force vectors. While the nominal FFS is largely invariant across postures, the synergy-limited FFS rotates with the hindlimb axis in the sagittal plane, and changes shape acutely in the horizontal plane.

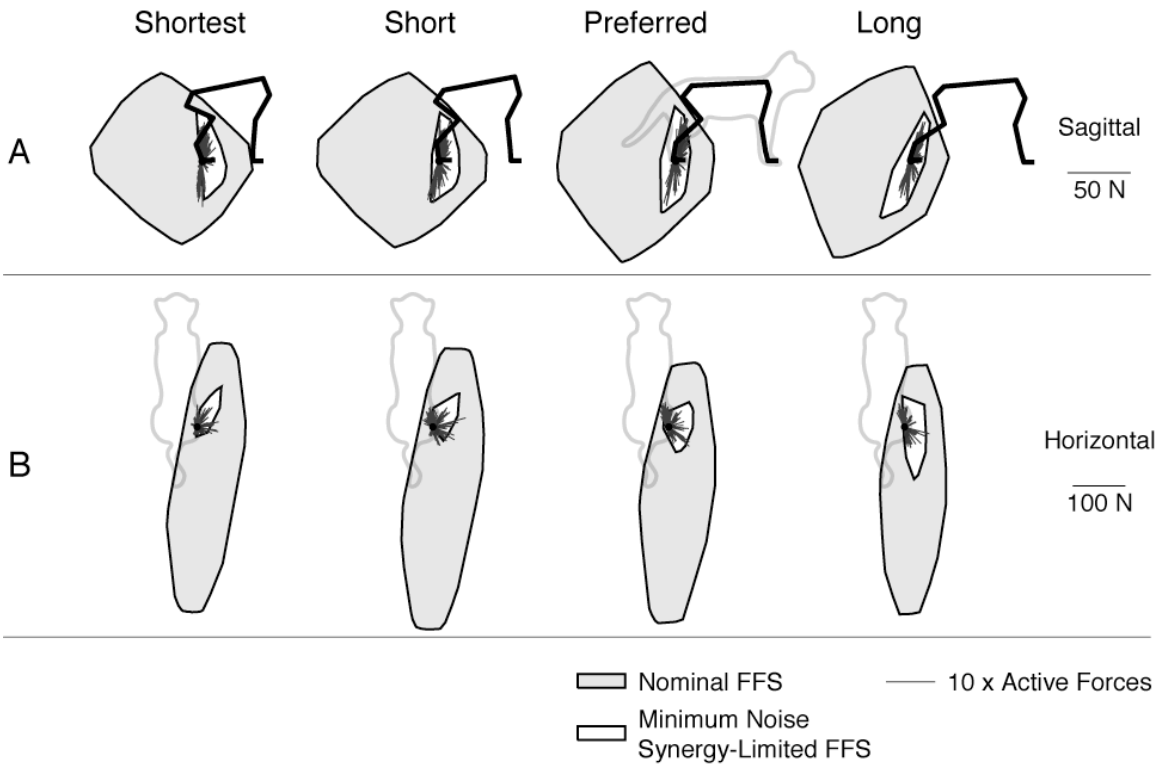

Figure 3.4. Nominal FFS (white), minimum-noise synergy-limited FFS (gray), and active postural forces (dark gray; magnified 10x) for cat *Bi* in all postures. Active postural response forces are averaged across time windows as in Torres-Oviedo et al. (2006). A: sagittal projection. B: horizontal projection. The synergy-limited FFS is a substantially better predictor of the distribution of postural forces than the nominal FFS at all postures, Particularly in the sagittal plane, where the synergy-limited FFS rotates closely with the envelope of postural forces. While the nominal FFS predicts almost no change in force production in the horizontal plane as posture varies, the synergy-limited FFS predicts stereotypical changes along a posterior diagonal axis (downwards and to the right, in the figure) at long (L) posture and increased anterior forces (upwards, in the figure) at shortest (SS) posture, as is observed experimentally (Macpherson 1994).

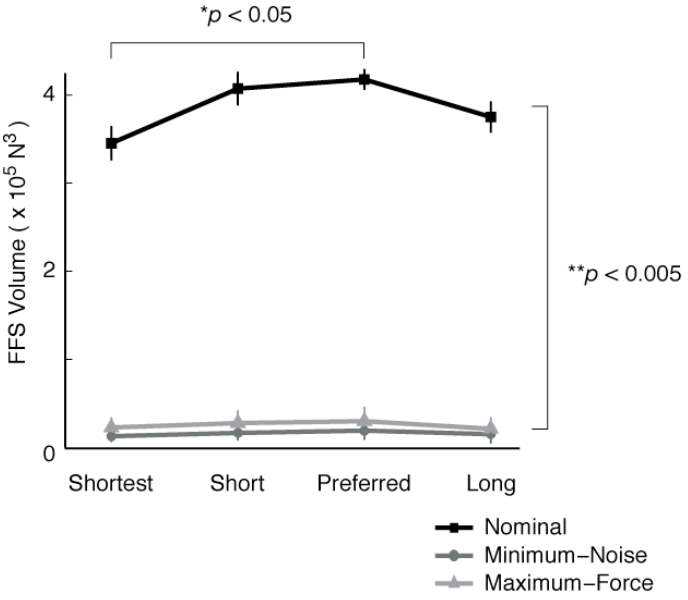

Figure 3.5. Changes in nominal and synergy-limited FFS volume with posture. Data are presented as $\mu \pm \sigma$. Synergy-limited FFSs have significantly reduced volume (multiple ANOVA; $F = 1556.01$, $^{**}p << 0.005$) compared to nominal FFSs. Tukey-Kramer pairwise comparisons applied post-hoc detected significant differences between the synergy-limited FFS volumes and nominal FFS volumes but no difference between the two optimization criteria. There was a significant main effect of postural configuration ($F = 4.47$, $^{*}p < 0.012$); post-hoc tests revealed that FFS volumes in preferred (P) posture were significantly higher than in shortest (SS) posture. No effect of animal was detected ($F = 1.53$, $p < 0.23$). To increase statistical power, separate ANOVAs were performed to test the effect of posture on the three (nominal, minimum-noise, maximum-force) datasets; these results indicated significant effects of postural configuration on the nominal FFS data ($F = 11.8$, $p < 0.004$) but not on the synergy-limited FFS data ($F = 0.31$, $p < 0.82$; $F = 0.25$, $p < 0.86$).

DISCUSSION

The primary motivation of this work was to demonstrate the feasibility of the functional muscle synergy architecture proposed in our previous, experimental study (Torres-Oviedo et al. 2006) in the context of a detailed biomechanical model. Here we show that simulated synergy force vectors rotate monotonically with the limb axis in the sagittal plane as posture varies (Figure 3.2), similar to that shown during experiments in the behaving animal. This result is important because it suggests that synergies can be coordinated throughout the workspace to perform functional tasks in extrinsic coordinates with a parsimonious internal model based on a polar coordinate transformation. In the case of balance control, the gravitational vector remains fixed although the synergy force vectors vary with postural configuration. This type of computation is documented in the nervous system; for example, a cascade of polar transformations occurs in the first stages of voluntary reaching (Flanders and Soechting 1990). It is thought that the initial proprioceptive frame for the transformation – at the level of the dorsal spinocerebellar tract – is likely a polar scheme based on limb length and orientation (Bosco et al. 1996; Poppele et al. 2002). Mechanistically, this transformation does not have to be explicit; as a neural substrate capable of computation in different reference frames has been demonstrated (Avillac et al. 2005). More work is required in this exciting area.

The second result, is that we demonstrate the muscle synergy organization comes at a "cost" in terms of the force-production capability of the limb. When the synergy architecture was imposed, it caused a dramatic reduction in FFS volume (Figure 3.5). This indicates that large regions of the FFS are inaccessible with only the synergies recruited for postural control. Based on this result we predict that tasks like locomotion will recruit additional synergies to reach the remainder of the FFS. Synergies that are "shared" among tasks and "specific" to particular tasks have been identified in other animal and human preparations (d'Avella and Bizzi 2005; Krishnamoorthy et al. 2004). However, it is only by examining muscle synergies in a biomechanical context that we are able to compactly illustrate why this might be the case.

The considerable changes in both FFS volume and shape associated with the synergy organization also suggest it may prove valuable to consider the implications of muscle synergies when using models to predict behaviors involving submaximal forces,

as opposed to "maximal" tasks (e.g., Kargo et al. 2002; Kuo and Zajac 1993; Valero-Cuevas et al. 1998), where behavior is likely limited by biomechanics alone. We have previously demonstrated that the nominal FFS is a weak predictor of postural forces in preferred posture (McKay et al. 2007). In contrast, the nominal FFS has been demonstrated as a good predictor of endpoint force in other tasks, for example for forces ranging between 200 and 650 N in the human lower limb (Schmidt et al. 2003) and maximal forces in the finger (Valero-Cuevas et al. 1998). Our results suggest that this disparity is because the forces required for the postural task are small enough (~1-2 N) that the constraints associated with the nominal FFS are simply not active. However, when we overlaid the experimental active postural response forces and the synergy-limited FFSs, we noted favorable agreement throughout the workspace (Figure 3.4), suggesting that the limited range of forces available with the synergy organization was determining behavior.

These results were generally independent of the optimization criteria used to derive the synergies. While both optimization criteria used here predict behavior in some circumstances (Crowninshield and Brand 1981; Kurtzer et al. 2006; Valero-Cuevas 2000), the primary reason for selecting these particular criteria from the many models of their type that have been proposed (Crowninshield and Brand 1981) was the drastically different solutions they produce (Figure 3.1). Although the specific criterion that best predicts postural muscle activation patterns is unknown, we can hypothesize that any function laying between the extremes of penalizing muscle activation relatively drastically ("minimum-noise") or not at all ("maximum-force") would yield similar results. We also noted with interest that the drastically different, but functionally equivalent muscle patterns illustrate the difficulty to the experimenter posed by biomechanical redundancy when inferring differences in function from redundant datasets. Although variations in muscle synergy composition may be observed across trials or subjects (e.g, d'Avella and Bizzi 2005; Torres-Oviedo et al. 2006), the functional significance of such differences may be occluded by biomechanical redundancy.

Energetic optimality has historically been an elegant guiding principle in the study of movement (cf. Alexander 1989; Hoyt and Taylor 1981). When examining the motor hierarchy, both biomechanical and neural optimality principles may be

simultaneously active. We noted that the volume of the nominal FFS, which reflects biomechanical limitations on force production, was significantly higher at the preferred posture (Fig. 5), consistent with the idea that the kinematics of this self-selected posture optimize this criterion. Similarly, Fung and Macpherson (1995) have used an inverse dynamic analysis to demonstrate that the preferred posture kinematics minimize total joint torques for antigravity support. At other postures, the limb is levered at the girdle, preserving the intralimb geometry and locally minimizing joint torques. Similar kinematic invariance has been demonstrated repeatedly across species (Helms-Tillery et al. 1995; Sumbre et al. 2006). Therefore, we were surprised that the volume of the synergy-limited FFS, which reflects the combined biomechanical and neural limitations on force production for the task, did not vary significantly across postural configurations. These results suggest that synergy force vectors may be specifically selected among all possible force vectors to minimize posture-dependent changes in synergy-limited FFS volume. This is but one of many possible "neural optimality" criteria that may work in concert with kinematic criteria; the contributions of both types of mechanisms should be considered to fully understand the neuromechanical coordination of the task.

CHAPTER 4
THE FORCE CONSTRAINT STRATEGY REFLECTS OPTIMAL COORDINATION ACROSS LIMBS

INTRODUCTION

The goal of this study was to understand the neural and biomechanical mechanisms underlying the patterns of ground reaction forces during postural tasks in cats known as the force constraint strategy (Macpherson 1988a; b). When a postural perturbation is issued, either as a translation of the support surface in any of several directions in the horizontal plane, or as a rotation of the support surface in the pitch or roll axes, stereotyped, directionally-specific patterns of muscle activity known as the automatic postural response (APR) are elicited at about 60 ms after perturbation onset. Due to neuromechanical delays, changes appear in the ground reaction forces at each of the limbs approximately 60 ms later. During this active period, the ground reaction force at each hindlimb tends to be directed along a diagonal axis either towards or away from the center of mass (CoM), regardless of the perturbation direction.

Comparison of forces during the active and passive periods of the postural response suggests that the force constraint strategy may result from active control mechanisms within the nervous system. During the passive period 0-20 ms after perturbation onset, the musculoskeletal system is stabilized only by background postural tone. However, during this early period there is no evidence of the stereotypy observed during the active response, and the ground reaction forces in each limb are simply directed in the direction of the perturbation. Because of this difference, it was suggested by Macpherson (1988a) that the nervous system might address the inter-limb redundancy in partitioning an appropriate response force among the limbs by controlling the magnitude of the ground reaction force at each hindlimb without modulating its direction.

The stereotypical force directions in the force constraint strategy do not reflect limitations in the force production capability of the hindlimb, also supporting the role of active nervous system control. Previous neurophysiological studies suggested that the diagonal axis is a primary torque direction for single muscles within the hindlimb (Lawrence et al. 1993; Nichols et al. 1993). These studies suggested that the force

production capability of the hindlimb might be limited to diagonal forces, in which case the force constraint strategy would be attributable to purely biomechanical mechanisms. To test this, we calculated the manifold of forces that a detailed musculoskeletal model of the isolated hindlimb (Burkholder and Nichols 2004) could produce given the constraints on the activation of individual muscles (the feasible force set, or FFS; McKay et al., 2007). We demonstrated that while larger forces were feasible in the anterior-posterior directions, the hindlimb could generate forces significantly larger than those observed during postural control in any direction.

Altering the postural configuration of the animal can modify the force constraint strategy without drastic changes in muscle activity, suggesting that biomechanical factors other than the biomechanical constraints of the isolated hindlimb may play a role. When cats are required to perform the postural task in different postural configurations created by shortening the stance distance between the fore- and hind-feet, the reliance on diagonal forces in the hindlimbs is relaxed, and a wider range of force directions is observed (Macpherson 1994). The changes in ground reaction forces can be attributed primarily to biomechanical mechanisms, because the tuning curves of individual muscles with respect to perturbation direction scale, but do not appreciably shift, across postural configurations (Torres-Oviedo et al. 2006). Despite this, in our analyses of the hindlimb musculoskeletal model, we demonstrated that the hindlimb FFS does not vary appreciably across postural configurations (McKay and Ting 2008), suggesting that the biomechanical constraints on force production in the hindlimb were not a likely source for these changes. However, because we previously considered the hindlimb in isolation, we could not estimate the effects that interactions between redundant limbs would have on motor solutions.

A simplified control scheme based on functional muscle synergies that map muscle activation patterns to force vectors that rotate with the limb axis may explain the pattern of variation with postural configuration (Torres-Oviedo et al. 2006). Muscle synergies have been proposed as a general control strategy used by the nervous system to simplify control problems by coupling the activation of multiple muscles into groups (Bernstein 1967). Muscle synergies are defined as common patterns of activation across multiple muscles that may be organized in terms of biomechanical function, for example,

propulsion or body support in human locomotion (Neptune et al. 2009) or crank propulsion in human pedaling (Raasch and Zajac 1999). Previously, five muscle synergies were identified that were adequate to describe the activity of muscles throughout the hindlimb during the postural task (Torres-Oviedo et al. 2006). Each muscle synergy was correlated with a unique ground reaction force vector that rotated with the axis of the hindlimb in the sagittal plane as the postural configuration was varied. Because of this rotation, although four of the five muscle synergies produced diagonally-oriented force vectors in the longest postural configuration, in the shorter postural configurations, the force vectors were directed primarily downward, producing a wider range of force projections in the horizontal plane.

We previously verified that functional muscle synergy constraints were feasible and limited the force production capability of the hindlimb; however, because we considered only a single limb, we could not test the feasibility of controlling a muscle synergy organization in the context of multiple limbs. One limitation of the previous analysis was that the presumed causal relationship between the identified muscle synergies and the identified muscle synergy force vectors could not be verified within the biomechanical constraints of the musculoskeletal system. To address this critique, we demonstrated in the musculoskeletal model that simulated muscle synergies could produce force vectors that rotated in the sagittal plane as postural configuration was varied, in a manner very similar to that observed in experimental data (McKay and Ting 2008). In further analyses, we demonstrated that when the muscles in the model were constrained to activate in simulated muscle synergies, the volume of the hindlimb FFS was drastically diminished, and exhibited changes with postural configuration. This suggested that muscle synergy constraints could limit the set of forces that were feasible for the postural task to near the regimes observed in data, consistent with a role of muscle synergies as the primary determinant of the force constraint strategy. However, because we considered only the constraints on force production in a single limb, we could not determine whether the control of the experimentally-observed muscle synergies in multiple limbs would produce the postural forces observed in each limb for particular perturbation directions.

Simplified neuromechanical models suggest that functional muscle synergies may emerge from the optimal control of individual muscles. Other researchers have demonstrated that the optimal control of individual muscles can produce low-dimension muscle patterns similar to muscle synergies although no central constraints on muscle activation may exist in the nervous system (Kurtzer et al. 2006; Todorov 2004). Therefore, functional muscle synergies observed during postural control may simply serve as a convenient basis with which to describe muscle patterns generated by the optimal control of individual muscles during the postural task, rather than reflecting nervous system constraints on muscle activation. However, it was unclear from these studies whether or not this phenomenon was universal, due to the abstract (Todorov 2004) or highly biomechanically-constrained (Kurtzer et al. 2006) nature of the neuromechanical models used.

Simulations of the optimal control of individual muscles to regulate the center of mass (CoM) in an inverted pendulum model explain aspects of the postural response, but cannot predict force patterns. The CoM is a strong determinant of muscle activation patterns during postural control, as similar muscle patterns are recruited during translation and rotation perturbations of the support surface that cause similar CoM motion, although opposite changes may be elicited in individual joint angles (Ting and Macpherson 2004). In an inverted pendulum model of postural control, the optimal control of individual muscles to regulate the CoM reproduced the temporal patterning of muscles throughout the cat hindlimb both before and after peripheral neuropathy (Lockhart and Ting 2007). However, because the musculoskeletal system was abstracted to a pendulum, variables like ground reaction forces could not be predicted. Additionally, because only diagonal perturbations were considered, the model was unable to predict muscle tuning curves.

Here, we hypothesized that the forces observed in the force constraint strategy reflected the optimal motor solution for controlling the CoM given the constraints of the quadrupedal musculoskeletal system. In a quadrupedal model, we simulated the optimal feedforward control of individual muscles to generate net forces and moments at the CoM suitable for countering the disturbances induced by postural perturbations. We demonstrate that the optimal control of individual muscles reproduces the diagonal forces

associated with the force constraint strategy; across postural configurations, the changes in postural forces and stereotypical scaling of muscle tuning curves are also reproduced. When we simulated control of the center of pressure (CoP), un-physiological forces were predicted, demonstrating that the choice of the task variable is critical to accurately predicting postural force patterns. We also simulated the control of simulated muscle synergies derived from experimentally-observed synergy force vectors. Muscle synergy control predicted ground reaction force patterns that were very similar to those predicted by optimal muscle control and to experimental data, verifying that low-dimension control strategies are feasible to produce appropriate control of the CoM across postural configurations. Additionally, the force patterns predicted by muscle synergy control exhibited active unloading, in which the flexion responses of the limbs are produced by activation of flexor muscles rather than the deactivation of extensor muscles used in weight support. Active unloading was represented in the experimental data, but was not captured by the optimal muscle control solution. This suggests that aspects of the force constraint strategy may satisfy additional criteria besides those explicitly modeled by our optimal control formulation. We propose that using a common set of muscle synergies may allow a low dimension approximation of the optimal control of the musculoskeletal system, possibly enabling faster computation time, but at the expense of increased energetic cost compared to optimal muscle control.

METHODS

SUMMARY

To quantify possible differences in motor performance and energetic cost associated with controlling muscle synergies or individual muscles, we simulated balance tasks in a quadrupedal neuromechanical model of a cat. We created the quadrupedal model by extending an existing model of the cat hindlimb (Bunderson et al. 2010; McKay et al. 2007; McKay and Ting 2008). The hindlimb model was parameterized to match three healthy cats performing balance tasks in either a self-selected (*preferred*) postural configuration, or in any of three altered postural configurations created by manipulating the distance between the fore- and hind-feet (Torres-Oviedo et al. 2006).

Because a musculoskeletal model of the forelimb was unavailable, we modeled the forelimbs in two ways. In the *symmetrical* quadrupedal model, we assumed that the musculoskeletal capabilities of the forelimbs were identical to those of the hindlimbs. In the *asymmetrical* quadrupedal model, we assumed that the musculoskeletal capabilities of the forelimbs allowed only vertical forces, so that they could be used only as struts. We viewed these two models as corresponding to high (the symmetrical model) and low (the asymmetrical model) amounts of musculoskeletal redundancy during balance tasks.

In each simulation, either individual muscles or five muscle synergies in each limb were activated to generate net restoring forces and moments at the CoM, or net corrections in the CoP, that were appropriate to correct disturbances introduced by support surface translation perturbations. Muscle synergies were based on synergy force vectors previously observed in the preferred postural configurations of the same animals (McKay and Ting 2008).

Simulations were performed to minimize each of three cost functions: minimum control cost, in terms of either total squared muscle activation ($\sum e^2$) or total squared muscle synergy activation ($\sum c^2$), or minimum energetic cost, in terms of the total squared activation of each muscle weighted by its mass ($\sum (m \bullet e)^2$). We compared the patterns of horizontal-plane forces predicted by the simulations to each other and to experimental data, and quantified the performance of each simulation in terms of the amount of simulated muscle activation.

EXPERIMENTAL DATASET

We based all simulations on previously-collected data of three healthy cats (*Bi*, *Ru*, *Ni*). The cats were trained to stand unrestrained with weight evenly distributed on four force plates mounted on a moveable perturbation platform and to remain in place when the platform translated in any of 12 directions in the horizontal plane (Figure 4.1A). Perturbations were 15 cm/s velocity and 5 cm amplitude (Macpherson et al. 1987). The cats performed the task in either a control postural configuration (*preferred* configuration), or in up to three altered postural configurations created by manipulating the stance distance between the fore- and hind-feet. The following stance distances were examined in each of the animals: *Bi*: 30 cm, 27 cm (preferred), 20 cm, and 13 cm; *Ru*: 40 cm, 29 cm (preferred), 24 cm, and 18 cm; *Ni*: 29 cm (preferred), 24 cm, and 18 cm. A minimum of five trials of each perturbation direction in each stance distance were collected.

For each cat, EMG, kinematic, and ground reaction force data were collected during each trial. Chronic indwelling EMG from 16 left hindlimb muscles and 3D ground reaction forces at each paw were collected at 1,000 Hz. Details of the EMG processing and analyses for these animals were presented in an earlier work (Torres-Oviedo et al. 2006). Ground reaction forces were low-pass filtered at 100 Hz. Positions of kinematic markers located on the platform and the left sides of the body were collected at 100 Hz and used to estimate sagittal- and frontal-plane joint angles of the hindlimb. Locations of joint centers were estimated from marker positions by subtracting off joint radii, skin widths, and marker widths and subsequently used to compute joint angles.

CoM location was estimated based on ground reaction force data and kinematic data. For each animal in each postural configuration, baseline CoM location in the horizontal plane was estimated as the location of the CoP averaged during the background period of each trial (300-150 ms before perturbation onset) and then averaged across trials. CoM location in the horizontal plane at any time point was then estimated by calculating the net horizontal plane forces, dividing by the mass, and then integrating twice (Ting and Macpherson 2004). CoM height was estimated from the positions and masses of body segments during the background period of each trial and then averaged across trials.

The constraints for the simulated balance tasks were based on the net forces and moments at the CoM, as well as the net changes in the CoP, averaged across cats during the active period of the automatic postural response (APR, Macpherson, 1988a;b). After perturbation onset, the EMG activity associated with the APR occurs at a latency of 60 ms. Initial APR muscle activity results in changes in kinetic and kinematic variables after an additional neuromechanical delay of about 60 ms. We therefore defined the active period of the postural response for either ground reaction force, CoM, or CoP data as an 80 ms window beginning 120 ms after perturbation onset. Because we were interested in the changes in ground reaction forces, CoM kinetics, and CoP position associated with the active response, baseline levels calculated over a 150 ms window before perturbation onset were removed.

Simulations attempted to reconstruct the average ground reaction forces during each perturbation direction exhibited by each cat during the active period of the APR. As with the CoM kinetics and CoP position variables, average ground reaction forces were calculated over an 80 ms window beginning 120 ms after perturbation onset. Baseline levels calculated over a 150 ms window before perturbation onset were removed, and active ground reaction forces were then averaged for each perturbation direction of each cat in each postural configuration.

NEUROMECHANICAL MODELS

Hindlimb model

All simulations were based on an existing musculoskeletal model of the cat hindlimb. The hindlimb musuloskeletal model is three-dimensional, with seven rotational degrees of freedom – three at the hip joint, and two at each of the hip and ankle – and 31 muscles (Burkholder and Nichols 2004; McKay et al. 2007; McKay and Ting 2008). A fully dynamic version of the model is available for detailed forward simulations (Bunderson et al. 2008; Bunderson et al. 2010). However, because of the small changes in joint angles (≤6°) observed during the balance tasks discussed here, a static version was appropriate. In the formulation used here, the hindlimb model is a matrix equation relating 31-element muscle activation vectors $\bar{e}$ to the 3D ground reaction force

$f_{RH} = \left[f_X \; f_Y \; f_Z \right]^T$ at the limb endpoint. The equation for the right hindlimb model is therefore:

$$\bar{f}_{RH} = H_{RH}(\bar{q}) \cdot \bar{e}_{RH}$$

In this equation, $H_{RH}(\bar{q})$ designates the right hindlimb model and its dependence on the seven joint angles $\bar{q}$. To avoid supermaximal activation of muscles, we constrained the elements of $\bar{e}$ to the unit interval in all simulations. Detailed descriptions of the model $H_{RH}(\bar{q})$, and the procedure for identifying best-match values of $\bar{q}$ for each cat in each postural configuration have been presented previously (McKay and Ting 2008).

Symmetrical quadrupedal model

To create the symmetrical quadrupedal musculoskeletal model, we reflected the hindlimb model across the sagittal and frontal planes. After concatenating the additional limbs, the quadrupedal model relates 124-element muscle activation vectors $\bar{e}$ (31 elements per limb) to both the 3D ground reaction force $\bar{f}$ at the endpoint of each limb and to the 6D reaction force and moment $\left[\bar{f}_{CoM}{}^T \; \bar{m}_{CoM}{}^T \right]^T$ at the CoM. The net reaction force at the CoM $\bar{f}_{CoM}$ is the sum of the ground reaction forces at each limb endpoint. The net reaction moment at the CoM $\bar{m}_{CoM}$ is the sum of moments at the CoM due to each ground reaction force, calculated via the cross product with the vectors from the CoM to the endpoints of each limb.

We oriented the endpoints of the four limbs in the quadrupedal model symmetrically with respect to the CoM location (Figure 4.4). In all postural configurations, the stance width between the left and right limbs was assumed to be 8 cm and the stance distance between the fore- and hind-limbs was assumed to be the nominal stance distance reported above. Preliminary examinations revealed that more detailed kinematic estimates of endpoint position did not appreciably change the results of the simulations. The height of the CoM above the plane of the feet was estimated from kinematic data and morphological parameters separately for each cat in each postural configuration. Across postural configurations, mean CoM heights for each animal were as follows (mean ± SD): *Bi*: 12.6 ± 0.4 cm; *Ru*: 15.2 ± 0.4 cm; *Ni*: 12.7 ± 0.8 cm.

Asymmetrical quadrupedal model with strut forelimbs

To create the asymmetrical quadrupedal musculoskeletal model, we constrained the symmetrical model so that the forelimbs could exert only vertical forces. This was accomplished by setting the $\bar{f}_X$ and $\bar{f}_Z$ rows of the musculoskeletal models for the forelimbs to zero; otherwise, the symmetrical and asymmetrical quadrupedal models are identical. Particularly in shorter postural configurations, the forelimbs have been described as "struts," exerting primarily vertical, rather than shear, forces (Macpherson 1994). This modification ensured that the lateral components of postural forces in the simulations were generated by the hindlimbs alone, similar to the anterior-posterior asymmetries observed in experimental data.

Muscle synergies

We simulated muscle synergies as patterns of coactivation across multiple muscles in each limb. Muscle synergies were assumed to be identical across limbs. Mathematically, this relationship is $\bar{e}_{RH} = W \cdot \bar{c}_{RH}$ for the right hindlimb, where each column of W comprises an individual muscle synergy, and $\bar{c}_{RH}$ is a vector of muscle synergy activations (Torres-Oviedo et al. 2006). In all simulations, we constrained the elements of W and $\bar{c}$ to be nonnegative. The equation that relates the muscle synergy activation in the right hindlimb to the 3D ground reaction force at the endpoint is:

$$\bar{f}_{RH} = H_{RH}(\bar{q}) \cdot W \cdot \bar{c}_{RH}$$

All muscle synergies used here were based on 5 muscle synergy force vectors extracted from ground reaction force data from the preferred postural configuration of each cat during the APR (Torres-Oviedo et al. 2006). Using these synergy force vectors, we subsequently identified the muscle synergies in the model as the patterns of simulated muscle activation that generated each synergy force vector with the lowest total squared muscle activation (McKay and Ting 2008).

SIMULATED BALANCE TASKS

In each simulation, either individual muscles or five muscle synergies in each limb were activated to generate net restoring forces and moments at the CoM (the CoM task), or net corrections in the CoP (the CoP task) appropriate to counter the effects of postural perturbations.

In the CoM task, net forces were directed in the direction of the perturbation in the horizontal plane, and 2.5 N in magnitude, and directed in the direction of the perturbation in the horizontal plane, and net moments were directed perpendicular to the direction of the perturbation and 0.75 N-m in magnitude (Figure 4.3B). For example, during anterior perturbations, a 2.5 N directly anterior CoM force, and an 0.75 N-m CoM moment clockwise about the leftwards axis were required. For all cats, the net vertical CoM force was constrained to 30 N to resist gravity, and the vertical ground reaction force at each foot was constrained to be nonnegative, so that no limbs could "pull." No constraints were placed on the vertical ("yaw") moment at the CoM. In simulations of muscle synergies, muscle synergy activations were further constrained to be nonnegative with respect to a background level identified by constraining the net vertical CoM force to 30 N while constraining the net horizontal forces to zero.

In the CoP task, corrections in CoP location were 3.3 cm in magnitude and directed opposite the direction of the perturbation (Figure 4.3C). CoP was defined as the spatial average of the foot locations, weighted by the vertical ground reaction force at each foot. CoP has been hypothesized to be an important regulated variable in the nervous system because the deviation between the CoP and the vertical projection of the CoM into the horizontal plane (the CoG) determines the instantaneous stability of the musculoskeletal system in some contexts (Winter 1995). One criticism of the CoP as a regulated variable is that CoP location is not affected by – and therefore is not a good candidate variable to explain – horizontal plane forces. Corrections in CoP location corresponded to an equivalent net moment at the CoG of 1.0 N-m magnitude, directed perpendicular to the direction of the perturbation. Constraints on vertical forces and numerical procedures were otherwise identical to the CoM task.

Cost functions

Simulations were performed to minimize each of three criteria, or cost functions. In optimal muscle control, simulations were performed to minimize either the control cost, the total squared muscle activation ($\sum e^2$), or an estimate of the energetic cost, the total squared activation of each muscle weighted by its mass ($\sum (m \bullet e)^2$). In muscle synergy control, both of these cost functions were minimized in the presence of muscle synergy constraints, as well as with the addition of muscle synergy control cost, total

squared muscle synergy activation ($\sum c^2$). All simulations were formulated as constrained quadratic programming problems and solved with *quadprog.m* in Matlab (The Mathworks, Natick, MA, USA).

We developed the mass-weighted muscle activation cost function ($\sum(m \bullet e)^2$) to obtain a more accurate proxy for minimizing the energy usage in the muscles than squared muscle activation. Minimizing squared muscle activation or squared muscle synergy activation minimize control cost, which is often assumed in control theory as a proxy for the amount of energy used in a control task, particularly in the context of the neural control of movement (Fagg et al. 2002; Todorov and Jordan 2002). In the simple muscle model used here, minimizing squared muscle activation is numerically identical to minimizing squared muscle stress, which has also been presented as a proxy for maximizing endurance, or equivalently minimizing energy (Crowninshield and Brand 1981). However, neither minimizing control cost nor minimizing muscle stress is necessarily directly related to minimizing the metabolic energy expended in the muscles (O'Sullivan et al. 2009). ATP hydrolysis activity, and therefore the rate of energy usage (Joules/second) in single human muscle fibers is related to fiber stress (N/cm^2) (Szentesi et al. 2001). The total rate of energy usage in any given muscle is therefore proportional to the muscle stress multiplied by the total volume of muscle fibers, assumed to be the muscle volume. Because the density of mammalian muscle is approximately constant (Yamaguchi 2001), the volume of each muscle is proportional to its mass, so that by weighting the stress of each muscle by its mass, the total squared energy usage $(Joules/second)^2$ can be minimized to within a constant.

COMPARISONS BETWEEN MODELS

To determine which simulated central coordination process best approximated the central coordination process used by cats during postural perturbations, we quantified the fits of ground reaction forces predicted in each simulated balance task to experimental data. For each postural configuration in each cat, we calculated the coefficient of determination (R^2) and uncentered squared correlation coefficient (uncentered-R^2) between the modeled forces and average experimental forces across the 12 perturbation directions for which experimental data was available. We primarily considered fits to hindlimb forces in the horizontal (X-Z) plane, as the vertical forces were largely uniform

across models due to the constraints of the task; however, fits to 3D forces were considered as necessary. Values for each fit statistic were subjected to two-way ANOVA (factors: model type × animal) with Tukey-Kramer post-hoc tests. Fit statistics for the symmetrical and asymmetrical models were treated separately; in the symmetrical model, only data from the preferred postural configuration of each cat was considered. All results were evaluated at a significance level of $\alpha = 0.05$. All averaged data are presented as means ± SD.

We also compared the total muscle activation and energetic cost associated with each central coordination process in the asymmetrical model. We calculated the RMS simulated hindlimb muscle activation predicted by each central coordination process for each postural configuration in each cat. These values were then subjected to two-way ANOVA (factors: model type × animal) with Tukey-Kramer post-hoc tests. Subsequent statistical analyses are detailed as necessary in the presentation of Results.

FORCE PRODUCTION IN THE ISOLATED HINDLIMB

Because initial simulations of optimal muscle control in the symmetrical four-hindlimb model predicted large forces along the anterior-posterior axis in the hindlimbs, we examined how anisotropies in the force production capability of the isolated hindlimb might inform the distribution of the forces among the limbs. We considered the isolated left hindlimb parameterized to cat *Bi* in the preferred postural configuration. We identified the unique pattern of muscle activation or muscle synergy activation that produced a 1 N force in directions distributed throughout the horizontal plane in 5° increments while minimizing each of the cost functions described above, using quadratic programming as elsewhere. Subsequently we examined the dependence of the each cost function on the direction of hindlimb force.

FORCE CONTRIBUTIONS OF SUBSETS OF MUSCLE SYNERGIES

To better illustrate the biomechanical functions of each muscle synergy in the model, we also examined the force contributions of each muscle synergy, as well as subsets of muscle synergies, to the CoM control postural task. We calculated the fits to experimental ground reaction force data provided by each muscle synergy and compared them to each other as well as to the fit provided by optimal muscle control.

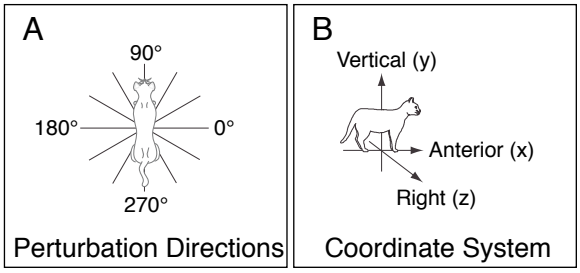

Figure 4.1. Coordinate frames for support-surface translation perturbations. A: Perturbations were delivered in 12 evenly-spaced directions in the horizontal (x-z) plane. B: Coordinate system used in the simulations.

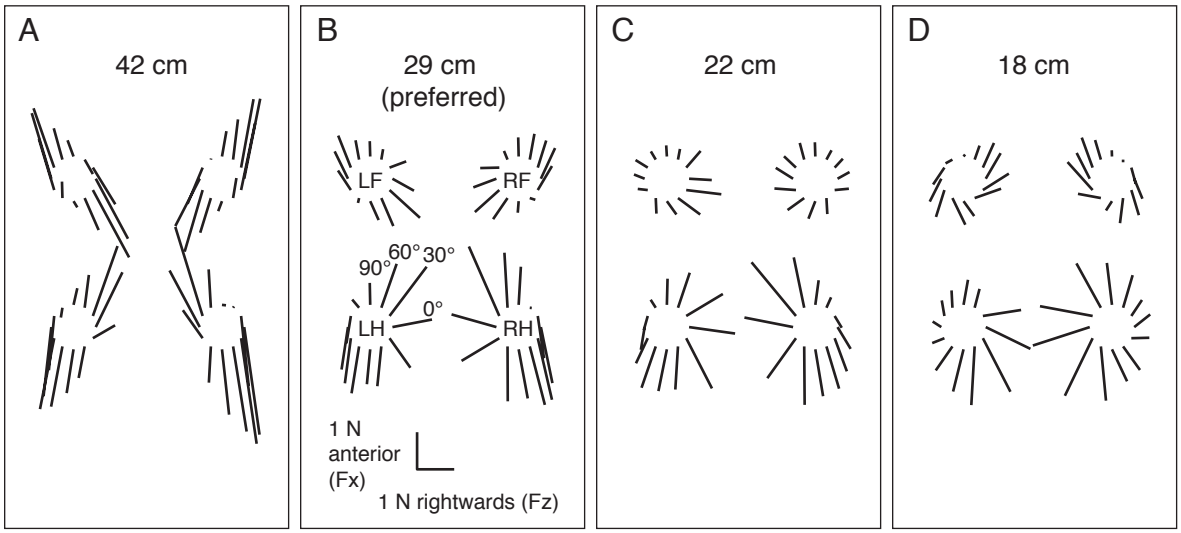

Figure 4.2. Changes in active force responses with postural configuration. Data shown are taken from cat *Ru*. A-D: in each panel, force vectors are drawn for each limb (clockwise from top left: LF, left forelimb; RF, right forelimb; RH, right hindlimb; LH, left hindlimb) with their origins offset in the direction of platform motion towards 0°, 30°, 60°, etc, as annotated in the self-selected postural configuration, B.

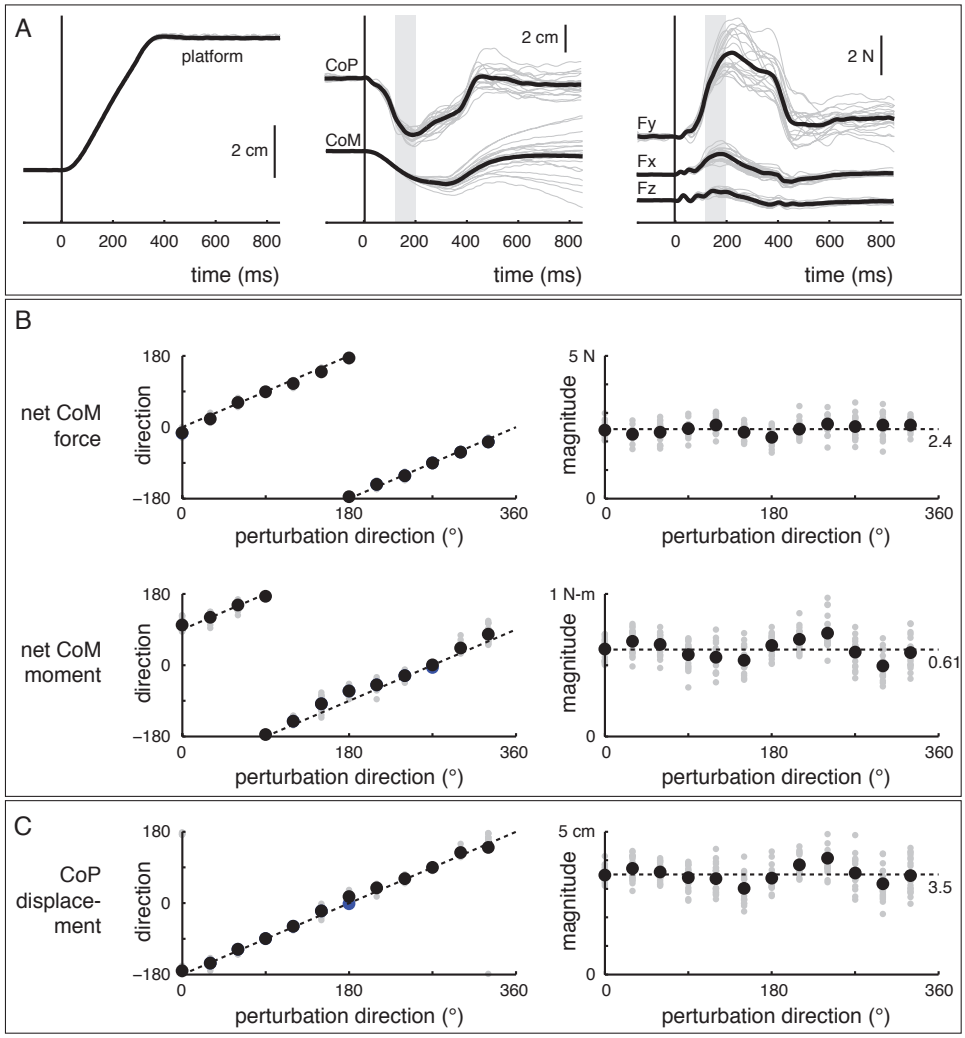

Figure 4.3. Approximation of net CoM kinetics and CoP excursion by the simulated tasks. A: left to right; time traces of platform position, CoM location with respect to the platform, and left-hindlimb ground reaction forces (GRF) for 20 perturbations towards 60° for cat *Bi* in the preferred postural configuration (27 cm). Gray bars: the active period of the force response, 120-200 ms after perturbation onset. B: Average net horizontal-plane forces and moments at the CoM for cat *Bi*, preferred stance distance, presented in polar coordinates. Upper: net CoM force direction and magnitude. Lower: net CoM moment direction and magnitude. Light gray dots represent experimental data; black dots represent average values. Dashed lines on direction plots designate the force and moment horizontal-plane directions used as task constraints in the model. Dashed lines on magnitude plots designate mean values. C: Average direction and magnitude of CoP displacements for *Bi*, preferred stance distance. Legend as in B.

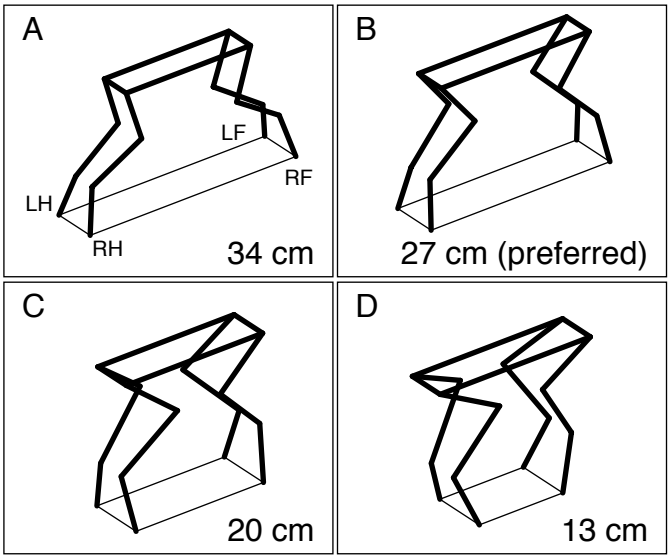

Figure 4.4. Simulated kinematics of symmetrical quadrupedal musculoskeletal models. Data shown are for cat *Bi*. A-D: simulated kinematics for stance distances 34, 27, 20, and 13 cm. LH: left hindlimb; LF: left forelimb; RF: right forelimb; RH: right hindlimb.

RESULTS

EXPERIMENTAL DATA

Translation perturbations to standing balance induced a typical disturbance in the CoM location. In all perturbation directions, the CoM initially lagged behind the platform position, introducing errors that were not fully corrected until after the termination of the perturbation (Figure 4.3, middle panel) (Lockhart and Ting 2007; Welch and Ting 2009). After the corrective muscular response, weight was redistributed and the CoM was transferred to a different location.

Ground reaction forces displayed typical stereotypical patterns of variation associated with the force constraint strategy (Macpherson 1988a; b) (Figure 4.2). In the long and preferred postural configurations (Figure 4.2A,B), limb forces were approximately symmetrical among the four limbs and directed towards the CoM.

In the preferred postural configuration, the hindlimbs of all cats exhibited stereotypical ground reaction force directions corresponding to perturbation directions where they were loaded (0°-90° for the left hindlimb) or unloaded (150°-300° for the left hindlimb). Considering the left hindlimb of cat *Ru* in the preferred postural configuration (Figure 4.2B), similar CoM-directed forces ground reaction forces were observed during all perturbation directions where the hindlimb was loaded (0°-90°). During anterior-rightwards perturbations towards 60°, the left hindlimb was nearly maximally loaded (sustaining a loading force of 10.6 N, vs. 6.9 N during quiet standing) and exhibited a shear ground reaction force (1.3 N) towards 70.9°, approximately along the perturbation direction and towards the CoM. In contrast, in posterior-leftwards perturbations where the hindlimb was unloaded, posterior-directed shear forces were observed. During perturbations towards 210°, the hindlimb almost completely unloaded, sustaining a loading force of only 1.8 N, and exhibited a shear ground reaction force that was directed almost entirely posterior (262.3°).

The forelimbs also exhibited two stereotypical ground reaction force directions corresponding to perturbation directions where they were loaded (270°-360° for the left forelimb) or unloaded (90°-180° for the left forelimb) in the preferred postural configuration. In particular, during posterior-rightwards perturbations towards 300°, the

left forelimb of cat *Ru* (Figure 4.2B) was nearly maximally loaded (sustaining a loading force of 11.8 N vs. 7.8 N during quiet standing) and exhibited a shear ground reaction force (0.8 N) approximately in the direction of the perturbation and the CoM (292.9°). In contrast, during anterior-leftwards perturbations towards 150°, the left forelimb almost entirely unloaded (loading force of 2.3 N) and exhibited a shear ground reaction force (0.9 N) that was directed approximately 40° away from the perturbation direction, approximately anterior (111.6°).

In postural configurations shorter than the preferred configuration of the animal, a wider range of force directions was observed in the both the forelimbs and the hindlimbs, and asymmetries appeared between the forces exhibited by the forelimbs and the hindlimbs (Figure 4.2C,D). Considering the same perturbation directions as above in the short postural configuration of cat *Ru* (Figure 4.2C), the left hindlimb exhibited responses similar to those observed in the preferred postural configuration. However, the force directions observed in the forelimb approached a linear dependence on the perturbation direction; between the preferred and short postural configurations, the average angle deviation between the forelimb force direction and the perturbation direction decreased from 27.5 ± 24.8° to 18.6 ± 13.0°.

MUSCLE SYNERGY CONTROL OF THE COM PREDICTS POSTURAL FORCES IN THE SYMMETRICAL MODEL

In the symmetrical musculoskeletal model, muscle synergy control of the CoM predicted significantly higher R^2 fits to experimental data than all other simulated control types in the preferred postural configuration ($p<0.05$, $F(4,22) = 3.87$, post-hoc tests). Simulated ground reaction forces for representative animal *Ru* are presented in Figure 4.5. All simulated ground reaction forces were symmetrical because of the symmetry of the musculoskeletal model, Ground reaction force magnitudes were significantly larger ($p<<1e-6$, $F(3,138)=44.7$) in optimal muscle control than in muscle synergy control in both the CoM and the CoP tasks (post-hoc tests). Across animals and tasks, the average horizontal-plane force magnitude was 2.8 ± 1.4 N in optimal muscle control and 0.8 ± 0.4 in muscle synergy control. Forces predicted by optimal muscle control tended to be directed near the anterior-posterior axis for all perturbation directions in both the CoM

and CoP tasks. Grand mean fit data for the symmetrical musculoskeletal model are summarized in Table 5.1.

Anisotropic biomechanical capabilities predict large anterior-posterior forces in optimal muscle control

Because we were interested in how the properties of the musculoskeletal system might determine the particular force directions selected during the simulated tasks, we performed additional analyses in the isolated left hindlimb of cat *Bi* in the preferred postural configuration. We quantified the minimum cost – in $\sum e^2$ or in $\sum c^2$ – associated with generating a 1 N horizontal force directed along the unit circle in the horizontal plane in 5° increments (Figure 4.6).

Analysis of the cost curves demonstrated that the forces near the anterior-posterior axis observed in optimal muscle control in the symmetrical model reflected force directions that were highly favorable given the force production capability of the hindlimb model. The optimal muscle control cost curve was characterized by two minima, near 90° and 270°, because of the prevalence of individual muscles with horizontal-plane force projections near those directions (cf. Bunderson et al., 2010, McKay et al., 2007). In contrast, the cost curve for muscle synergy control was relatively flat from approximately 210°-60°, corresponding to the region between the force directions of muscle synergy 1 and muscle synergy 2, the primary loading and unloading muscle synergies. This suggested that combinations of muscle synergies 1 and 2 could be obtained to generate a 1 N horizontal-plane force in a wide range of directions with a comparable relative cost, leading to the wider range of force directions predicted by muscle synergy control than by optimal muscle control. Peak values of cost curves were located near 180° in both optimal muscle control and optimal synergy control, corresponding to pure adduction forces.

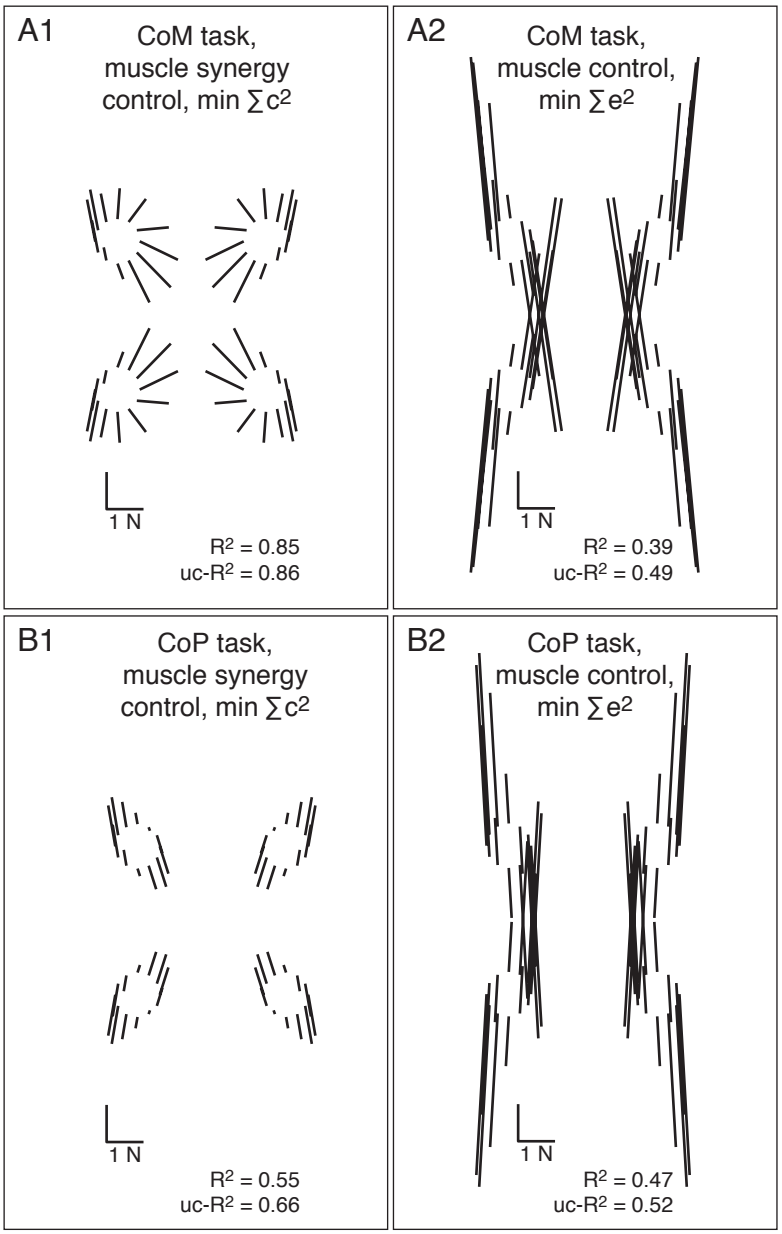

Figure 4.5. Simulated ground reaction forces predicted by the optimal control of muscle synergies and individual muscles in the symmetrical quadrupedal model. All data correspond to the 29 cm (preferred) postural configuration of *Ru* (Figure 4.2B); *Bi* and *Ni* are similar. A1-2: CoM task. A1: muscle synergy control, $\sum c^2$. A2: muscle control, $\sum e^2$. B1-2: CoP task. B1: muscle synergy control, $\sum c^2$. B2: muscle control, $\sum e^2$.

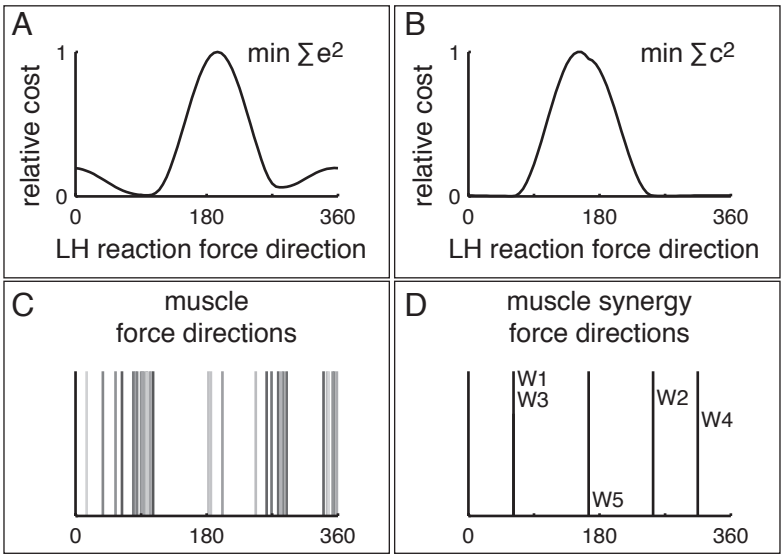

Figure 4.6. Normalized costs of force production with individual muscles or muscle synergies in the isolated hindlimb. Data shown were correspond to the left hindlimb of cat *Bi* in the preferred postural configuration; other cats are similar. A-B: normalized minimum cost of a 1 N ground reaction force produced in any direction in the horizontal plane assuming control of individual muscles (A) or muscle synergies (B). Note that flat regions correspond to low costs relative to the maximum, not to cost values of zero. C: distribution of horizontal-plane directions of single muscle forces in the left hindlimb. Each vertical line depicts the force direction of an individual muscle; darker lines correspond to muscles with higher maximal force (F_{MAX}) values. D: distribution of horizontal-plane directions of muscle synergy forces in the left hindlimb. Relative heights of labels W1-W5 correspond to the relative force magnitudes of each muscle synergy.

Table 4.1. Grand mean symmetrical model fits to preferred postural configuration ground reaction force data. Values are presented as mean (SD).

Metric	Control	Cost Function	Task	
			CoM	CoP
X-Z R^2	Muscle	$\sum e^2$	0.46 (0.07)	0.47 (0.03)
		$\sum (m \bullet e)^2$	0.41 (0.06)	0.47 (0.04)
	Muscle synergy	$\sum e^2$	0.58 (0.06)	0.36 (0.31)
		$\sum (m \bullet e)^2$	0.58 (0.12)	0.37 (0.32)
		$\sum c^2$	0.82 (0.05)	0.59 (0.06)
X-Z uc-R^2	Muscle	$\sum e^2$	0.45 (0.06)	0.47 (0.07)
		$\sum (m \bullet e)^2$	0.47 (0.03)	0.47 (0.07)
	Muscle synergy	$\sum e^2$	0.54 (0.12)	0.41 (0.16)
		$\sum (m \bullet e)^2$	0.59 (0.05)	0.44 (0.15)
		$\sum c^2$	0.87 (0.04)	0.74 (0.07)
XYZ R^2	Muscle	$\sum e^2$	0.82 (0.06)	0.76 (0.05)
		$\sum (m \bullet e)^2$	0.73 (0.05)	0.72 (0.05)
	Muscle synergy	$\sum e^2$	0.93 (0.02)	0.89 (0.04)
		$\sum (m \bullet e)^2$	0.93 (0.02)	0.91 (0.03)
		$\sum c^2$	0.96 (0.01)	0.95 (0.02)

OPTIMAL MUSCLE CONTROL AND MUSCLE SYNERGY CONTROL OF THE COM PREDICT LOADING FORCES IN THE ASYMMETRICAL MODEL

Simulated ground reaction forces predicted by optimal muscle control and muscle synergy control recreated the stereotypical loading forces observed in the force constraint strategy in the CoM task; however, optimal muscle control failed to predict active unloading forces observed in experimental data. Simulated ground reaction forces for cat *Ni* are presented in Figure 4.7. Overall, optimal muscle control and muscle synergy control predicted similar overall fits to data (Table 5.2), with the exception that in the shorter postures, optimal muscle control predicted forces during limb unloading (in the left hindlimb, corresponding to perturbation directions between 180°-270°) that were significantly larger in magnitude (1.9 ± 1.0 vs. 1.0 ± 0.4; $p<2.4e-6$, $F(2,69)=15.7$) than those predicted by muscle synergy control.

Muscle tuning predicted by optimal muscle control and muscle synergy control

Similar overall muscle tuning was predicted by both optimal muscle control and muscle synergy control. Representative examples are shown in Figure 4.8. Muscle activation patterns in the left hindlimb predicted by optimal muscle control exhibited generally unimodal tuning, with maxima near medial-lateral perturbation directions: 0° or 180°. Muscle tuning curves generally smoothly scaled across postural configurations, rather than shifting tuning direction, with the exception of three muscles in *Ru*: *lateral gastrocnemius*, *plantaris*, and *soleus*. In all cats, several strong muscles, including *vastus lateralis* (F_{MAX} = 147 N), *adductor femoris* (102 N), and *flexor hallicus longus* (105 N) were tuned approximately symmetrically with respect to their background level in optimal muscle control. These muscles tended to be maximally activated in rightwards perturbations where the left hindlimb was loaded and maximally inactivated in leftwards perturbations where the left hindlimb was unloaded.

Muscle activation patterns in the left hindlimb predicted by muscle synergy control exhibited bimodal tuning in several cases that likely resulted from limitations in the specific method used to parameterize the simulated muscle synergies. Although in some muscles bimodal tuning may be expected from experimental data (e.g., *sartorius*, see Torres-Oviedo et al., 2006, Figure 6), in general, this result is unphysiological. As an

example, the simulated activity of *tibialis anterior* in the model parameterized to cat *Ru* exhibited two tuning curve peaks of comparable magnitude at 30° and 210° in all postural configurations. Because muscle synergy tuning curves were uniformly unimodal – with the exception of muscle synergy 2 in *Ni*, which exhibited a second tuning peak in the preferred postural configuration only, bimodal muscle tuning must result from the partial participation of individual muscles in multiple simulated muscle synergies with different functions. We therefore attribute this unphysiological result to limitations in the specific method used to identify the simulated muscle synergies used here. Closer examination of the tuning curves revealed that the peak near 180° resulted from the action of muscle synergy 2, consistent with the unloading function expected of the ankle flexor *tibialis anterior*, the 30° peak resulted from a small contribution from muscle synergy 3. Each simulated muscle synergy was used here was individually optimal in that each corresponded to the minimum muscle activation required to generate the experimentally-observed synergy force vector associated with it. However, practical limitations prevented the identification of more globally-optimal sets of muscle synergies, which would presumably eliminate the problem of muscles participating in multiple muscle synergies with conflicting functions. More sophisticated methods for synergy parameterization are an active area of research (Kargo et al. 2010; Neptune et al. 2009).

MUSCLE SYNERGIES 1-3 APPROXIMATE THE OPTIMAL MUSCLE CONTROL

Muscle synergies 1 and 3 are responsible for active loading

Across animals, we found that the force contributions of muscle synergies 1-3 were sufficient to recreate postural force data equivalently to optimal muscle control. The individual force contributions of muscle synergies 1 and 3, muscle synergy 2, and muscle synergies 4 and 5 during the CoM task for *Ru* are presented in Figure 4.9. The grand mean fits to experimental data predicted by combination of muscle synergies are presented in Figure 4.10.

The combined force contributions of muscle synergies 1 and 3 were generally sufficient to recreate the active loading response observed during the postural response throughout the workspace. The combined force contributions of muscle synergies 1 and 3 in cat *Ru* are presented in Figure 4.9A. Muscle synergies 1 and 3 both produced anterior

ground reaction forces appropriate for the loading response of the limb in the preferred postural configuration. However, the force vectors associated with each of muscle synergies 1 and 3 generalized across the workspace in different ways. In all cats, the anterior component of the force vector corresponding to muscle synergy 1 rotated from the anterior to the posterior half plane between the preferred and short postural configurations. Sagittal-plane muscle synergy force directions are summarized in Table 5.3. Although muscle synergy 1 was appropriate to produce loading vertical forces throughout the workspace, its posterior force vector projection made it inappropriate for the necessary anterior component of the loading force in the short and shortest postural configurations. Because of this rotation, the anterior ground reaction force component of the loading response was primarily supplied by muscle synergy 3 in the shorter postural configurations.

Synergy 2 is responsible for active unloading

The force contributions of muscle synergy 2 were responsible for nearly the entirety of the active unloading response. The force contributions of muscle synergy 2 in cat Ru are presented in Figure 4.9B. Because optimal muscle control did not perform active unloading, across animals, the combined force contributions of muscle synergies 1 and 3 without the contribution of muscle synergy 2 were sufficient to fit experimental data comparably to optimal muscle control ($p>0.05$ ANOVA, post-hoc tests).

Synergies 4-5 exhibit small force magnitudes

Muscle synergies 4 and 5 together were characterized by small force magnitudes and appeared to function primarily to complement the primary action of muscle synergies 1-3. The combined force contributions of muscle synergies 4 and 5 in cat Ru are presented in Figure 4.9C.

Because of their smaller force magnitudes, it is also likely that muscle synergies 4 and 5 may represent higher-order aspects of the postural task that are not captured in the static representation here; for example, limb stabilization during force production (Bunderson et al. 2008; van Antwerp et al. 2007) or cancelling interaction torques associated with the primary loading leg.

Muscle synergy control predicts higher energetic costs than optimal muscle control

Muscle synergy control in the CoM task predicted significantly higher RMS muscle activation than optimal muscle control ($p<0.001$, $F(2,25)=11.7$, post hoc tests). This contrast was preserved across animals ($p<0.16$, $F(2,25)=1.98$) and postural configurations ($p<0.19$, $F(3,25)=1.70$). Across animals and postural configurations, grand mean RMS muscle activation during the CoM task was 0.08 ± 0.03 for muscle synergy control, $\sum c^2$, 0.06 ± 0.03 for muscle synergy control, $\sum e^2$, and 0.04 ± 0.002 for optimal muscle control, $\sum e^2$. The grand mean RMS muscle activation for the three control types is presented in Figure 4.11.

Minimizing $\sum(m \bullet e)^2$ *predicts similar forces and muscle tuning to minimizing* $\sum e^2$ *but with unphysiological recruitment of small muscles*

Minimizing $\sum e^2$ and minimizing $\sum(m \bullet e)^2$ produced approximately similar force patterns, particularly if only the preferred postural configuration was considered (Figure 4.12B,C). The two cost functions also predicted similar muscle tuning that differed primarily in magnitude, rather than direction. For example, across cats, the average activation of the relatively heavy muscle *adductor femoris* (29.2 g) was significantly lower in $\sum(m \bullet e)^2$ simulations than in $\sum e^2$ simulations, (0.01 ± 0.002 vs. 0.08 ± 0.003; $p<0.01$, t-test), although the peak tuning direction (30°) was unchanged. Conversely, the average activation of the relatively light muscle *flexor hallicus longus* (2.0 g) was significantly higher in $\sum(m \bullet e)^2$ simulations than in $\sum e^2$ simulations (0.25 ± 0.07 vs. 0.04 ± 0.007; $p<0.05$, t-test), although its peak tuning direction in the preferred postural configuration (0°) was unchanged.

Overall, minimizing $\sum(m \bullet e)^2$ predicted unphysiological high levels of activation in the smallest muscles in the model, with peak values near maximal activation (1.0), suggesting that this cost function is not a good representation of the central coordination process used during the postural task.. Muscle activation values in the $\sum e^2$ and $\sum(m \bullet e)^2$ simulations as functions of muscle mass and maximal muscle force are summarized in Figure 4.13. Despite the marked differences in activation levels of individual muscles predicted by the two cost functions, we attribute the overall similarity of the force patterns predicted by each to the fact that in the musculoskeletal model used here, the maximum force of each muscle is generally proportional to its mass (Figure 4.14).

Therefore, although the $\sum(m \bullet e)^2$ cost function preferentially recruits smaller muscles, these same muscles tend to be weaker, so that the larger muscles in the model still dominated the overall behavior. We expect that many other musculoskeletal models would exhibit a similar property. Additionally, many candidate cost functions related to $\sum e^2$ would likely predict similar solutions, which largely reflect the anisotropic properties of the musculoskeletal system, rather than the details of the specific cost function used (Crowninshield and Brand 1981; Herzog and Leonard 1991).

Optimal muscle control of CoP predicts anterior ground reaction forces during both loading and unloading

Ground reaction forces predicted by optimal muscle control of the CoP were directed anteriorly for all perturbation directions, resulting significantly degraded fits to data ($p<1e-6$, $F(1,40)=41.9$) in CoP control vs. CoM control in all animals ($p<0.70$, $F(2,40)=0.36$). Predictions were very similar across cats and across $\sum e^2$ and $\sum(m \bullet e)^2$ simulations. In each postural configuration of each cat, only two horizontal-plane force directions were observed; one of which corresponded to the background force vector, observed when the limb was loaded, and the other of which was offset by approximately 15°. This is expected because shear forces are unconstrained in the CoP task; therefore, the minimizations relied on the most biomechanically favorable muscles, the majority of which produced ground reaction forces near the anterior axis (Figure 4.6). In the preferred postural configuration of *Bi*, forces were directed towards 87.4° when the limb was loaded and 100.2° when the limb was unloaded in $\sum e^2$ simulations, and towards 87.4° (loaded) and 79.1° (unloaded) in $\sum(m \bullet e)^2$ simulations; other cats and postural configurations were similar. Across animals, postural configurations, and cost functions, mean R^2 values were 0.08 ± 0.15 for CoP control vs. 0.56 ± 0.31 for CoM control.

Uncompensated direction reversal of muscle synergy 1 predicts disrupted loading forces in optimal muscle synergy control of CoP

In the long and preferred postural configuration of each cat, ground reaction forces predicted by muscle synergy control of the CoP exhibited the bimodal distribution of force directions in loading and unloading typical of the force constraint strategy. Because they were not specified as a task constraint, hindlimb horizontal force magnitudes were significantly lower in CoP control than in CoM control ($p<<1e-6$, t-

test). The grand mean hindlimb horizontal force magnitudes were 1.01 ± 0.77 N in CoP control vs. 1.80 ± 1.02 N in CoM control. However, in general, the distribution of force directions was very similar to observed data, resulting in relatively high R^2 values (0.66 ± 0.11 in CoP control vs. 0.85 ± 0.05 in CoM control).

In the shorter postural configurations, muscle synergy CoP control predicted loading forces that were directed either laterally (cat *Bi*) or posterior (*Ni* and *Ru*), leading to significantly degraded overall fits to data ($p<<1e-6$, $F(1,17)=36.65$) that depended strongly on postural configuration ($p<0.0001$, $F(1,17)=24.14$) but not on animal ($p<0.80$, $F(2,17)=0.23$) (see Table 1.2). Comparison of the muscle synergy tuning curves from CoP control with those from CoM control revealed that these differences could be attributed to significantly attenuated recruitment of muscle synergies 3-5 ($p<2.3e-5$, $F(4,10)=27.4$, post hoc tests), which are recruited in the CoM task to compensate for the reversal of the anterior force component of muscle synergy 1 between the preferred and short postural configurations. Therefore, the posterior loading forces observed in the CoP task primarily result from the sign reversal of muscle synergy 1, that remains uncompensated by the action of muscle synergy 3 because the net shear force is unconstrained. Across animals, the mean ratios of the peak activation of each muscle synergy in the CoP task to that in the CoM task were 1.04 ± 0.27, 0.56 ± 0.21, 0.03 ± 0.03, 0.02 ± 0.02 for muscle synergies 1-5, respectively.

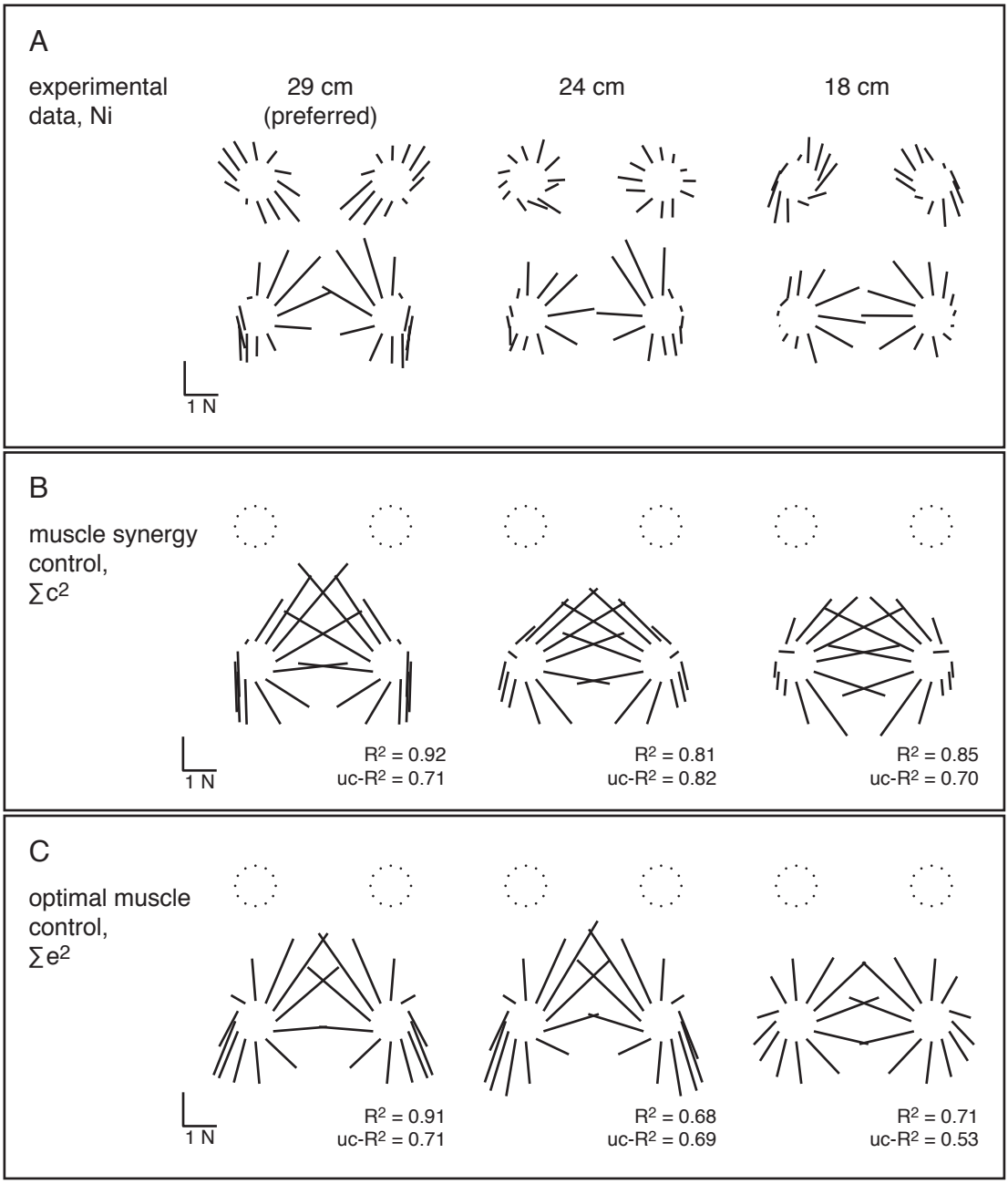

Figure 4.7. Simulated ground reaction forces predicted by the asymmetrical quadrupedal model parameterized to cat *Ni*. A: average forces taken from experimental data. B: simulated ground reaction forces predicted by muscle synergy control, minimizing $\sum c^2$. C: simulated ground reaction forces predicted by optimal muscle control, minimizing $\sum e^2$.

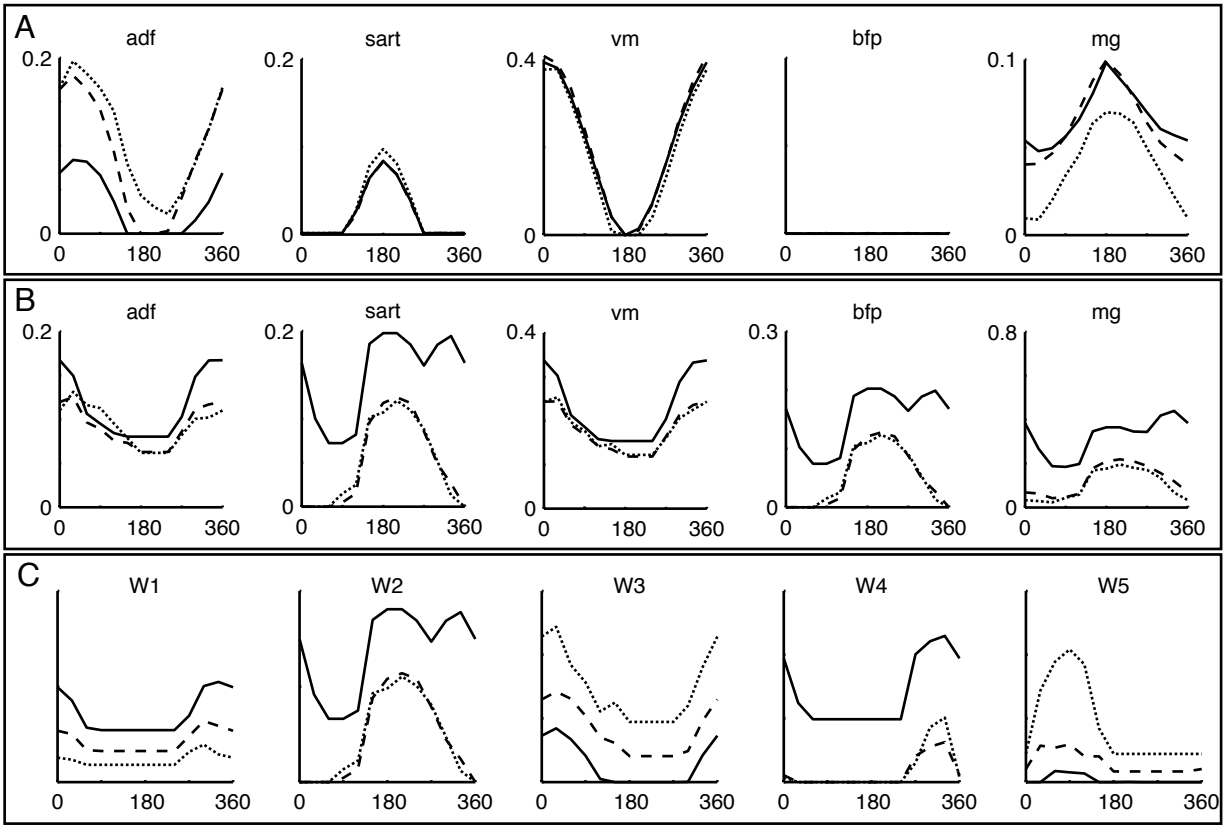

Figure 4.8. Simulated muscle and muscle synergy tuning curves predicted by optimal muscle control and muscle synergy control. Data are from the model parameterized to cat *Ni*. In all panels, solid, dashed, and dotted lines correspond to 29 cm (preferred), 24 cm, and 18 cm stance distance, respectively. A: muscle tuning curves predicted by optimal muscle control, $\sum e^2$ muscle designators are summarized in Table 4.7. B: muscle tuning curves predicted by muscle synergy control, $\sum c^2$. C: muscle synergy tuning curves predicted by muscle synergy control, $\sum c^2$. W1-W5 correspond to muscle synergies 1-5. Note different scales for MG in A and B.

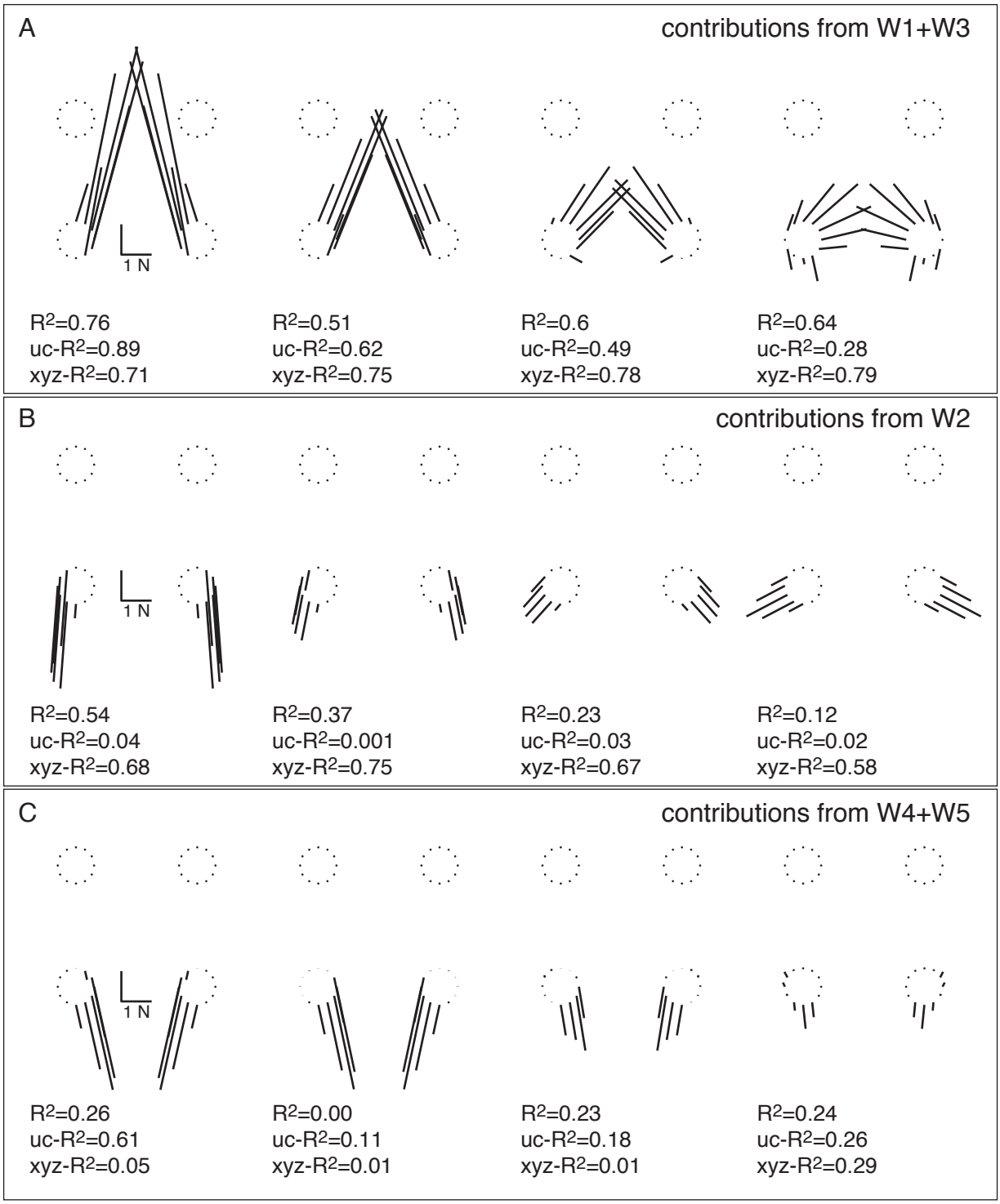

Figure 4.9. Decomposition of force contributions of muscle synergies in *Ru* (experimental data shown in Figure 4.2). In all panels, left to right corresponds to 42 cm, 29 cm (preferred), 22 cm, and 18 cm stance distance. A: contribution of muscle synergies 1 and 3. B: contribution of muscle synergy 2. C: contribution of muscle synergies 4 and 5.

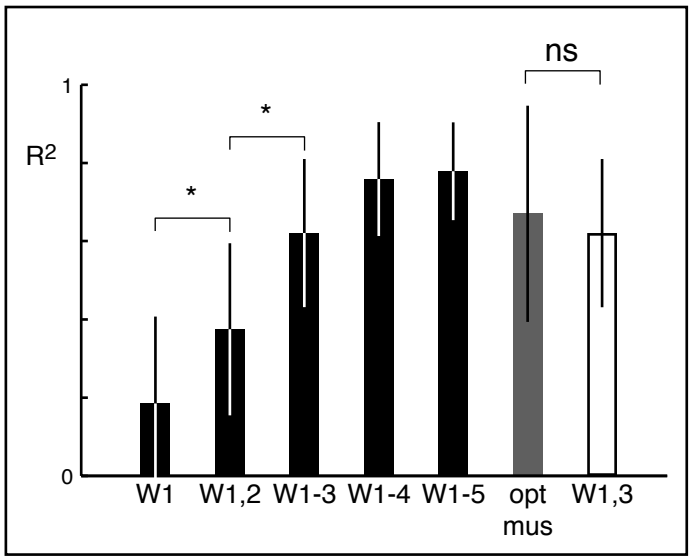

Figure 4.10. Approximation of optimal muscle control solution with muscle synergies. Black bars: R^2 values between modeled forces and data predicted by increasing numbers of synergies included in the approximation. W1: contribution of muscle synergy 1; W1,2: contribution of muscle synergies 1 and 2, etc. Gray bar: R^2 value between optimal muscle control forces and data. White bar: contribution of muscle synergies 1 and 3 only. *p<0.05, ANOVA, post-hoc tests. ns: p>0.05.

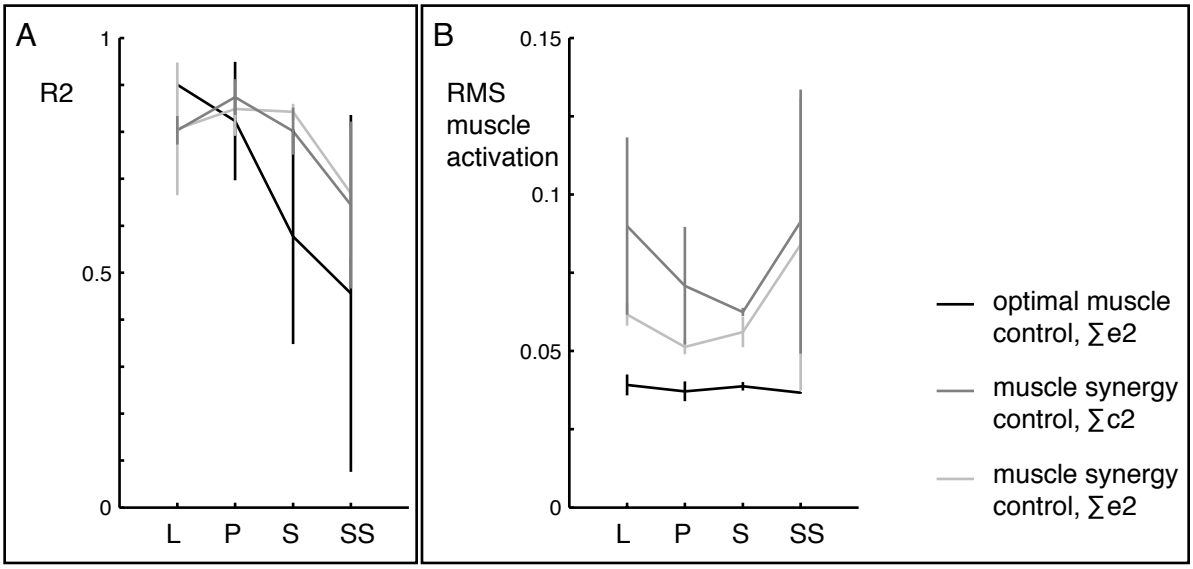

Figure 4.11. Fits to ground reaction force data and energetic costs predicted by the asymmetrical model. A: Average model fits to horizontal-plane hindlimb forces from experimental data across animals in each postural configuration. L: long; P: preferred; S: short; SS: shortest. B: Average simulated RMS muscle activation across animals in each postural configuration.

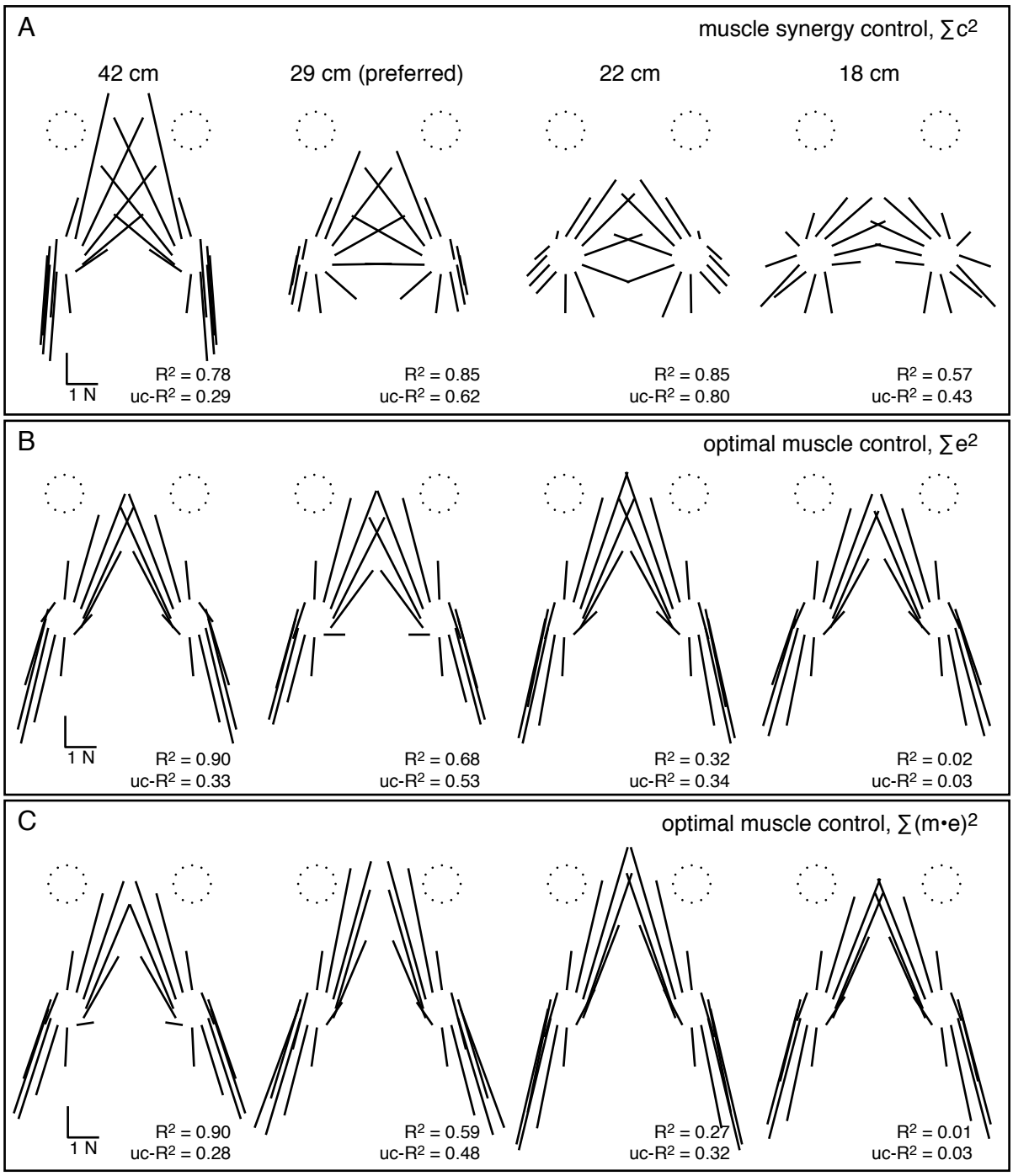

Figure 4.12. Simulated ground reaction forces predicted by the asymmetrical quadrupedal model parameterized to cat *Ru* (experimental data shown in Figure 4.2). A: simulated ground reaction forces predicted by muscle synergy control, minimizing sum-squared muscle synergy activation. B: simulated ground reaction forces predicted by optimal muscle control, minimizing sum-squared muscle activation. C: simulated ground reaction forces predicted by optimal muscle control, minimizing sum-squared muscle activation weighted by muscle mass.

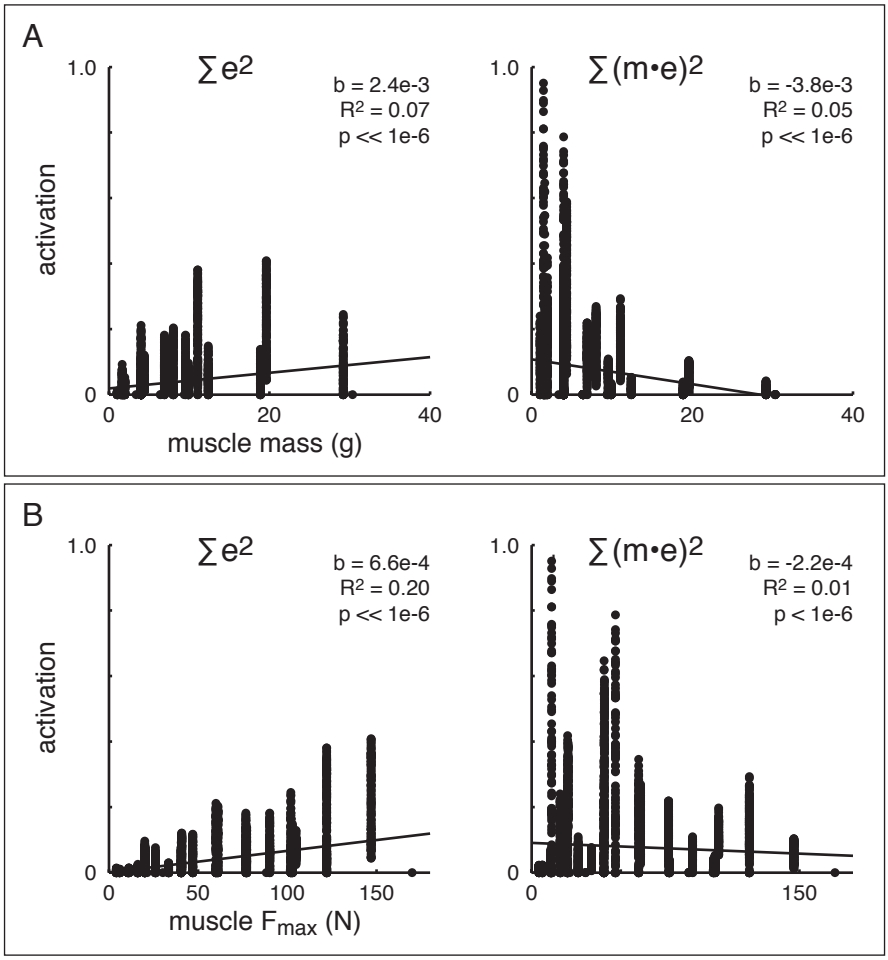

Figure 4.13. Distribution of muscle activation predicted by optimal muscle control in $\sum e^2$ and $\sum(m \bullet e)^2$ cost functions. A: scatterplots of predicted muscle activation values vs. muscle mass. Left: $\sum e^2$. Right: $\sum(m \bullet e)^2$. B: scatterplots of predicted muscle activation values vs. maximal muscle force. Left: $\sum e^2$. Right: $\sum(m \bullet e)^2$.

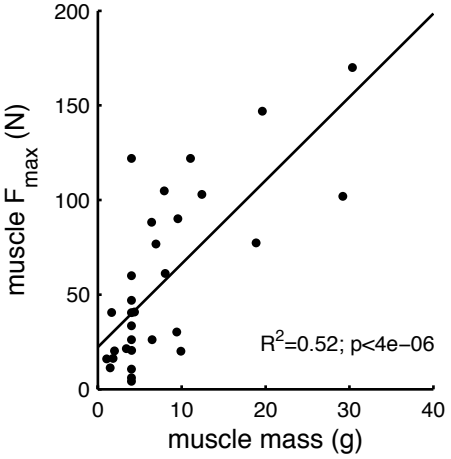

Figure 4.14. Approximately linear relationship between the mass and the maximal force F_{MAX} of individual muscles in the model of the cat hindlimb.

Table 4.2. Grand mean asymmetrical model fits to ground reaction force data. Values are presented as mean (SD).

Metric	Control	Cost Function	Task	
			CoM	CoP
X-Z R^2	Muscle	$\sum e^2$	0.67 (0.28)	0.08 (0.15)
		$\sum (m \bullet e)^2$	0.45 (0.32)	0.08 (0.15)
	Muscle synergy	$\sum e^2$	0.80 (0.11)	0.33 (0.30)
		$\sum (m \bullet e)^2$	0.76 (0.18)	0.34 (0.30)
		$\sum c^2$	0.78 (0.13)	0.34 (0.33)
X-Z uc-R^2	Muscle	$\sum e^2$	0.51 (0.22)	0.24 (0.23)
		$\sum (m \bullet e)^2$	0.34 (0.16)	0.24 (0.24)
	Muscle synergy	$\sum e^2$	0.58 (0.21)	0.37 (0.27)
		$\sum (m \bullet e)^2$	0.55 (0.22)	0.37 (0.28)
		$\sum c^2$	0.59 (0.18)	0.50 (0.30)
XYZ R^2	Muscle	$\sum e^2$	0.90 (0.08)	0.80 (0.05)
		$\sum (m \bullet e)^2$	0.81 (0.08)	0.83 (0.04)
	Muscle synergy	$\sum e^2$	0.93 (0.04)	0.87 (0.05)
		$\sum (m \bullet e)^2$	0.92 (0.04)	0.88 (0.06)
		$\sum c^2$	0.89 (0.05)	0.92 (0.03)

Table 4.3. Synergy force vector directions in the right hindlimb (sagittal-plane).

SFV	Cat	Model				Data			
		L	P	S	SS	L	P	S	SS
1	*Bi*	-113°	-97.2°	-89°	-74.9°	-103°	-97.2°	-91.1°	-85.6°
	Ru	-112	-96.7	-80.1	-69.7	-108	-96.7	-90.2	-85.3
	Ni		-97	-82.8	-75.7		-97	-91	-86.7
2	*Bi*	64	79.7	74.2	82.9	74.3	79.7	85.8	91.3
	Ru	69.1	80.3	84.5	85.6	68.7	80.3	86.9	91.7
	Ni		78.7	83.2	85.9		78.7	84.7	89
3	*Bi*	-119	-106	-101	-86.6	-111	-106	-99.5	-94
	Ru	167	173	179	-174	162	173	180	-176
	Ni		-122	-113	-99.4		-122	-116	-111
4	*Bi*	-49.6	-7.5	4.63	17.5	-12.9	-7.5	-1.4	4.1
	Ru	1.7	12.4	20.5	27	0.822	12.4	19	23.8
	Ni		-7	8.7	11.4		-7	-1	3.3
5	*Bi*	75.2	90.9	88.7	96	85.5	90.9	97	102
	Ru	86.1	98.3	105	106	86.7	98.3	105	110
	Ni		-138	-132	-122		-138	-132	-128

Table 4.4. Synergy force vector directions in the right hindlimb (dorsal-plane).

SFV	Cat	Model				Data			
		L	P	S	SS	L	P	S	SS
1	*Bi*	-87°	-61.9°	16.4°	73.2°	-73°	-61.9°	-16°	49°
	Ru	-85	-72.4	69.8	78.2	-83.3	-72.4	-4.38	65.6
	Ni		-62.2	45.8	67.6		-62.2	-15.2	41.9
2	*Bi*	93.9	106	86.9	87.1	101	106	126	-157
	Ru	94.3	101	132	152	95.2	101	121	-138
	Ni		88.1	103	95.1		88.1	86	69.4
3	*Bi*	-79.8	-62.2	-51.2	18.4	-68.4	-62.2	-49.3	-26.3
	Ru	-63	-66.6	-69.3	-70.6	-65.6	-66.6	-66.7	-66.6
	Ni		-54	-37.6	-21.1		-54	-48.7	-43.8
4	*Bi*	37	45.2	49.7	53.4	44.7	45.2	45.4	45.3
	Ru	77.4	78	80.7	84.3	78.3	78	77.7	77.3
	Ni		50.3	53.8	57.9		50.3	50.5	50.5
5	*Bi*	96.2	-165	83	-91.8	126	-165	-115	-105
	Ru	110	-103	-108	-117	120	-103	-97.2	-95.5
	Ni		-90	-89.4	-90.3		-90	-90	-90

Table 4.5. Synergy force vector magnitudes in the right hindlimb (sagittal-plane).

SFV	Cat	Model				Data			
		L	P	S	SS	L	P	S	SS
1	*Bi*	2.74 N	2.26 N	1.74 N	1.67 N	-	2.26 N	-	-
	Ru	3.45	3.09	2.65	2.5	-	3.09	-	-
	Ni		4.37	3.65	3.87	-	4.37	-	-
2	*Bi*	1.29	1.41	1.3	1.4	-	1.41	-	-
	Ru	1.68	1.75	1.74	1.7	-	1.75	-	-
	Ni		1.33	1.33	1.36	-	1.33	-	-
3	*Bi*	1.19	0.989	0.764	0.696	-	0.989	-	-
	Ru	0.202	0.219	0.206	0.17	-	0.219	-	-
	Ni		0.51	0.397	0.4	-	0.51	-	-
4	*Bi*	0.162	0.152	0.198	0.213	-	0.152	-	-
	Ru	0.331	0.364	0.406	0.409	-	0.364	-	-
	Ni		0.119	0.138	0.142	-	0.119	-	-
5	*Bi*	0.247	0.269	0.241	0.259	-	0.269	-	-
	Ru	0.115	0.121	0.118	0.111	-	0.121	-	-
	Ni		0.121	0.109	0.104	-	0.121	-	-

The mark (-) designates that the synergy force vector magnitudes in these postural configurations were fixed to the preferred-configuration value by construction.

Table 4.6. Synergy force vector magnitudes in the right hindlimb (dorsal-plane).

SFV	Cat	Model				Data			
		L	P	S	SS	L	P	S	SS
1	*Bi*	1.06 N	0.32 N	0.108 N	0.453 N	0.515 N	0.32 N	0.157 N	0.23 N
	Ru	1.3	0.379	0.486	0.886	0.978	0.379	0.115	0.277
	Ni		0.601	0.641	1.04		0.601	0.29	0.376
2	*Bi*	0.569	0.263	0.353	0.173	0.389	0.263	0.127	0.0813
	Ru	0.602	0.3	0.223	0.282	0.637	0.3	0.112	0.0775
	Ni		0.261	0.16	0.0975		0.261	0.123	0.0243
3	*Bi*	0.59	0.301	0.193	0.132	0.381	0.301	0.216	0.157
	Ru	0.221	0.237	0.22	0.18	0.228	0.237	0.239	0.238
	Ni		0.332	0.253	0.182		0.332	0.295	0.27
4	*Bi*	0.175	0.213	0.259	0.253	0.211	0.213	0.214	0.213
	Ru	0.34	0.364	0.386	0.366	0.372	0.364	0.353	0.342
	Ni		0.153	0.168	0.164		0.153	0.154	0.154
5	*Bi*	0.0636	0.0158	0.00532	0.0269	0.0261	0.0158	0.036	0.06
	Ru	0.00842	0.0179	0.0313	0.0342	0.00793	0.0179	0.0312	0.0409
	Ni		0.0904	0.0726	0.0554		0.0904	0.0815	0.0746

Table 4.7. Muscles included in the musculoskeletal model.

Designator	Name	Mass (g)	F_{MAX} (N)
ADF	Adductor femoris	29.2	102
ADL	Adductor lounges	1.48	11.3
BFA	Biceps femoris anterior	4	47
BFP	Biceps femoris posterior	30.3	170
EDL	Extensor digitorum longus	3.4	21.5
FDL	Flexor digitorum longus	1.99	20.3
FHL	Flexor hallucis longus	7.93	105
GMAX	Gluteus maximus	4	6
GMED	Gluteus medius	4	60
GMIN	Gluteus minimus	4	4.21
GRAC	Gracilis	9.41	30.2
LG	Lateral gastrocnemius	12.4	103
MG	Medial gastrocnemius	9.55	90.2
PB	Peroneus brevis	4	33.5
PEC	Pectineus	4	10.6
PL	Peroneus longus	1.81	16.3
PLAN	Plantaris	6.94	76.8
PSOAS	Psoas minor	4	122
PT	Peroneus tertius	1.06	16
PYR	Pyriformis	4	26.1
QF	Quadratus femoris	4	40.5
RF	Rectus femoris	11.1	122
SART	Sartorius	9.93	20.1
SM	Semimembranosus	18.9	77.3
SOL	Soleus	4.03	20.5
ST	Semitendinosus	6.42	88.2
TA	Tibialis anterior	6.47	26.2
TP	Tibialis posterior	1.65	40.6
VI	Vastus intermedius	4.39	40.8
VL	Vastus lateralis	19.6	147
VM	Vastus medius	8.04	61.1

DISCUSSION

We reproduced force patterns during postural tasks in cats by optimally controlling the quadrupedal musculoskeletal system to regulate the CoM. A low-dimension controller based on muscle synergies derived from experimental data was also sufficient to approximate this optimal strategy across postural configurations, although it required higher energetic cost. Interestingly, muscle synergy control recreated the active unloading observed in experimental animals. This suggests that aspects of the force constraint strategy may satisfy additional criteria besides those explicitly modeled by our optimal control formulation. Our results support the hypothesis that the forces observed in the force constraint strategy reflect the optimal motor solution for controlling the CoM given the constraints of the musculoskeletal system.

Muscle synergy control predicts similar forces but higher energetic costs compared to optimal muscle control

The simplification associated with low dimension control based on muscle synergies comes at an appreciable cost, in terms of simulated muscle activation, compared to that of optimal muscle control. In simulated reaching movements, it has been demonstrated that the control of muscle synergies constructed from optimality criteria can approximate the motor solutions predicted by the optimal control of individual muscles both in a detailed musculoskeletal model of the frog hindlimb (Berniker et al. 2009) as well as in an abstract model of reaching (Chhabra and Jacobs 2006). However, because simulations of this type typically seek to verify the feasibility of the low-dimension control architecture provided by muscle synergies, they typically do not attempt to recreate experimental data. Conversely, simulations of muscle synergy control in the context of experimental data typically do not compare cost increases associated with muscle synergy control in the context of realistic movements (Kargo et al. 2010; Neptune et al. 2009). Although the simulated muscle synergies used here were identified to satisfy the constraints of the experimentally-observed muscle synergy force vectors with the lowest amounts of simulated muscle activation, simulations of muscle synergy control required significantly higher muscle activation than simulations of optimal muscle control in all cases.

Optimal muscle solutions may serve as the endpoint of ongoing adaptive processes

The minimizations presented here may be descriptive of the control process used by the nervous system without specifically considering its implementation. We do not interpret these results to mean that the nervous system explicitly performs optimal control, in the sense that an engineering control system would. Implementations of the simple feedforward optimal control modeled here (Fagg et al. 2002; Shah et al. 2004), as well as more sophisticated optimal control architectures such as the Kalman filter (Denève et al. 2007) have been presented on more realistic neural substrates.

The control process used by the nervous system may be developed over time as a result of ongoing adaptative processes. These processes may be difficult to observe over experimental timescales, but can be revealed by examining the timecourse of compensation and recovery after deficit. For example, after cats experience a deficit that disrupts the balance of sensory feedback that is available for the temporal patterning of muscle activity, their temporal coordination patterns converge towards a novel optimal solution that is appropriate to the new constraints imposed by the deficit (Lockhart and Ting 2007). Although this adaptation can be observed over the course of days, it remains incomplete on practical timescales.

Similarly, deficits such as the pathological muscle synergies observed in hemiplegic stroke provide some of the most compelling evidence that a muscle synergy architecture may be the best representation for the way that muscles are controlled in the unaffected nervous system. Considering a locomotion task in hemiplegic subjects, Clark and colleagues (2010) demonstrated that muscle synergies in the unaffected leg were also expressed in the affected leg, but that they were co-recruited, so as to function as a single unit. Evidence suggests that disrupting this type of pathological coupling requires overcoming certain thresholds or constraints within the nervous system, because focused interventions can be designed to disrupt these types of pathological coupling through appropriate biofeedback (Ellis et al. 2005). We speculate that typical muscle patterns may result from multiple similar fragmentation processes over the course of learning and development.

Higher-order muscle synergies may allow the generalization of motor solutions to other conditions

The different patterns of generalization throughout the workspace of muscle synergies 1 and 3 suggest that higher-order muscle synergies may function in part to extend the range of conditions for which an existing motor solution is appropriate. Here, in the preferred postural configuration, the functions of muscle synergies 1 and 3 – as described by the force vectors they produce – are partially redundant. This is particularly true in cat *Bi*, for which they produce force vectors that are separated by only about 10° in the sagittal plane. However, by considering other postural configurations, it becomes evident why both are required: because muscle synergies 1 and 3 exhibit different patterns of generalization, muscle synergy 3 augments the function of muscle synergy 1 so that it is appropriate in the other postural configurations. It seems likely that muscle synergy 5 may serve a similar role in generalization, as it is modulated to its highest levels in the shortest postural configuration in all cats.

Penalizing contraction time may recreate active unloading in optimal muscle control

The primary differences between forces predicted by muscle synergy control and forces predicted by optimal muscle control occurred when the limb was unloaded. Because muscle synergy activations were constrained to be nonnegative with respect to the background level, additional muscle synergy activation was required in these perturbation directions to actively unload the limb, a function performed by muscle synergy 2 in all cats. This active unloading was not observed in optimal muscle control, as it requires the coactivation of flexors and extensors, and hence would result in greater than the minimum control cost.

It is possible that constraining the optimal muscle control model to actively unload would recreate the forces observed in these perturbation directions. This constraint could be justified by the fact that there is a strong pressure to generate the active postural response as fast as possible, and the dynamics of muscle activation are faster than the dynamics of muscle inactivation.

It is likely that there are significant evolutionary pressures associated with generating appropriate postural responses rapidly and robustly, so that the APR occurs as rapidly as computational constraints will allow. In support of this idea, deficits introduced

in lesion studies have the general effect of delaying, but never accelerating, postural responses (Stapley et al. 2002). Similarly, deficits in any one sensory modality are robustly compensated for through sensory reweighting (Peterka 2002). As a result, when there is explicit sensory loss in the visual, vestibular, or somatosensory systems, the spatial tuning characteristics of individual muscles are retained (Inglis et al. 1994; Stapley et al. 2002).

Strut forelimbs may represent musculoskeletal and neural constraints

The constraints on forelimb force production applied in the asymmetrical quadrupedal model likely represent underlying, and possibly complementary, mechanisms of both the musculoskeletal and neural systems. The skeletal morphology of the elbow is likely able to support significantly higher compressive forces than that of the knee, so that in a purely mechanical sense, the forelimbs are likely more suited to use as struts than the hindlimbs (T.J. Burkholder, personal communication). In the preferred and long postural configurations, the forelimbs do generate horizontal-plane forces that are comparable in magnitude to those in the hindlimbs, suggesting that they may not be purely biomechanically constrained to only generate vertical forces. However, between the long and shortest postural configuration, the sagittal-plane angle of the forelimb varies over a range of roughly 20°, which may suffice to rotate forces directed along the limb axis to be exactly vertical (Fung and Macpherson 1995). Unfortunately, a detailed quantification of the musculoskeletal mechanics of the forelimb is not yet available.

Evidence suggests that the overall neural control of the forelimbs is likely to be markedly different from that of the hindlimbs, perhaps complementing their different morphology. During postural tasks, the muscle activity in the forelimbs has been qualitatively described as exhibiting muscle coordination patterns wherein muscles throughout the limb are coactivated or co-inactivated. This is unique to the forelimbs, as muscle activity in the hindlimbs is characterized by reciprocal inhibition between muscles on opposite sides of the limb (Macpherson et al. 1989). Interestingly, during locomotion, there is evidence that forelimb muscle activity during locomotion is actually more complex than that of the hindlimb, exhibiting a greater number of unique bursts of temporal muscle activity over the gait cycle (Krouchev et al. 2006). In preliminary studies, we have also observed a higher number of muscle synergies in the forelimb than

in the hindlimb (unpublished observations), suggesting that the uniform co-activation or co-inactivation pattern may result from the orderly recruitment of a motor repertoire that is more sophisticated overall than that of the hindlimbs.

CHAPTER 5
CONCLUSIONS

Here, I identified constraints within the nervous and musculoskeletal systems that determine the muscle activity and ground reaction forces observed during the APR in cats. I demonstrated that biomechanical constraints on force production in the isolated hindlimb do not uniquely determine the characteristic patterns of force activity observed during the APR, although in the presence of muscle synergy constraints they introduce characteristic features of postural forces. When I considered the coordination of four limbs, I demonstrated that the optimal feedforward control of the musculoskeletal system to stabilize the CoM recreated the muscle activity and ground reaction forces observed during the APR very well. The optimal control of five muscle synergies in each limb based on experimental data was also sufficient to appropriately stabilize the CoM across postural configurations, although it required a higher energetic cost than would be required if individual muscles were controlled. Overall, these results support the hypothesis that the force constraint strategy and related muscle activity represent the optimal motor solution for controlling the CoM given the constraints of the musculoskeletal system.

While a low dimension neural control structure based on muscle synergies is feasible to regulate the CoM, any decreases in the resulting costs of computation may require increases in the costs of execution. This tradeoff may reflect the fact that information representation in the nervous system may be limited by metabolic constraints, making some computational structures more favorable than others (Denève et al. 2007; Olshausen and Field 2004). Similarly, controlling muscle synergies may also speed motor learning. In a model of birdsong, Fiete and colleagues (2004) demonstrated that increasing the sparseness of the descending drive from premotor areas increased the rate of learning, because synaptic interference was reduced.

NEUROANATOMICAL BASES OF THE APR

Identifying neuroanatomical bases for the APR is an area of ongoing research. It is known that cortical control is not necessary for the APR, as the decerebrate cat can

produce rudimentary postural responses, both in terms of muscle activation (Honeycutt et al. 2009) and force responses (Honeycutt and Nichols 2010). Cerebral cortex may instead play a role as a meta-modulator, primarily by adjusting central "set" before postural tasks in a long loop involving the basal ganglia, and adapting strategies across repetitions in a second long loop involving the cerebellum (Jacobs and Horak 2007). For example, APR muscular activity can be voluntarily suppressed when subjects intend to take a step in response to a perturbation with characteristics that are expected, but only the later phase of the response can be voluntarily suppressed when perturbation characteristics are randomized, suggesting some degree of involvement of cerebral cortex in the later portions of the timecourse (Burleigh and Horak 1996). The contributions of vestibular and visual information, which is incorporated in parallel with lower-level mechanisms, at longer latencies, may not be critical (Deliagina et al. 2008). Cats with vestibular lesion can generate generally appropriate, although hypermetric, responses to translation perturbations (Inglis and Macpherson 1995). The role of the cerebellum may be particularly important during motor learning; cerebellar lesions preclude proper scaling of postural responses to repeated perturbations of known magnitude (Horak and Diener 1994).

The primary role of higher centers may be to provide tonic drive to spinal circuits via descending pathways in the ventral spinal cord (Deliagina et al. 2008). It is known that the APR requires supraspinal influences, because the ability of chronic spinal cats to balance is typically permanently disrupted, although they are typically able to recover weight support and some limited lateral stability (Pratt et al. 1994). However, in the presence of appropriate descending drive, postural responses may emerge largely from spinal mechanisms. Laterally-hemisected rabbits recover rudimentary postural responses relatively quickly (Lyalka et al. 2005). Even in the absence of appropriate descending drive, some rudimentary responses may also occur. Cats spinalized at the lumbrosacral level do exhibit incomplete extensor responses, but not flexor responses, although flexors are active in other behaviors like paw shake (Macpherson and Fung 1999).

CLINICAL RELEVANCE

Here, I considered the mechanisms of standing balance in cats. Although these studies are of a scientific rather than a clinical nature, they may ultimately contribute to

an increased understanding of the mechanisms of standing balance in both healthy and impaired populations. Towards this, ongoing studies in our laboratory translate many of the ideas and techniques developed here to research in human subjects. Developing a better understanding of the mechanisms of standing balance would be beneficial, because it might lead to superior clinical interventions and strategies to avoid falls. Falls are a leading cause of morbidity and mortality among adults aged 65 and older (Stevens 2005). In 2006, approximately 5.8 million (almost 16%) of persons aged 65 and older reported falling at least once during the preceding three months, and 1.8 million (nearly 5% of all older adults) sustained some type of fall-related injury (Stevens et al. 2008). The most recent estimates for the direct medical costs associated with these type of fatal and nonfatal fall-related injuries – the year 2000 – was approximately $19 billion annually (Stevens 2005).

FUTURE STUDIES

The models and analyses used here could be used to guide future investigations in the neural control of movement. The most obvious extension is to generalize the results in the context of a fully dynamic model of the cat hindlimb. The static cat hindlimb model was appropriate because of the quasi-static nature of the postural task. Additionally, the use of a static model enabled analytical techniques – as in the FFS analysis – that would be improbable or impossible to implement in a dynamic model. Encouragingly, the general results of the static model – that the force production capability of the hindlimb appears to be biased along the anterior-posterior axis – has been qualitatively confirmed in later studies using a fully dynamic version of the model (Bunderson et al. 2010), suggesting that these results can be generalized to more complex dynamic conditions.

One interesting question concerning the results of Chapters 2 and 3 is whether the rotation of synergy force vectors with the limb axis we observed depends critically on the particular synergy force vectors and intralimb geometry selected by the animals. Because the mechanical action of individual muscles can vary widely depending on the state of other muscles and joints (van Antwerp et al. 2007), it seems likely that details of intralimb geometry may significantly affect the pattern of synergy force vector rotation we observed. It is also known that the intralimb geometry itself is tightly regulated

according to energetic constraints in parallel with the regulation observed during the APR (Fung and Macpherson 1995), suggesting that these parallel postural circuits may hold exciting insights. Similarly, the particular synergy force vector, and balance of muscles included in each muscle synergy may influence the degree to which the rotation with the limb axis is observed. By considering the particular intralimb geometry and synergy force vectors selected by the animals in the context of the possibilities enabled by, for example, Monte Carlo simulation, it could be determined whether animals were tightly controlling these quantities to the benefit of the generalizability of muscle synergies.

The degree to which the use of other cost functions to identify simulated muscle synergies in the hindlimb model would produce different patterns of generalization across postural configurations is also unknown, and may be an interesting area for investigation. We used simulated muscle synergies, rather than using experimentally-observed muscle synergies directly, because of the difficulties associated with quantitatively incorporating experimentally-observed EMG data into musculoskeletal models. In the few neuromechanical simulations of muscle synergies that have been attempted, muscle synergies were either simulated based on experimental force data (Kargo et al. 2010), or derived from an optimization routine using incomplete experimental EMG data as an initial guess (Neptune et al. 2009). Therefore, to test the feasibility of the muscle synergy-synergy force vector relationship, we adopted an approach similar to that of the former study. We derived simulated muscle synergies from the synergy force vectors observed in the postural configuration of each cat with either of two different optimization criteria; one that penalized the activation of muscles in the simulated muscle synergy strongly, and one that did not penalize muscle activation at all. We demonstrated that simulated muscle synergies derived from both criteria produced force vectors that rotated in the sagittal plane as postural configuration was varied, in a manner that was very similar to that observed in experimental data (McKay and Ting 2008). We hypothesized that similar optimization criteria laying between these two extremes would result in a similar synergy force vector rotation; however, this was not tested rigorously.

It will be possible to fully account for asymmetries between the forelimbs and hindlimbs in the quadrupedal model of Chapter 4 once a detailed anatomical model of the cat forelimb becomes available. However, in order to do so, the muscle activity in the

forelimb will need to be characterized. The muscle synergy organization of the forelimb is likely highly different than that of the hindlimb – in both cats and humans standing quadrupedally, for example, qualitatively different patterns of muscle activation are observed between the forelimbs and hindlimbs during postural control (Macpherson et al. 1989). In general, the forelimbs are used as "struts," with muscles throughout the limb coactivating or co-inactivating in response to loading or unloading, whereas the hindlimbs are used as "levers," leading to patterns of reciprocal inhibition. In preliminary investigations, I have found that a higher number of EMG principal components is observed in the forelimb than in the hindlimb. This is consistent with the results of Krouchev and colleagues, who identified 11 distinct patterns of muscle activity in the cat forelimb during locomotion, but only 7 in the hindlimb (Krouchev et al. 2006). However, due to the paucity of data, these results were not pursued further.

One of the most interesting extensions of Chapter 4 would be to use a more detailed muscle model that was better suited to estimating the energy used during the postural task. The relationship between fiber type composition and rates of instantaneous ATP hydrolysis during isometric force production in human skeletal muscle has been reported (Szentesi et al. 2001). By better delineating the muscles in the hindlimb model according to fiber type, a better proxy for energy usage could be obtained.

The quadrupedal model in Chapter 4 could also be extended to a feedback formulation once the dynamics of mediolateral balance are better characterized. Although the inverted pendulum formulation has been used to characterize the dynamics of anterior-posterior and diagonal perturbations, where the loaded hindlimb or limbs dominates the dynamics (Lockhart and Ting 2007; Welch and Ting 2009), the dynamics of mediolateral perturbations are still difficult to treat.

The results of Appendix A point to the conclusion that the dimension reduction associated with the APR takes place within the nervous system. Overall, many studies in our laboratory assume or hypothesize that the CoM is the variable that is regulated by the nervous system during postural control, and that this regulation occurs in a feedback manner (Lockhart and Ting 2007; Welch 2008). Considered in the context of feedback control, the results of Chapter 4 suggest that multiple patterns of sensory information – i.e., joint angles, are mapped within the nervous system to similar estimates of the CoM

kinematics, and that these kinematic estimates are mapped to motor responses. For simplicity, in Appendix A, we treated the entire nervous system as a "black box." Specific linkages between somatosensory components and motor components were not examined. However, if the CoM kinematic estimate is encoded within the nervous system, a simple and testable prediction would be that disturbances in the CoM would map to unique motor patterns, whereas disturbances in local variables like joint angles would not. In the context of PCA, this could be tested by carefully examining the identified component bases for functional linkages between CoM kinematics and motor output patterns. Similarly, the kinematics of reduced proprioceptive frames, such as limb length and orientation, which have been demonstrated to be encoded in the dorsal spinal cerebellar tract (DSCT) (Bosco et al. 1996) could be performed. Extending the analysis of Appendix A to include more detailed elements of the hypothesized sensorimotor transformation – filling in the "black box" – would likely provide more insight than applying more sophisticated nonlinear dimension reduction methods than PCA, for example, Isomap and Locally-Linear Embedding (Roweis and Saul 2000; Tenenbaum et al. 2000). One of the principal observations we have made based on many studies is that quasi-linear relationships like low-dimensional dynamics may emerge from the interactions between many nonlinear neuromechanical elements (Ting and McKay 2007); therefore, identifying the linear relationships in the context of an overall framework for postural control may be more useful than characterizing the overall nonlinear transformation compactly without the hypothesized structure.

CONCLUSION

I integrated techniques from musculoskeletal modeling, control systems engineering, and data analysis to identify neural and biomechanical constraints that determine the muscle activity and ground reaction forces during the automatic postural response (APR) in cats. I demonstrated that biomechanical constraints on force production in a single hindlimb do not uniquely determine the characteristic patterns of force activity observed during the APR; however, when I considered the coordination of four limbs, I demonstrated that the optimal feedforward control of individual muscles to stabilize the CoM recreated the muscle activity and ground reaction forces observed during the APR very well. These results support the hypothesis that the force constraint

strategy and related muscle activity represent the optimal motor solution for controlling the CoM given the constraints of the musculoskeletal system.

This work advances our understanding how the constraints and features of the nervous and musculoskeletal systems interact to produce motor behaviors. In the future, this understanding may inform improved clinical interventions, prosthetic applications, and the general design of distributed, hierarchal systems.

APPENDIX A

THE NERVOUS SYSTEM REDUCES THE DIMENSION OF SENSORY INFLOW DURING PERTURBATION RESPONSES

INTRODUCTION

During postural perturbations, the nervous system must use sensory signals from all segments of the body in order to rapidly and appropriately activate many muscles to maintain stability. We have hypothesized that in the final stage of this sensorimotor transformation, muscles are recruited in groups, called muscle synergies, rather than individually, reducing the number of degrees of freedom that must be controlled (Ting and McKay 2007). Previously, we subjected muscle activity in multiple muscles during postural perturbations in both cats and humans (Torres-Oviedo et al. 2006; Torres-Oviedo and Ting 2007) to a components analysis technique called nonnegative matrix factorization (NNMF, Lee and Seung 1999). We demonstrated that between 4 and 6 muscle synergies were sufficient to reconstruct the activity in up to 16 individual muscles during the postural task, consistent with the hypothesis that the number of degrees of freedom that are controlled by the nervous system is fewer than the number of muscles (Torres-Oviedo et al. 2006; Torres-Oviedo and Ting 2007).

The primary objective of this study was to address critiques of our previous studies that the small number of postural muscle synergies may simply reflect either limitations in the complexity of the postural task, or artifacts of the subsequent analyses, rather than a muscle synergy organization within the nervous system. Because our multidirectional perturbation paradigm typically involves perturbations in various directions within the horizontal plane, the repertoire of muscle activity that is evoked might be expected to lie on a two-dimensional manifold, whether individual muscles or muscle synergies are recruited. Therefore, the first objective of this study was to examine the dimension of the perturbation effects in a complex, redundant, biomechanical system acting in the gravitational field. For generality, we used a general technique with no constraints on sign – principal components analysis, or PCA (Basilevsky 1994) – as the primary method of dimension estimation.

The second objective of this study was to address the more nuanced critique that the small number of postural muscle synergies may simply reflect dependencies in the sensory information elicited by postural perturbations and used to pattern muscular responses, rather than dependencies in muscle activation enforced by a muscle synergy organization within the nervous system. Towards this, we systematically investigated the relationship between the dimension of applied perturbations, somatosensory information, muscle activity, and motor outputs during postural tasks. Somatosensory information from the joints and skin is critical to the timing of muscle activity during postural responses (Bolton and Misiaszek 2009; Inglis et al. 1994; Stapley et al. 2002). However, this somatosensory information does not reflect the dynamics of the perturbation itself, but rather, reflects the dynamics of the perturbation after mechanical filtering through the musculoskeletal system, which may limit its complexity. If postural perturbations fail to fully excite the dynamics of the musculoskeletal system, or excite the dynamics in a stereotyped, low-dimension fashion, later stages in the sensorimotor transformation would presumably have insufficient sensory inflow to generate complex muscle activation patterns, whether or not muscle synergy constraints are present. It is also likely that the natural sensory frames of the musculoskeletal system also filter somatosensory information. For example, the maximal lengthening directions of individual muscles within the isolated cat hindlimb lie preferentially near the parasagittal plane (Bunderson et al. 2010). The relative amount and accuracy of reflex feedback regarding the lengths of muscles in the hindlimb therefore depends on the degree to which postural perturbations excite these neuromechanical feedback pathways.

To determine whether muscle synergies identified during postural perturbations simply reflect limitations in the complexity of the postural task, we have previously altered the biomechanical context of the postural task in cats (Torres-Oviedo et al. 2006), with the intent that different biomechanical contexts might elicit novel muscle activation patterns. We required cats to perform two different postural perturbation tasks: translation perturbations, wherein the support surface was rapidly translated in any of several directions in the horizontal plane, and rotation perturbations, wherein the support surface was rapidly rotated in any of several combinations of pitch and roll. Because these two types of perturbations elicit apparently opposite changes in the angles of joints

throughout the body (Nashner 1976; Ting and Macpherson 2004), we reasoned that they would elicit different patterns of sensory information, and therefore would be likely to recruit novel muscle activation patterns. Despite this, we observed that muscle synergies from translation perturbations were sufficient to reconstruct muscle activity during rotation perturbations, suggesting that the same underlying neuronal networks were being recruited during both perturbation types. We also observed that each muscle synergy could be robustly correlated to a "functional motor output" – a unique reaction force vector at the ground. Further, when the cats were forced to perform the postural task in different postural configurations created by altering the distance between the fore- and hind-feet, the force vectors rotated with the limb axis in the sagittal plane. If the relationship between muscle synergy activation and force vector generation were causal, it would be consistent with the hypothesis that muscle synergies may be organized within and recruited by the nervous system in terms of the motor outputs that they produce. Later, in a musculoskeletal model of the cat hindlimb, we demonstrated that this hypothesized causal relationship was biomechanically feasible, as the force vectors produced by simulated muscle synergies exhibited a similar pattern of rotation with the limb axis as the hindlimb was moved throughout the workspace (McKay and Ting 2008).

A limitation of the previous study was that we did not quantitatively address the degree to which alterations in the biomechanical context of the postural task affected its sensory context. The patterning of the "initial burst" of muscle activity of the automatic postural response (APR), beginning about 40-60 ms after perturbation in onset, and the active changes in biomechanical variables, beginning about 60 later, relies heavily on somatosensory information from the joints and the skin encoding changes in kinematic and kinetic variables – joint angles, joint angular velocities, and reaction forces at the ground – within the first 30 ms after the onset of a postural perturbation (Ting and Macpherson 2004). Proprioceptive information regarding the angles and angular velocities of joints throughout the hindlimb is represented at the dorsal root level during locomotion in afferents from multiple sensory modalities including muscle spindles, Golgi tendon organs, and cutaneous and hair follicle receptors (Weber et al. 2007). Second, cutaneous information regarding loading forces at the ground is required for appropriate foot placement in spinal cats during locomotion (Rossignol et al. 2008) and

provides the only unambiguous estimate of CoM excursion direction during postural disturbances (Ting and Macpherson 2004).

The sensory context of the postural task is not trivial to estimate because the somatosensory information used during postural tasks likely reflects the combined dynamics of the platform and the musculoskeletal system. The kinematic and kinetic variables represented in somatosensory information are likely to be highly correlated during postural perturbations because of purely biomechanical factors; for example, the angles of the hip, knee and ankle in anesthetized cats lie along a plane in three-dimensional joint space in the absence of neural control (Bosco et al. 2000). Therefore, dimension reduction within the musculoskeletal system may be a possible source of constraint on the dimension of elicited muscle activity and functional motor outputs (Figure A.1). This is in contrast to reduced preparations where the influence of sensory information as a determinant of muscle activity dimension can be eliminated, for example by deafferentation (Cheung et al. 2005), explicitly modulated, for example by tendon vibration (Kargo and Giszter 2008), or presumably bypassed entirely, for example by spinal iontophoresis (Saltiel et al. 2001). It is also unlikely that despite the established roles of vestibular and visual information in postural control during continuous perturbations (Kuo 2005; Peterka 2002), these sensory modalities either cannot be or is not used to compensate for deficiencies or dependencies in somatosensory information in postural control during transient perturbations. Following vestibular lesion, cats exhibit hypermetric, but appropriately-patterned postural responses to support surface translations, even when standing in total darkness (Inglis and Macpherson 1995). In contrast, when somatosensory information is disrupted after peripheral neuropathy, the onset of muscle activity is delayed and its timecourse of activation is disrupted (Lockhart and Ting 2007; Stapley et al. 2002), similar to results in humans after peripheral neuropathy (Bloem et al. 2000; Bloem et al. 2002; Inglis et al. 1994).

Here, we were interested in three primary questions. First, do translation and rotation perturbations elicit high, or low-dimension somatosensory information? Although we considered translations in directions distributed throughout the horizontal plane, and rotations distributed throughout the pitch and roll axes, all of the conditions in each perturbation type can be summarized by only two parameters – either anterior and

lateral Cartesian coordinates in translation, or pitch and roll rotational coordinates in rotation. Dependencies between perturbation conditions may therefore fail to fully excite the dynamics of the musculoskeletal system, constraining the dimension of somatosensory information to that of the perturbation, 2. In this case, the dimension of muscle activity and motor outputs may be constrained by the dimension of the somatosensory information rather than dimension reduction within the nervous system (Figure A.2, A1).

Second, if the somatosensory information elicited by translation and rotation perturbations is greater than two-dimensional, is it mapped by the nervous system to lower-dimension muscle activity and motor outputs? If the postural response was governed by the feedback of local variables like joint angles, in the absence of any central constraints on dimension, we would expect the dimension of the perturbations to be retained throughout the sensorimotor transformation (Figure A.2, A2).

Third, and finally, do translation and rotation perturbations elicit similar, or different patterns of somatosensory information and motor outputs (Figure A.2, B-C)? We hypothesize that different patterns of somatosensory information lead to the recruitment of identical muscle synergies in translation and rotation perturbations. However, if similar somatosensory information is elicited in both perturbation types due the dynamics of the musculoskeletal system, recruitment of identical muscle synergies would be expected without explicit dimension reduction within the nervous system. Similarly, considering motor outputs, we have previously proposed that the recruitment of identical muscle synergies during translation and rotation perturbations leads to a conserved pattern of force outputs. By extension, these forces would be expected to be used in the different overall biomechanical contexts associated with the two perturbation types. However, it was unknown whether such hypothesized multifunctionality could be quantified.

To address these questions, we estimated and compared the dimension of somatosensory information, muscle activity, and motor outputs during translation and rotation perturbations. Because of the long computational and neuromechanical latencies inherent to the automatic postural response in cats, somatosensory inputs and motor outputs can be observed in discrete epochs during balance tasks (Ting and Macpherson

2004). Therefore, we directly estimated and compared the dimension of somatosensory inputs, muscle activity, and functional motor outputs during standing balance in unrestrained cats.

We present three primary findings. First, we demonstrate that although both translation and rotation perturbation paradigms are by construction two-dimensional, both types give rise to somatosensory inflow that is significantly higher dimension. Second, by directly comparing the dimension of somatosensory inputs, muscle activity, and motor outputs, we demonstrate that that sensorimotor transformation during postural perturbations is not one-to-one, as would be expected if low dimension muscle activity and motor outputs solely reflected limitations in the available somatosensory information. Third, by quantifying the similarity of identified principal component bases of somatosensory information and motor outputs using shared subspace dimensionality (SSD, Cheung et al. 2005), we demonstrate that distinct patterns of somatosensory information and motor outputs are elicited across translation and rotation perturbations – suggesting that altering the biomechanical context of the postural task alters the sensory context – as well as across the somatosensory input and motor output epochs – suggesting that feedback of local variables is insufficient to explain the patterning of the postural task. Finally, we show that our results are generally robust to changes in dimension estimation methods, as well as demonstrating that the dimension estimates of muscle activity from our implementation of PCA were consistent with those using non-negative matrix factorization.

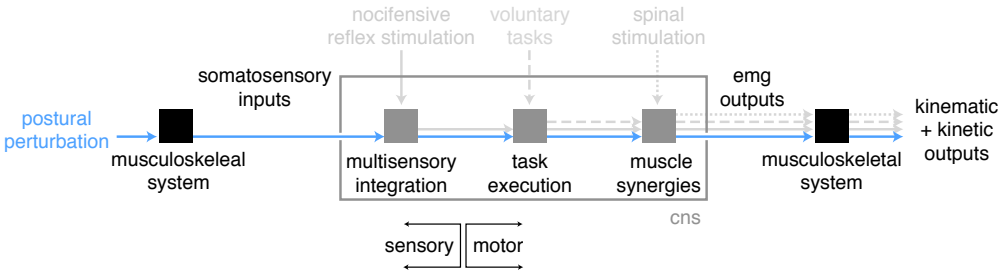

Figure A.1. Somatosensory information elicited during reactive postural tasks reflects the combined dynamics of postural perturbations and the musculoskeletal system. In this hypothesized organization for postural control (blue lines), postural perturbations are transformed through joints, muscles, and reflexes (musculoskeletal system, black box) to somatosensory inputs. Networks within the CNS (gray, enclosed by dark gray box) integrate these inputs to form an estimate of the relevant aspects of the body's state which is used to centrally control the postural task via the activation of muscle synergies, and subsequent muscle activation (EMG) and motor outputs. In this study, we estimated and compared the dimensionality of somatosensory inputs, EMG outputs, and kinematic and kinetic outputs during postural perturbation tasks. Other studies of muscle synergies (light gray lines) progressively isolate motor pathways, including the muscle synergy block hypothesized to be the source of dimensionality reduction. Examples include nocifensive reflex stimulation (light gray solid line, Kargo and Giszter 2008; Tresch et al. 1999), voluntary movements (light gray dashed line, d'Avella et al. 2006; Holdefer and Miller 2002), and spinal stimulation (light gray dotted line, Mushahwar et al. 2004; Saltiel et al. 2005).

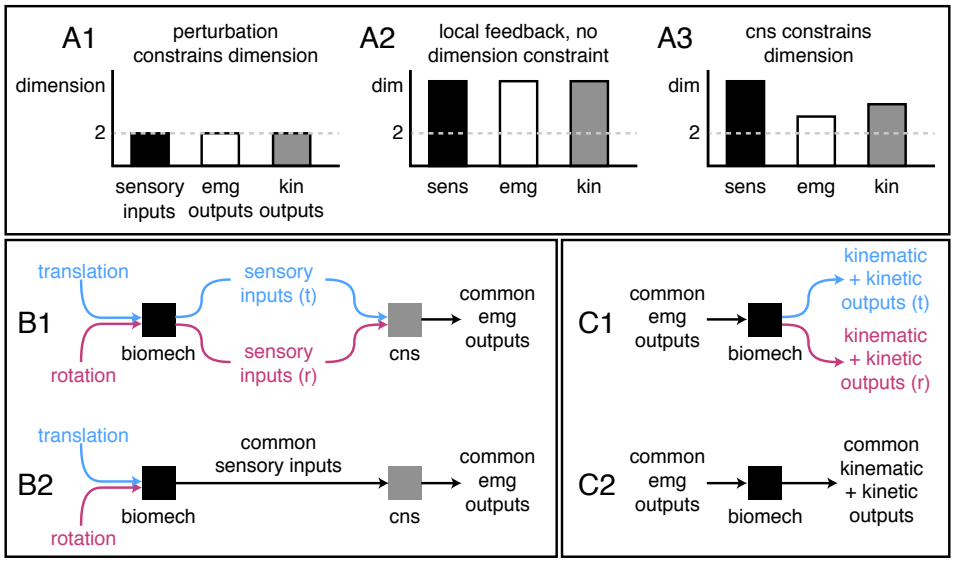

Figure A.2. Hypotheses investigated in the study. A: Three possible relationships between dimension of somatosensory inputs, muscle activity, and kinematic and kinetic motor outputs during postural perturbation tasks. A1: Dependencies between perturbation conditions fail to fully excite the dynamics of the musculoskeletal system, and therefore constrain the dimension of elicited somatosensory information to the perturbation dimension (2). In this scheme, the dimension of EMG and functional motor outputs is constrained by the dimension of sensory information – a task constraint – rather than dimension reduction within the nervous system. A2: Perturbations elicit somatosensory information of higher dimension, but EMG and functional motor outputs result from feedback of local variables, without central dimension constraints. A3: Perturbations elicit high dimension somatosensory information which is mapped by the nervous system to low-dimension EMG and functional motor outputs. B: Two possible relationships between the somatosensory information elicited by translation and rotation perturbations. B1: Translation and rotation perturbations elicit unique somatosensory information that is conveyed by the nervous system to identical muscle activation patterns, reducing the dimension of the muscle activity. B2: Due to the dynamics of the musculoskeletal system, translation and rotation perturbations elicit identical somatosensory information. In this scheme, interdependencies in somatosensory information result in common muscle synergies without explicit dimension reduction within the nervous system. C: Two possible relationships between muscle activity patterns and functional motor outputs. C1: Common muscle activity patterns elicit different functional motor outputs depending on biomechanical context. C2: Deterministic relationship between muscle activity patterns and motor outputs.

METHODS

SUMMARY

We considered previously collected data of seven cats during translation and rotation perturbations. To estimate somatosensory information and motor outputs, we calculated the mean changes in the angles and angular velocities of joints from across the body, as well the changes in reaction forces at the ground, during a *somatosensory input* time window immediately after perturbation onset and during a *motor output* time window after the onset of muscle activity. We assembled these mean values, as well as average muscle activity during the initial burst of the APR, into matrices and estimated their dimension using PCA based on the data correlation matrix. We performed three primary analyses. First, to determine whether the dimension of somatosensory information might be limited by the dimension of applied perturbations, we compared the dimension of kinematic and kinetic variables during the somatosensory input period to the nominal dimension of the perturbation and to the dimension of control data that was randomly shuffled. We considered data from both perturbation types separately, comparing their dimension to the nominal perturbation dimension 2, as well as data from both perturbation types together, comparing their dimension to the nominal perturbation dimension 3. Second, to determine whether muscle activity and motor outputs elicited during postural perturbations were of comparable or lower dimension than somatosensory inputs, we directly compared the dimension of somatosensory inputs, muscle activity, and motor outputs. Third, to determine whether translation and rotation perturbations elicited similar or different somatosensory information, muscle activity, and motor outputs, we quantified the similarity between principal component bases identified in each perturbation type using SSD. Additionally, to test whether the sensorimotor transformation could be well-characterized by local feedback of kinematic and kinetic variables, we quantified the similarity between principal component bases identified in the somatosensory input and the motor output periods using SSD. Finally, we compared our results with those of a different formulation of PCA (cov-PCA), as well as with those of NNMF.

EXPERIMENTAL PROCEDURES

Previously-collected data of seven healthy cats (*An*, *Be*, *Kn*, *So*, *Sq*, *St*, and *Wo*) were examined. The unrestrained cats withstood perturbations of the support surface either as translations in the horizontal plane (15 cm/s, 50 mm amplitude) or as rotations in combinations of pitch and roll (40 °/s, 6° amplitude) (Macpherson et al. 1987; Ting and Macpherson 2004). Perturbations were delivered in either 12 or 16 directions depending on the animal (Table A.1). A minimum of five trials of each perturbation direction were collected. Two of the cats received additional translation perturbations in a short stance distance condition wherein the distance between the forelimbs and hindlimbs was reduced by approximately 30%.

Chronic indwelling EMG from 16 left hindlimb muscles and 3D ground reaction forces at each paw were collected at 1,000 Hz. The muscles sampled in each cat are summarized in Table A.2. Raw EMG signals were high-pass filtered at 35 Hz, demeaned, rectified, and low-pass filtered at 100 Hz. EMG signals were normalized to the maximum EMG observed in each muscle over all conditions for each cat. Ground reaction forces were low-pass filtered at 100 Hz. In rotation trials, ground reaction forces were rotated into Earth-based coordinates based on the measured pitch and roll of the platform. Positions of kinematic markers located on the platform and the left (*An*, *Be*, *Kn*, *Wo*) or both (*So*, *Sq*, *St*) sides of the body were collected at 100 Hz and used to estimate sagittal- and frontal-plane joint angles and joint angular velocities. Locations of joint centers were estimated from marker positions by subtracting off joint radii, skin widths, and marker widths. Sagittal- and frontal-plane joint angles were computed from the positions of joint centers. Joint angular velocity time traces were numerically derived from joint angle time traces and low-pass filtered at 5 Hz.

SOMATOSENSORY INPUT , MOTOR OUTPUT, AND EMG QUANTIFICATION

We treated measured kinematic and kinetic variables as proxies for somatosensory information and functional motor outputs. We determined changes in muscle activity, kinematic, and kinetic variables during translation and rotation perturbations by examining changes in mean levels during specific time periods as reported in previous studies (Figure A.3) (Ting and Macpherson 2004). To estimate somatosensory information, during each trial ensembles of joint angles, joint angular

velocities, and ground reaction forces were sampled during a *somatosensory input* time window occurring 0-30 ms after perturbation onset. Baseline levels during a background window 250-100 ms before perturbation onset were removed. Ensembles of electromyograms (EMG) were sampled during background, and during the initial burst of the APR, 60-120 ms after perturbation onset. Only EMG samples during the APR were included in the later dimension analyses. To estimate functional motor outputs, ensembles of joint angles, joint angular velocities, and ground reaction forces were sampled during a *motor output* time window occurring 120-200 ms after perturbation onset during each trial, allowing an appropriate electromechanical delay for muscle activation to dissipate to the periphery. We were interested in changes in kinematic and kinetic variables, which correspond to the disturbances introduced by postural perturbations and the subsequent corrections of the active response, rather than their absolute levels, which may depend on the initial state of the animal (kinematic configuration, phase of postural sway, etc.). Therefore, the mean values for each trial were expressed as changes from one period to the next to highlight changes in slope.

To determine whether the magnitudes of changes in kinematic and kinetic variables during the somatosensory input and motor output periods were comparable across perturbation types, the mean values for each period of each trial were subjected to two-way ANOVA (factors: data type (joint angle, joint angular velocity, or ground reaction force) $\times$ perturbation type (translation vs. rotation)). Results were evaluated at a significance level of $\alpha = 0.05$. Additionally, to determine whether the magnitudes of changes were comparable across time periods, mean values from both perturbation types were pooled and subjected to a second two-way ANOVA (data type $\times$ time period) evaluated at a significance level of $\alpha = 0.05$.

To determine whether muscles tended to activate, rather than deactivate, during the APR, the percentage of trials and muscles in which the APR level was positive with respect to the background level was calculated for each cat. These percentages were subjected to one-way ANOVA on perturbation type ($\alpha = 0.05$), as well as to t-tests against the value corresponding to no bias (50%). Results were evaluated at a

significance level of $\alpha = 0.05$, adjusted with a Bonferroni correction for multiple comparisons ($\alpha = 0.025$; n = 2).

DIMENSION ESTIMATION WITH PCA

The dimension of ensembles of joint angles, joint angular velocities, forces, and EMG data for each cat was estimated with PCA. Each experimental variable for each cat was first normalized to have unit variance over all available samples of each perturbation type, to ensure that each variable was expressed on a consistent scale during different time periods and that each variable was counted equally in the subsequent analyses. We primarily considered data from translation and rotation perturbations separately; however, in some cases data from both perturbation types were pooled before dimension estimation.

The data were then assembled into matrices grouped by variable type and by time period. Principal components (PCs) were then calculated as the eigenvectors of the correlation matrix of each data matrix. In this formulation of PCA, the amount of variance contributed by each PC (also referred to as the *latent variance*) is described directly by the associated eigenvalue. PCs corresponding to eigenvalues ≥ 1.0 explain more variance than any given variable of the original dataset and are typically retained; others are typically discarded (Basilevsky 1994; Widmer et al. 2003). We therefore defined dimension to be the number of PCs corresponding to eigenvalues ≥ 1.0. As a control condition, the dimension of each data matrix was typically determined before and after the elements of the matrix were randomly shuffled to remove correlation structure (Gentner and Classen 2006).

IDENTIFICATION OF SHARED COMPONENTS WITH SSD

We quantified the similarity between identified sets if PCs with their shared subspace dimensionality, or SSD (Cheung et al. 2005; Gentner and Classen 2006). SSD is a scalar that quantifies the number of principal angles between two subspaces that are smaller than a threshold value. To illustrate the idea of principal angles, consider two intersecting planes embedded in 3D space. The vector corresponding to their intersection is common to both planes, and the first principal angle between the subspaces is therefore angle between the intersection vector within the first plane and the intersection vector in

the second plane: 0°. The second principal angle is then the angle that one would commonly imagine between the two planes.

Given a pair of PC matrices, with each column corresponding to a basis vector and each row corresponding to a variable, the SSD analysis proceeds as follows. The principal angles between the subspaces are first calculated numerically (subspacea.m, Knyazev and Argentati 2002). After the principal angles are calculated, the SSD is defined to be the number of principal angles with cosines ≥ 0.90; equivalent to the number of principal angles in the interval (-25°,25°). In the case of fully overlapping subspaces, the SSD will be equal to the number of columns in the narrower of the two matrices. For this reason, we performed statistical comparisons on SSD values normalized to this maximum. SSD values normalized in this way describe whether two vector subspaces are mutually perpendicular (SSD=0), completely coplanar (SSD=1), or partially coplanar ($0 \leq SSD \leq 1$).

COMPARISON OF SOMATOSENSORY INPUT DIMENSION TO PERTURBATION DIMENSION AND TO SHUFFLED DATA

To determine whether somatosensory information is limited by the dimension of applied postural perturbations, we directly compared the dimension of kinematic and kinetic variables during the somatosensory input period to the dimension of the applied perturbations. We subjected the dimension estimates of somatosensory input variables across cats to a two-way ANOVA (data type × perturbation type). Data were pooled across factors that failed initial F-tests and subjected to one-tailed t-tests against the perturbation dimension (2). Results were evaluated at a significance level of $\alpha = 0.05$, adjusted with a Bonferroni correction for multiple comparisons ($\alpha = 0.0167$; $n = 3$). Additionally, we performed similar tests on the dimension of kinematic and kinetic data pooled from both translation and rotation perturbations. We subjected these data to a one-way ANOVA (data type). Data were pooled across factors that failed initial F-tests and subjected to one-tailed t-tests against the dimension of combined translation and rotation perturbations (3). Results were evaluated at a significance level of $\alpha = 0.05$, adjusted with a Bonferroni correction for multiple comparisons ($\alpha = 0.0167$; $n = 3$).

Next, to determine whether the correlation structure of somatosensory information reflected the dynamics of the musculoskeletal system as excited by the postural perturbations rather than random noise, we compared the dimension of somatosensory information before and after shuffling the data to disrupt the correlation structure. We performed a three-way ANOVA on the pooled somatosensory information dimension and shuffled data dimension (structure (data vs. shuffled data) × data type × perturbation type) evaluated at significance level of $\alpha = 0.05$. All averaged data are presented as means ± SD.

COMPARISON OF MOTOR OUTPUT DIMENSION AND SENSORY INPUT DIMENSION

To determine whether the nervous system reduces the dimension of somatosensory information in patterning muscle activity and motor outputs, we directly compared the dimension of somatosensory input and motor output variables. Dimension values were pooled across cats and subjected to three-way ANOVA (time window (somatosensory input vs. motor output or APR) × data type × perturbation type) at a significance level of $\alpha = 0.05$.

Additionally, to determine whether the correlation structure exhibited by motor outputs was significant, we compared the dimension of motor outputs before and after shuffling the data. The pooled motor output dimension and shuffled data dimension were subjected to a three-way ANOVA (structure × data type × perturbation type) evaluated at significance level of $\alpha = 0.05$.

COMPARISON OF PRINCIPAL COMPONENTS ACROSS TRANSLATION AND ROTATION PERTURBATIONS AND POSTURAL CONFIGURATIONS

To determine whether translation and rotation perturbations elicited identical or different somatosensory information and motor responses, we quantified the normalized SSD between sets of PCs identified in translation and rotation perturbations during both the sensory input and motor output periods. We subjected the normalized SSD values to a two-way ANOVA (data type × time window). Data were pooled across factors that failed initial F-tests and subjected to one-tailed t-tests against the value corresponding to

complete similarity (1). Results were evaluated at a significance level of $\alpha = 0.05$, adjusted with a Bonferroni correction for multiple comparisons ($\alpha = 0.0071$; n = 7). Additionally, to determine the degree to which EMG PCs were shared across postural configurations, we also quantified the SSD between sets of EMG PCs identified during translation perturbations in the preferred and short postural configurations. Because only two animals (*Be* and *Sq*) received perturbations in the short postural configuration, these results are presented without detailed statistical analysis.

COMPARISON OF PRINCIPAL COMPONENTS ACROSS THE SOMATOSENSORY INPUT AND MOTOR OUTPUT PERIODS

To determine whether changes in kinematic and kinetic variables were similar during the somatosensory input and motor output periods, as would be expected in a mechanical system dominated by mechanical feedback, we computed the SSD between sets of PCs identified during the somatosensory input and motor output periods. We subjected the normalized SSD values to a two-way ANOVA (data type $\times$ perturbation type). Data were pooled across factors that failed initial F-tests and subjected to t-tests against the value corresponding to complete similarity (1). Results were evaluated at a significance level of $\alpha = 0.05$, adjusted with a Bonferroni correction for multiple comparisons ($\alpha = 0.025$; n = 2).

COMPARISON WITH COVARIANCE-PCA AND NNMF

To verify the robustness of our dimension estimates, we compared the results of the primary, correlation-matrix based PCA with those of two alternative methods of dimension estimation. We first subjected kinematic and kinetic data to an alternative formulation of PCA based on the eigenvectors and eigenvalues of the data covariance matrix (covariance-PCA). In this formulation, dimension was defined as the number of covariance-PCs required for cumulative data reconstruction $R^2 \geq 0.90$. Dimension estimates of kinematic and kinetic variables from covariance-PCA and correlation-PCA were pooled and subjected to a three-way ANOVA (method (correlation-PCA vs. covariance-PCA) $\times$ time window $\times$ perturbation type) at a significance level of $\alpha = 0.05$. Second, the dimension of EMG data was estimated with both covariance-PCA and

nonnegative matrix factorization (NNMF) (Torres-Oviedo et al. 2006; Tresch et al. 1999). In this formulation, dimension was defined as the number of identified muscle synergies required for cumulative data VAF ≥ 0.90 (Torres-Oviedo et al. 2006). Dimension estimates of EMG were pooled from NNMF, covariance PCA, and correlation-PCA and subjected to a two-way ANOVA (method (correlation-PCA vs. covariance-PCA vs. NNMF) $\times$ perturbation type) at a significance level of $\alpha = 0.05$.

Table A.1. Summary of experimental conditions across cats.

	Pert Type	Stance	*An*	*Be*	*Kn*	*So*	*Sq*	*St*	*Wo*
# trials	translation	preferred	250	158	259	64	143	221	184
		short		181			169		
	rotation	preferred	225	233	220	166	164	185	
# directions	translation		16	12	16	12	12	16	16
	rotation		16	12	16	12	12	12	
kinematics			L	L+R	L	L+R	L+R	L+R	L

Abbreviations: L and R, left and right side kinematics.

Table A.2. Inclusive list of muscles recorded across cats.

Label	Muscle Name	*An*	*Be*	*Kn*	*So*	*Sq*	*St*	*Wo*
ADFM	*adductor femoris*		•		•	•		
BFMA	*biceps femoris anterior*		•		•	•		
BFMM	*biceps femoris medialis*	•	•	•	•	•		•
BFMP	*biceps femoris posterior*	•	•			•		
EDL	*extensor digitorum longus*	•	•		•	•		
FDL	*flexor digitorum longus*		•		•	•		
FHL	*flexor hallicus longus*		•		•	•		
GLUT	*gluteus*	•		•			•*	•
GRAC	*gracilis*		•			•		
ILPS	*Iliopsoas*			•				
LGAS	*lateral gastrocnemius*	•			•		•	•
MGAS	*medial gastrocnemius*	•	•			•		
PERB	*peroneus brevis*		•		•	•		
PLAN	*plantaris*	•			•	•		
PSMA	*psoas major*	•						
REFM	*rectus femoris*	•	•	•	•	•		•
SEMA	*semitendinosus anterior*		•	•	•			
SEMP	*semitendinosus posterior*	•	•	•	•	•		•
SOL	*soleus*	•		•			•	
SRTA	*sartorius anterior*	•	•	•	•	•		•
STEN	*semitendinosus*	•	•	•	•			•
TERM	*teres major*			•			•	•
TFL	*tensor fascia latae*	•						
TIBA	*tibialis anterior*	•		•	•	•		•
VLAT	*vastus lateralis*			•				
VMED	*vastus medialis*	•	•		•	•	•	

The designator * indicates that the muscle was recorded in the right hindlimb; other muscles were recorded in the left hindlimb.

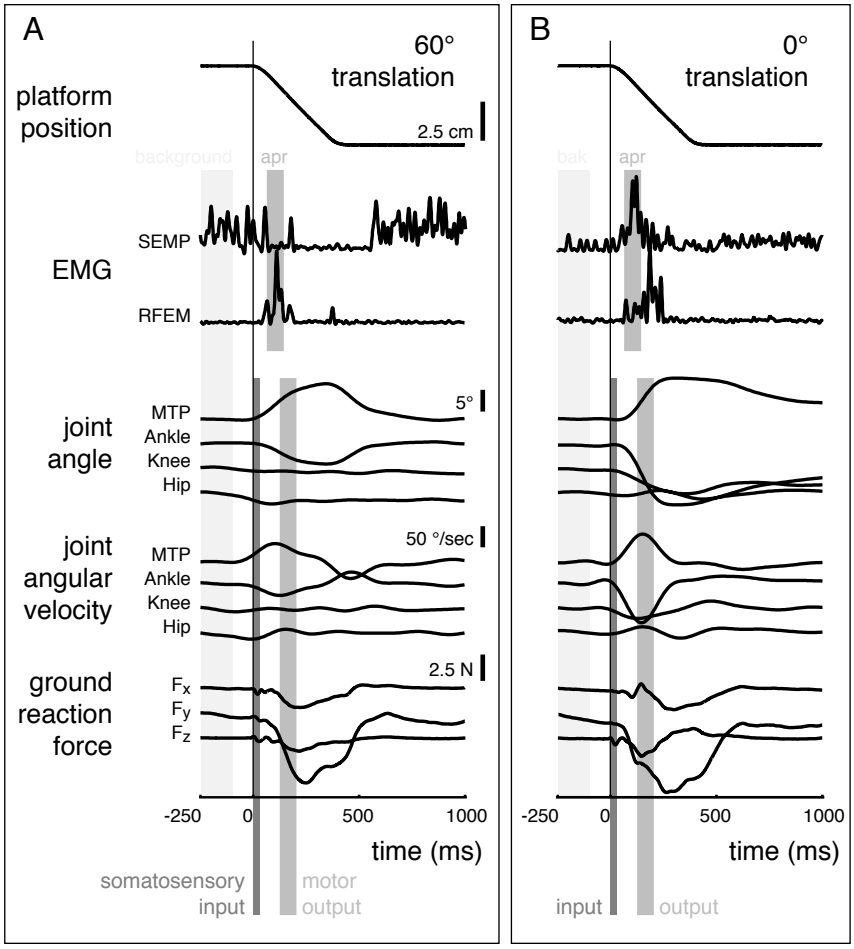

Figure A.3. Time windows used to estimate somatosensory input and motor output variables and muscle activation. A: changes in experimental variables from the left hindlimb during a translation perturbation towards 60°, diagonally forward and to the right. Sagittal-plane joint angles and joint angular velocities are shown. Shaded areas below EMG traces represent the background period and the initial burst of the APR. Other shaded areas the somatosensory input and motor output time periods. Note that the motor output period is earlier for electromyographic (EMG) than for biomechanical variables to account for neuromechanical delay. B: the same variables during a translation perturbation towards 0°. Background muscle activity depended on the state of the animal at the beginning of each trial: SEMP is inactivated during the motor output period in A but is activated during the motor output period in B, while REFM is activated in both. The level of background postural tone depends the state of the animal.

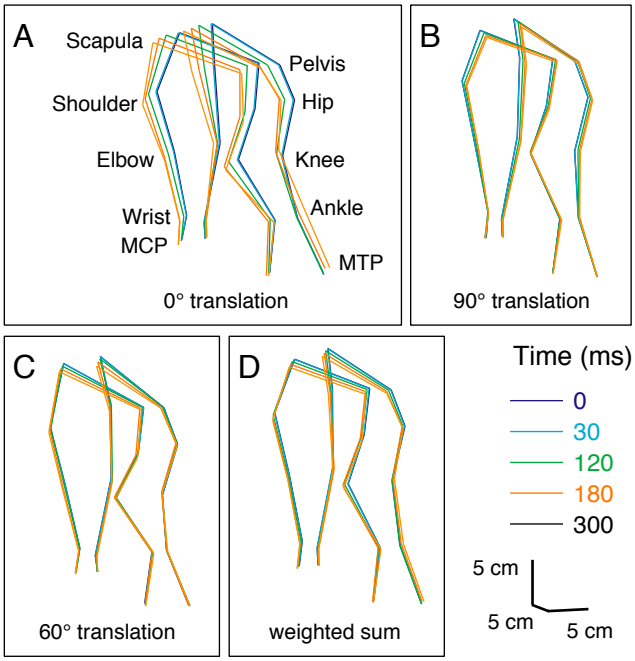

Figure A.4. Direction-dependent differences in joint kinematics during support-surface translations. A-C: Examples of joint motions induced by translation perturbations towards: A, 0°, rightward, B, 90°, forward, C, 60°, diagonally rightwards and forward. Large joint motions are induced by 0° perturbations, the direction in which the animal is the most biomechanically compliant. Smaller joint motions with different patterns of covariation are induced by 90° and 60° perturbations. D: Weighted sum of A and B for illustration of biomechanical nonlinearities. Although C and D are similar in general, the effects of 60° perturbations are not a simple sum of those of 0° and 90°. Note the additional motions at the knee and hip in the weighted sum that are suppressed in the 60° perturbation, the direction in which the animal is the most biomechanically stiff. Note that in all cases the animal does not return to a fully upright position until after the end of platform motion (> 300 ms).

RESULTS

SUMMARY

During the somatosensory input period, translation and rotation perturbations of the support surface caused small changes in the angles and angular velocities of joints throughout the body, as well as ground reaction forces at the feet. PCA revealed that these changes had more than two significant principal components. Although the number of significant principal components was equivalent between translation and rotation

perturbations, subsequent SSD analyses revealed that the components themselves were only partially shared across translation and rotation perturbations. Coordinated EMG activity during the initial burst of the APR in muscles throughout the hindlimb was also characterized by more than two significant principal components, but fewer than the number identified in somatosensory input variables. The number of significant EMG principal components was equivalent to the number of nonnegative muscle synergies identified through NNMF. Subsequent analyses revealed that EMG principal components were only partially shared across translation and rotation perturbations, but were completely shared between preferred- and short-stance distance conditions in both animals for which short-stance distance trials were available. After the onset of EMG activity, changes in the angles and angular velocities of joints throughout the body, as well as ground reaction forces at the feet during the motor output period were characterized by significant principal components that were fewer in number than those identified during the somatosensory input period.

TIMECOURSE OF RESPONSES TO POSTURAL PERTURBATIONS

Perturbations caused small, immediate changes in the angles and angular velocities of joints throughout the body and ground reaction forces at the feet during the sensory input period (Figure A.4). The magnitudes of these disturbances varied between translation and rotation perturbations ($p \leq 0.03$; $F(1,33)=5.1$). Rotation perturbations elicited larger initial disturbances in joint angles and joint angular velocities in comparison to translation perturbations, but smaller initial disturbances in ground reaction forces. This effect was quantified as a significant interaction between perturbation type and data type ($p < 0.01$; $F(2,33) = 4.9$). Across animals, the grand mean absolute change in joint angles during the sensory input period increased from $0.4 \pm 0.1°$ in translation to $0.7 \pm 0.2°$ in rotation. Similarly, the grand mean absolute change in joint angular velocities during the sensory input period increased from $8.5 \pm 2.5°$/sec in translation to $22.7 \pm 16.8°$/sec in rotation. In contrast, the grand mean absolute change in ground reaction forces during the sensory input period decreased from 0.2 ± 0.05 N in translation to 0.08 ± 0.01 N in rotation.

Animals exhibited coordinated muscle activity in response to the kinematic and kinetic disturbance introduced by the perturbations during the motor output period.

Muscles primarily activated, rather than deactivated, with respect to the level during the background period ($p < 0.025$; t-test, Bonferroni correction), although this bias was more pronounced in translation than rotation perturbations ($p << 0.001$; $F(1,11) = 65.4$). Across cats and sampled muscles, activation with respect to the background level was observed in 74 ± 3% of muscles and trials in translation and in 57 ± 5% of muscles and trials in rotation.

Kinematic and kinetic variables exhibited changes during the motor output period that were significantly larger than the changes observed during the sensory input period ($p < 0.021$; $F(1,74) = 10.2$). Across animals and perturbation types, the grand mean absolute change in joint angles increased from 0.6 ± 0.1° during the sensory input period to 4.8 ± 1.8° during the motor output period. The grand mean absolute change in joint angular velocities increased from 14.3 ± 8.6°/sec during the sensory input period to 28.8 ± 8.6°/sec during the motor output period, and the grand mean absolute change in ground reaction forces increased from 0.1 ± 0.03 N during the sensory input period to 1.1 ± 0.3 N during the motor output period. Horizontal plane forces exhibited the characteristic isotropic pattern during the sensory input period and center-of-mass directed anisotropic pattern during the motor output period first described by Macpherson as the force constraint strategy (Macpherson 1988a; Ting and Macpherson 2004). The magnitudes of changes in kinetic and kinematic variables during the motor output period exhibited a similar dependence on perturbation type as during the sensory input period. There was a strong main effect of perturbation type ($p << 0.001$; $F(1,33) = 67.8$) as well as a strong interaction effect, as changes to joint angles and joint angular velocities increased, whereas changes to force magnitude decreased, in rotation perturbations vs. translation perturbations ($p << 0.001$; $F(2,33) = 43.2$). Across animals, the grand mean absolute change in joint angles during the motor output period increased from 2.1 ± 0.6° in translation to 8.6 ± 1.6° in rotation. The grand mean absolute change in joint angular velocities during the motor output period increased from 15.9 ± 3.4°/sec in translation to 46.4 ± 10.9°/sec in rotation, and the grand mean absolute change ground reaction forces during the motor output period decreased from 1.7 ± 0.6 N in translation to 0.5 ± 0.07 N in rotation.

COMPARISON OF SOMATOSENSORY INPUT DIMENSION AND PERTURBATION DIMENSION

Across animals and perturbation types, kinematic and kinetic variables during the somatosensory input period were significantly higher-dimension than 2 ($p \leq 0.0167$), although perturbations were dimension 2 by construction. Across animals and perturbation types, the grand mean dimension of changes in kinematic and kinetic variables during the sensory input period was 8.7 ± 2.3 for joint angles, 8.2 ± 2.0 for joint angular velocities, and 3.5 ± 0.5 for forces. Tukey-Kramer tests applied post-hoc revealed that forces were significantly lower dimension than joint angles and joint angular velocities ($p<0.0001$). Inspection of the plots of the latent variances of the principal components suggested that significant correlation structure existed in the somatosensory information (Figure A.5). The first several components contributed variance greater than the 1.0 threshold, giving the plots characteristic steep curves. The number of components greater than the threshold was unchanged across translation and rotation perturbations ($p \leq 0.20$; $F(1,35) = 5.3$) but did depend on the data type ($p<<0.01$; $F(2,35) = 34.7$). Similar results were obtained when we examined data that was pooled from translation and rotation perturbations before dimension estimation. There was a highly significant effect of data type ($p<<0.01$; $F(2,17) = 20.57$). Across animals, the grand mean dimension was 8.8 ± 1.9 for joint angles, 7.8 ± 1.7 for joint angular velocities, and 3.5 ± 0.5 for forces; also similarly, forces were significantly lower dimension than joint angles and joint angular velocities ($p<0.001$). The only primary difference was observed in the t-test results against the combined perturbation dimension. Although the joint angle and joint angular velocity data were significantly higher dimension than the combined perturbation dimension 3, the force data was not significantly greater after Bonferroni correction ($p<0.038$).

Kinematic and kinetic variables during the somatosensory input period were significantly lower-dimension than structureless data ($p \leq 0.0001$; $F(1,73)=29.9$) in both translation and rotation perturbations ($p \leq 0.18$; $F(1,73)=1.8$). Across animals, perturbation types, and data types, the grand mean effect of shuffling the data was to raise the dimension from 6.8 ± 2.9 to 9.9 ± 4.3. Comparison of the plots of the latent variances of the principal components of the original and shuffled data suggested that the plots of shuffled

data were less steep in general, with additional eigenvalues greater than the 1.0 threshold (Figure A.3). Structureless data did retain the dimension dependence on data type from original data ($p \leq 0.0001$; $F(2,73)=43.99$). Across animals and perturbation types, the grand mean dimension of changes in shuffled kinematic and kinetic variables during the sensory input period was 12.0±3.7 for joint angles, 12.1±3.9 for joint angular velocities, and 5.6±0.8 for forces.

COMPARISON OF SOMATOSENSORY INPUT DIMENSION AND MOTOR OUTPUT DIMENSION

EMG, kinematic and kinetic variables during the motor output period were significantly lower-dimension than kinematic and kinetic variables during the somatosensory input period ($p << 0.0001$, $F(1,85)=34.6$) (Figure A.4). Across animals, data types, and perturbation types, somatosensory variables of were higher dimension than motor output variables and EMG (grand mean 6.8 ± 2.9 vs. 4.4 ± 2.2). Dimension values were unchanged across translation and rotation perturbations ($p \leq 0.39$; $F(1,85) = 0.7$) but depended strongly on the data type ($p << 0.0001$; $F(3,85) = 59.6$). Across animals and perturbation types, the grand mean dimension of changes in kinematic and kinetic variables during the motor output period, as well as EMG during the APR, was 6.2±1.1 for joint angles, 6.2±1.6 for joint angular velocities, 2.1±0.3 for forces, and 3.2±1.2 for EMG. Tukey-Kramer tests applied post-hoc revealed that contrasts between all data types except for that between joint angles and joint angular velocities were significant ($p \leq 0.05$). The grand mean dimension of changes in kinematic and kinetic variables during the motor output period, excluding EMG, was 4.8 ± 2.2.

The dimension of changes in kinematic and kinetic variables during the motor output period, as well as EMG during the APR, was significantly lower than that of structureless data ($p \leq 0.0001$; $F(1,98)=107.0$) in both translation and rotation perturbations ($p \leq 0.39$; $F(1,98)=0.74$), similar to the case of somatosensory information. Across animals, perturbation types, and data types, the grand mean effect of shuffling the motor output and EMG data was to increase the dimension from 4.4 ± 2.2 to 8.8±3.9. Structureless data retained the dimension dependence on data type from original data ($p \leq 0.0001$; $F(3,98)=41.5$). Across animals and perturbation types, the grand mean dimension of changes in shuffled kinematic and kinetic variables during the motor output

period, as well as EMG during the APR, was 11.7±3.8 for joint angles, 11.6±3.5 for joint angular velocities, 5.7±0.5 for forces, and 6.1±1.6 for EMG. An additional F-test applied post-hoc revealed that there was no significant difference in shuffled kinematic and kinetic data dimension between the sensory input and motor output periods ($p \leq 0.81$; $F(1,76)=0.06$).

COMPARISON OF PRINCIPAL COMPONENTS ACROSS TRANSLATION AND ROTATION PERTURBATIONS AND POSTURAL CONFIGURATIONS

SSD analysis suggested that somatosensory input PCs were more common across translation and rotation perturbations than motor output and EMG components ($p \leq 0.016$; $F(1,41)=6.4$), although the grand mean difference in normalized SSD magnitude was small: 0.39±0.17 for somatosensory inputs vs. 0.33±0.25 for motor outputs and EMG. Normalized SSD values depended strongly on data type ($p \leq 0.001$; $F(3,37)=9.2$). The grand mean values of normalized SSD across translation and rotation perturbations were: joint angles: 0.39±0.08, somatosensory, 0.23±0.10, motor; joint angular velocities: 0.33±0.08, somatosensory, 0.11±0.09, motor; forces: 0.47±0.27, somatosensory, 0.42±0.20, motor; EMG: 0.58±0.25, APR. All grand mean normalized SSD values were significantly less than 1.0, the number that would be expected if translation and rotation perturbations elicited identical somatosensory information or motor responses ($p \leq 0.00714$, t-tests with Bonferroni correction, n=7). Significant contrasts between EMG and joint angles ($p \leq 0.05$, Tukey-Kramer tests applied post-hoc) motivated an additional post-hoc F-test that revealed that pooled force and EMG components were significantly more common across translation and rotation perturbations than joint angle and joint angular velocity components (0.44±0.21 vs. 0.29±0.20; $p<0.03$; $F(1,40)=4.96$). Unnormalized grand mean values of SSD across translation and rotation perturbations were: joint angles: 3.5±1.4, somatosensory, 1.3±0.5, motor; joint angular velocities: 2.5±1.0, somatosensory, 0.7±0.5, motor; forces: 1.5±08, somatosensory, 0.8±0.4, motor; EMG: 1.5±0.6, APR. In both animals that received perturbations in the short stance conditions, the EMG principal component bases were completely shared, resulting in SSD values of 1.0.

COMPARISON OF KINEMATIC AND KINETIC PRINCIPAL COMPONENTS ACROSS THE SOMATOSENSORY INPUT AND MOTOR OUTPUT PERIODS

Normalized SSD values suggested that joint angle, joint angular velocity, and force PCs were more shared across the somatosensory input and motor output periods in rotation than in translation perturbations ($p \leq 0.0035$; $F(1,35)=9.8$). Grand mean normalized SSD across the somatosensory and motor periods increased from 0.31±0.26 in translation to 0.55±0.18 in rotation. This effect was equivalent across data types ($p \leq 0.73$; $F(2,35)=0.32$).

COMPARISON WITH COVARIANCE-PCA AND NNMF

Dimension estimates of kinematic and kinetic variables were significantly higher with covariance-PCA than with correlation-PCA ($p << 0.0001$; $F(1,150)=265.2$). Across animals, perturbation types, data types, and time windows, the grand mean dimension estimate of changes in kinematic and kinetic variables with covariance-PCA was 14.5±6.1, significantly higher than the estimate with correlation-PCA, 5.8±2.8. This contrast was observed in both translation and rotation perturbations ($p \leq 0.18$; $F(1,150)=1.8$) and in both the sensory input and motor output epochs ($p > 0.05$; $F(1,150)=3.9$). Inspection of the plots of cumulative reconstruction R^2 revealed curves that were markedly less steep than the latent variance plots considered in the correlation-PCA, suggesting that the covariance-PCA was compressing less variance in total into the first few components than correlation-PCA (Figure A.7).

EMG dimension estimates were significantly higher with covariance-PCA than with correlation-PCA ($p << 0.0001$; $F(2,35)=66.0$, Tukey-Kramer post-hoc tests), but not significantly different with NNMF ($p \leq 0.70$). These contrasts were observed in both translation and rotation perturbations ($p \leq 0.52$; $F(1,35)=0.42$). Inspection of the plots of cumulative reconstruction VAF revealed characteristic curves with a sharp bend around the number of identified synergies, typically 3 or 4. Across animals and perturbation types, the grand mean EMG dimension estimates were 3.2±1.2 for correlation-PCA, 2.3±1.0 for NNMF, and 11.1±3.3 for covariance-PCA.

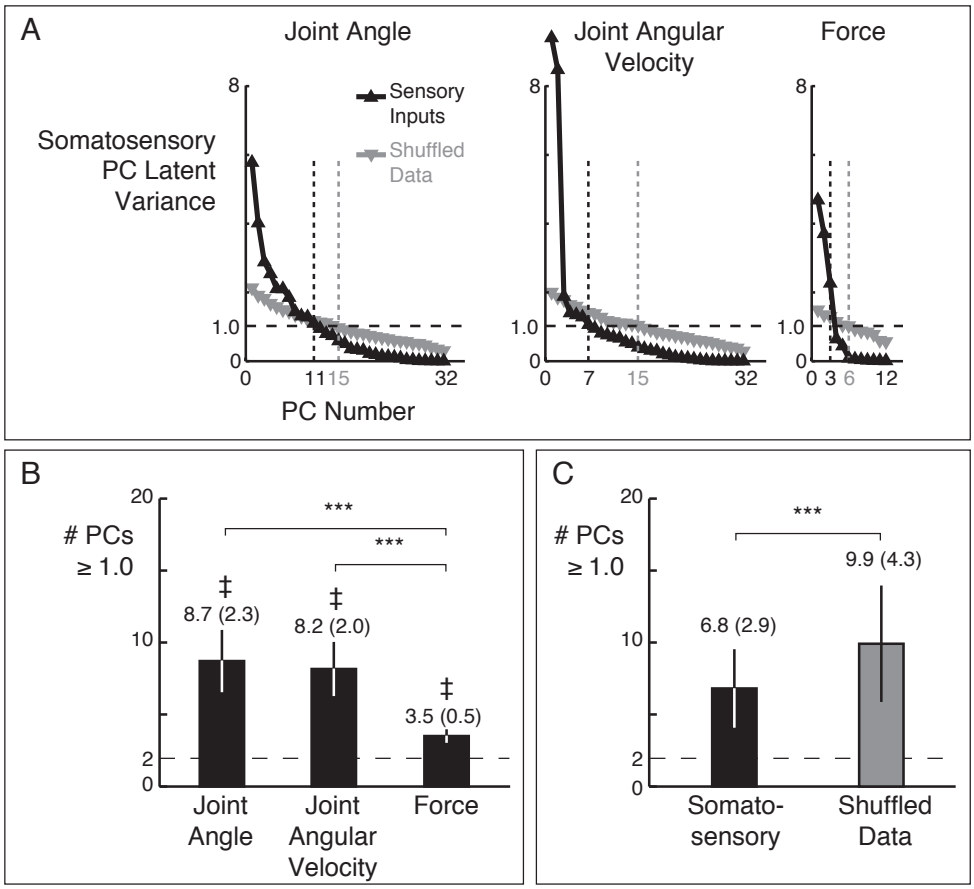

Figure A.5. Comparison of somatosensory information dimension to perturbation dimension and to shuffled data. A: Latent variance of PCs of kinematic and kinetic variables during the somatosensory period in translation perturbations in cat Be; rotation perturbations were similar. Left to right: joint angles, joint angular velocities, ground reaction forces. Higher-order principal components contribute less variance and can be neglected. Dashed vertical lines (black: data; gray: shuffled data) designate dimension, the number of PCs over the 1.0 threshold (dashed horizontal line). Variability in sensory variables (black) is compressed into fewer principal components than shuffled data (gray), such that the curve is more sharply concave upward with fewer singular values above the threshold. B: Comparison of somatosensory information dimension to perturbation dimension. Dashed line: dimension of applied perturbations, 2.0. Significant contrasts: ‡, $p \leq 0.0167$, t-test for mean = 2; ***$p < 0.0001$, ANOVA, Tukey-Kramer post-hoc tests. C: Comparison of somatosensory information dimension to shuffled data dimension. ***$p < 0.0001$, ANOVA.

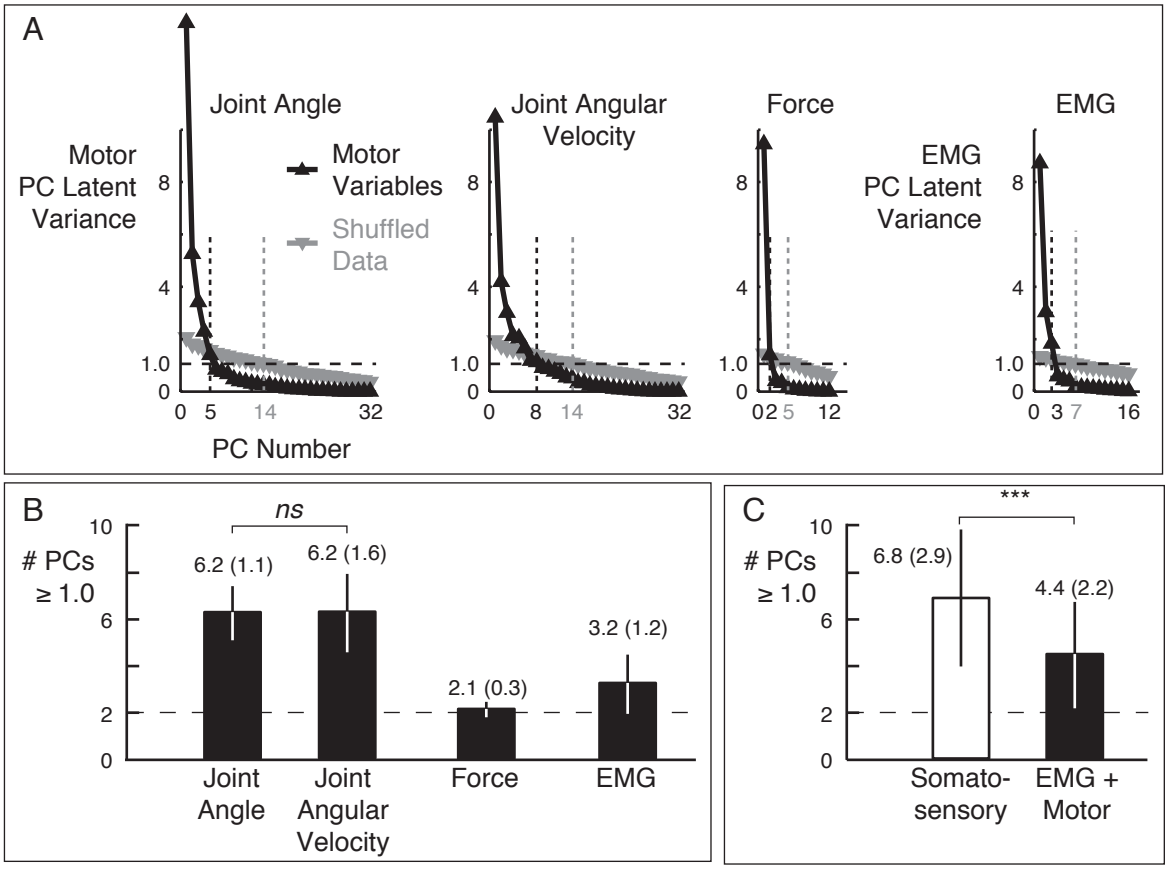

Figure A.6. Comparison of motor output dimension to somatosensory input dimension. A: Latent variance of PCs of kinematic, kinetic, and EMG variables during the motor output period in translation perturbations in cat Be; rotation perturbations were similar. Left to right: joint angles, joint angular velocities, ground reaction forces, EMG. Annotations as in Figure 4. B: Grand mean dimension of motor output variables across animals and perturbation types. Contrasts except for that marked ns are significant ($p \leq 0.05$, ANOVA, Tukey-Kramer post-hoc tests). C: Comparison of motor output dimension to somatosensory information dimension across animals, perturbation types, and data types. ***$p \leq 0.0001$, ANOVA.

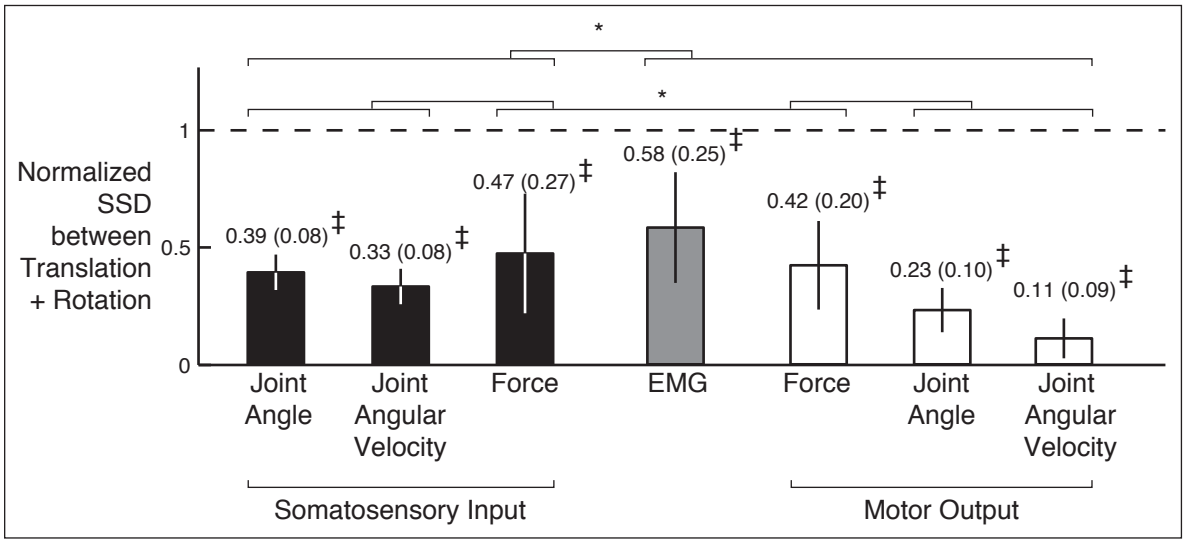

Figure A.7. Comparison of PCs across translation and rotation perturbations. Normalized SSD values less than 1.0 (dashed line) describe component bases that are partially orthogonal in translation and rotation perturbations. Black bars: somatosensory inputs. Gray bar: EMG. White bars: motor outputs. ‡, $p<0.00714$, t-test for mean = 1; *$p\leq0.05$, ANOVA.

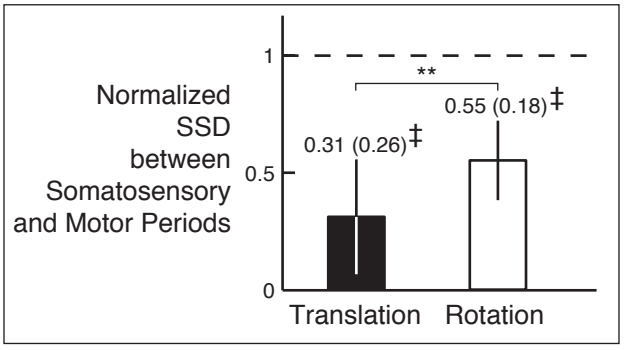

Figure A.8. Comparison of PCs across somatosensory input and motor output periods. Black bar: translation perturbations. White bar: Rotation perturbations. ‡, $p<0.025$, t-test for mean = 1; **$p<0.01$, ANOVA.

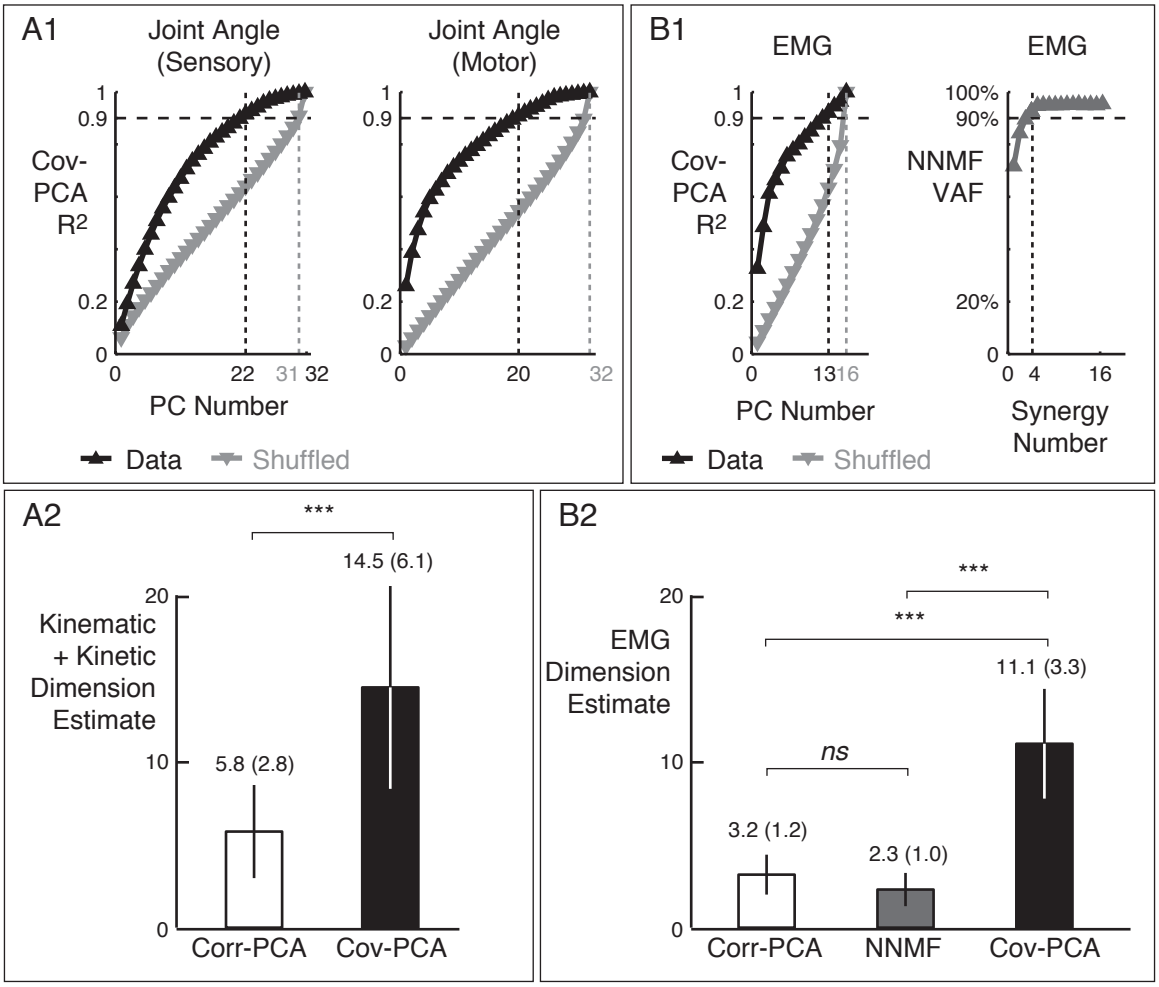

Figure A.9. Comparison of dimension estimates from correlation-PCA, covariance-PCA, and NNMF. A1: Representative plots of cumulative reconstruction R^2 for covariance-PCA of joint angle data during translation perturbations in cat Be; rotation perturbations, joint angles, and force data were similar. Left: somatosensory input period. Right: motor output period. Annotations as in Figure 4. B1: Plots of cumulative EMG reconstruction R^2 for covariance-PCA, and cumulative reconstruction VAF for NNMF, translation perturbations in Be. Left: covariance-PCA. Right: NNMF. A2: Comparison of grand mean dimension estimates of joint angles, joint angles, and forces with correlation-PCA and covariance-PCA. ***$p<0.0001$, ANOVA. B2: Comparison of grand mean EMG dimension estimates with correlation-PCA, NNMF, and covariance-PCA. ***$p<0.0001$; ns: $p<0.70$, ANOVA, post-hoc tests.

DISCUSSION

We demonstrated that two different types of planar postural perturbations caused disturbances to joint angles, joint angular velocities, and ground reaction forces that were greater than two-dimensional, and that exhibited more structure than would be expected by simple chance. We conclude that the identified components reflect the dynamics of the musculoskeletal system, as excited by the postural perturbations, and that somatosensory estimates derived directly from those variables will be greater than two-dimensional as well. Subsequent corrections in kinematic and kinetic variables due to the APR were lower-dimension than the original disturbances. We conclude that rather than the one-to-one mapping from disturbances to responses that would be expected with direct local feedback, the sensorimotor transformation from somatosensory information to motor responses must reduce the dimension of somatosensory information.

The somewhat counterintuitive idea that nominally planar postural perturbations can elicit changes in biomechanical variables of a higher dimension highlights a difference between unrestrained balance tasks and other motor paradigms. Here, with the intention of identifying lower bounds on the estimates of dimension of somatosensory variables, we performed a dimension analysis (correlation-PCA) that we regarded as conservative. The substantially increased dimension estimates we observed with covariance-PCA corroborate this interpretation. But even considering the lower bound dimension estimates obtained with correlation-PCA, we must conclude that in the unrestrained task presented here, planar perturbations are made more complex in the redundant kinematic chain due to the effects of gravity, and their effects vary depending on the animal's state, e.g., the phase of postural sway, and the level of background muscle tone. In other studies, even factors such as emotional state have been implicated as modulators of postural responses (Adkin et al. 2002). In contrast, in reaching tasks using a planar exoskeleton (e.g., Kurtzer et al. 2006), the mechanical dimensionality of the exoskeleton (two) may uniquely determine the dimensionality of the required joint torques (two) and the dimensionality of the required muscle activity patterns (two). Here, we conclude that the dimension of biomechanical variables reflect the dynamics of the musculoskeletal system, as excited by the postural perturbations, whereas in the exoskeleton case, the dimension reflects the dynamics of the experimental apparatus.

These data suggest that the CNS conveys higher-dimension somatosensory information to lower-dimension EMG and motor outputs. This finding, although relatively straightforward, is important because in most motor tasks, it is difficult to differentiate observed dimension constraints between neural or biomechanical sources (Macpherson 1991). During motor tasks, kinematic variables typically co-vary to some degree. It has been proposed that these patterns of co-variation may reflect specific control policies within the nervous system that couple kinematic variables into controlled degrees of freedom (Blickhan 1989; Ivanenko et al. 2008) while projecting irreducible motor noise into redundant, uncontrolled degrees of freedom (Scholz and Schöner 1999). But because neural outputs are transformed through biomechanical structures such as tendon networks, measured kinematic outputs can also reflect dimensional reduction in the biomechanical system (Gentner and Classen 2006; Schieber and Santello 2004). In some cases, such as the planar covariation of joint angles during locomotion, some dimensionality reduction is guaranteed by biomechanics alone (Bosco et al. 2000). Despite these examples, in many studies, biomechanical constraints on dimension are often ignored, simply because they are so difficult to quantify.

Because this study considered primarily the input-output relationships of the CNS during postural control, rather than specific underlying mechanisms (Figure 1), these results must be considered within a broader context in order to form hypotheses regarding the neural bases of this dimension reduction. The neural substrates that form and modify muscle activity for standing balance control are likely distributed throughout the spinal cord, with higher centers possibly contributing descending drive (Deliagina et al. 2008) and modulatory effects at long latencies (Jacobs and Horak 2007). Decerebrate cats can exhibit appropriate muscle tuning curves (Honeycutt et al. 2009), while spinalized cats exhibit disrupted responses to perturbation (Macpherson and Fung 1999). Because this organization is so diffuse, it could implement many candidate sensorimotor transformations.

One interpretation of these data is that the CNS may select and respond to only certain aspects, or even entire modalities, of the sensory inflow, so that multiple patterns of sensory information may elicit the same motor responses. Here, we noted that EMG and force data were lower dimension and were significantly more shared across

translation and rotation perturbations than kinematic data. These results could be taken to suggest that these elements are encoded within the nervous system and therefore conserved across conditions, whereas kinematic variables are not. Consistent with this hypothesis, the changes in the angles of ground reaction forces were previously implicated as the only variables that could consistently predict the direction of CoM acceleration, and therefore the antecedent muscle activity (Ting and Macpherson 2004). The primary difficulty with this interpretation is that proprioceptive information regarding angles and angular velocities of joints throughout the hindlimb is known to be represented at the dorsal root level during locomotion in afferents from multiple sensory modalities (Weber et al. 2007). Similarly, more abstract kinematic estimates of the length and orientation of the hindlimb is represented in the dorsal spino-cerebellar tract (Bosco et al. 2000). In contrast, although force has been implicated as an encoded variable in motor cortex (Georgopoulos et al. 1992), neurophysiological evidence regarding the nervous system encoding of ground reaction force is sparse. Finally, the fact that subjects are able to compensate for disrupted proprioceptive information including disrupted ground reaction force feedback (Peterka 2002) suggests that this simple explanation may be too limited.

These data are also consistent with the hypothesis that the dimension reduction comes at the final, output level of the CNS, due to muscle synergy constraints on the activation of muscles. In this interpretation, many sensory states elicit the recruitment of identical muscle synergies, reducing the dimension of the overall motor response. Although we did not examine muscle synergies explicitly, here, we carefully verified that the number of muscle synergies identified with NNMF agreed closely with the number of EMG PCs. Because we have previously observed a strong correspondence between muscle synergy recruitment and endpoint force, this interpretation also explains the similarity in dimension between the EMG and force data observed here.

One intuitive concept of motor learning is that the nervous system may explore the dynamics of the sensorimotor space, so changes in motor states associated with consistent changes in sensory states are reinforced. Sanger has used the postulate “good sensory coordinate systems are good motor coordinate systems” to describe this idea (1994). In the case of postural control in the cat, the force vectors associated with muscle

synergies are fixed with the limb axis as the postural configuration varies, similar to the polar coordinate frame used for proprioception of limb orientation identified in the dorso-spinal-cerebellar tract (Bosco et al. 2000), suggesting that the polar coordinate frame may be useful as both a sensory and a motor frame, and that the mapping between the two frames may be reinforced during development. This interpretation can also explain the dimension difference between the EMG and force data and the kinematic level. In the context of a single-joint movement, it has been proposed (Gottlieb 1996) that "no general relationship" exists between EMG and kinematic variables, and that any identified relationships are secondary to the EMG-muscle force relationship. It is probably more accurate to claim that relationships between EMG and kinematic variables are complex, nonlinear functions that must be assessed with the aid of musculoskeletal models. For example, we demonstrated that the endpoint force and acceleration associated with the activation of proximal muscles in a detailed, dynamic musculoskeletal model of the cat hindlimb depends strongly on the activation of muscles at the ankle (van Antwerp et al. 2007). The fact that different dynamic states can occur in the context of, or produce, identical kinematics, suggests that refining internal mappings between EMG and kinematics would be difficult, and that the conserved relationship between EMG and force may reflect mechanisms of development and learning, rather than hard rules.

Finally, we note that the fact that EMG PCs identified in translation and rotation perturbations were not completely similar – as quantified by normalized SSD – is not inconsistent with previous results suggesting that common muscle synergies are recruited in both perturbation types. There were no significant differences between the EMG dimension estimates obtained in translation and rotation perturbations or between PCA and NNMF, consistent with our previous results that identical synergies were recruited during both perturbation types. However, when we compared the EMG PCs identified in both perturbation types, we noted that the resulting normalized SSD values (0.58±0.25) were significantly lower than 1.0, the number corresponding to complete overlap between PC sets. Similarly, in an earlier study in which the SSD formulation was introduced, Cheung and colleagues reached a conclusion similar to that of our previous study – that muscle synergies that were generally common across experimental conditions resulted in similar low SSD values (table 1, Cheung et al. 2005). The reason for this disparity is

probably that the SSD metric does not account for the fact that muscles may be inactive without necessarily violating muscle synergy constraints. Here, the comparison of muscle activity between translation and rotation perturbations must be done carefully. Although the active force response observed during rotation perturbations is very similar to that observed in translation perturbations, some flexors remain silent during rotation perturbations, their role in flexing the limb having been largely assumed by the rotation of the platform (Ting and Macpherson 2004). To accommodate this, we have previously used muscle synergies identified in translation perturbations to reconstruct the muscle activity in rotation perturbations (Torres-Oviedo et al. 2006).

REFERENCES

Adamovich SV, Archambault PS, Ghafouri M, Levin MF, Poizner H, and Feldman AG. Hand trajectory invariance in reaching movements involving the trunk. *Experimental Brain Research* 138: 288-303, 2001.

Adkin AL, Frank JS, Carpenter MG, and Peysar GW. Fear of falling modifies anticipatory postural control. *Experimental Brain Research* 143: 160-170, 2002.

Alexander RM. Optimization and gaits in the locomotion of vertebrates. *Physiol Rev* 69: 1199-1227, 1989.

Avillac M, Denève S, Olivier E, Pouget A, and Duhamel JR. Reference frames for representing visual and tactile locations in parietal cortex. *Nat Neurosci* 8: 941-949, 2005.

Avis D, and Fukuda K. A Pivoting Algorithm for Convex Hulls and Vertex Enumeration of Arrangements and Polyhedra. *Discrete & Computational Geometry* 8: 295-313, 1992.

Basilevsky A. *Statistical Factor Analysis and Related Methods: Theory and Applications*. New York: Wiley, 1994.

Bauby CE, and Kuo AD. Active control of lateral balance in human walking. *J Biomech* 33: 1433-1440, 2000.

Berniker M, Jarc A, Bizzi E, and Tresch MC. Simplified and effective motor control based on muscle synergies to exploit musculoskeletal dynamics. *Proceedings of the National Academy of Sciences* 106: 7601-7606, 2009.

Bernstein N. *The Coordination and Regulation of Movements*. New York: Pergamon Press, 1967.

Blickhan R. The spring-mass model for running and hopping. *J Biomech* 22: 1217-1227, 1989.

Bloem BR, Allum JH, Carpenter MG, and Honegger F. Is lower leg proprioception essential for triggering human automatic postural responses? *Experimental Brain Research* 130: 375-391, 2000.

Bloem BR, Allum JH, Carpenter MG, Verschuuren JJ, and Honegger F. Triggering of balance corrections and compensatory strategies in a patient with total leg proprioceptive loss. *Experimental Brain Research* 142: 91-107, 2002.

Bolton DAE, and Misiaszek JE. Contribution of Hindpaw Cutaneous Inputs to the Control of Lateral Stability During Walking in the Cat. *J Neurophysiol* 102: 1711-1724, 2009.

Bonasera SJ, and Nichols TR. Mechanical actions of heterogenic reflexes among ankle stabilizers and their interactions with plantarflexors of the cat hindlimb. *J Neurophysiol* 75: 2050-2070, 1996.

Bosco G, Poppele RE, and Eian J. Reference frames for spinal proprioception: limb endpoint based or joint-level based? *J Neurophysiol* 83: 2931-2945, 2000.

Bosco G, Rankin AM, and Poppele RE. Representation of passive hindlimb postures in cat spinocerebellar activity. *J Neurophysiol* 76: 715-726, 1996.

Bunderson NE, Burkholder TJ, and Ting LH. Reduction of neuromuscular redundancy for postural force generation using an intrinsic stability criterion. *J Biomech* 41: 1537-1544, 2008.

Bunderson NE, McKay JL, Ting LH, and Burkholder TJ. Directional constraint of endpoint force emerges from hindlimb anatomy. *J Exp Biol* 213: 2131-2141, 2010.

Burkholder TJ, and Lieber RL. Sarcomere length operating range of vertebrate muscles during movement. *J Exp Biol* 204: 1529-1536, 2001.

Burkholder TJ, and Nichols TR. The mechanical action of proprioceptive length feedback in a model of cat hindlimb. *Motor Control* 4: 201-220, 2000.

Burkholder TJ, and Nichols TR. Three-dimensional model of the feline hindlimb. *J Morphol* 261: 118-129, 2004.

Burleigh A, and Horak F. Influence of instruction, prediction, and afferent sensory information on the postural organization of step initiation. *J Neurophysiol* 75: 1619-1628, 1996.

Cheung VC, d'Avella A, and Bizzi E. Adjustments of motor pattern for load compensation via modulated activations of muscle synergies during natural behaviors. *J Neurophysiol* 101: 1235-1257, 2009.

Cheung VCK, d'Avella A, Tresch MC, and Bizzi E. Central and sensory contributions to the activation and organization of muscle synergies during natural motor behaviors. *J Neurosci* 25: 6419-6434, 2005.

Chhabra M, and Jacobs RA. Properties of synergies arising from a theory of optimal motor behavior. *Neural Comput* 18: 2320-2342, 2006.

Clark DJ, Ting LH, Zajac FE, Neptune RR, and Kautz SA. Merging of Healthy Motor Modules Predicts Reduced Locomotor Performance and Muscle Coordination Complexity Post-Stroke. *J Neurophysiol* 103: 844-857, 2010.

Crowninshield RD, and Brand RA. A physiologically based criterion of muscle force prediction in locomotion. *J Biomech* 14: 793-801, 1981.

d'Avella A, and Bizzi E. Shared and specific muscle synergies in natural motor behaviors. *Proc Natl Acad Sci USA* 102: 3076-3081, 2005.

d'Avella A, Portone A, Fernandez L, and Lacquaniti F. Control of Fast-Reaching Movements by Muscle Synergy Combinations. *J Neurosci* 26: 7791-7810, 2006.

Deliagina TG, Beloozerova IN, Zelenin PV, and Orlovsky GN. Spinal and supraspinal postural networks. *Brain Res Rev* 57: 212-221, 2008.

Denève S, Duhamel J-R, and Pouget A. Optimal Sensorimotor Integration in Recurrent Cortical Networks: A Neural Implementation of Kalman Filters. *J Neurosci* 27: 5744-5756, 2007.

Dimitrova D, Nutt J, and Horak FB. Abnormal force patterns for multidirectional postural responses in patients with Parkinson's disease. *Exp Brain Res* 156: 183-195, 2004.

Dunbar DC, Horak FB, Macpherson JM, and Rushmer DS. Neural control of quadrupedal and bipedal stance: implications for the evolution of erect posture. *Am J Phys Anthropol* 69: 93-105, 1986.

Ellis MD, Holubar BG, Acosta AM, Beer RF, and Dewald JP. Modifiability of abnormal isometric elbow and shoulder joint torque coupling after stroke. *Muscle Nerve* 32: 170-178, 2005.

Fagg AH, Shah A, and Barto AG. A Computational Model of Muscle Recruitment for Wrist Movements. *J Neurophysiol* 88: 3348-3358, 2002.

Fiete IR, Hahnloser RHR, Fee MS, and Seung HS. Temporal Sparseness of the Premotor Drive Is Important for Rapid Learning in a Neural Network Model of Birdsong. *J Neurophysiol* 92: 2274-2282, 2004.

Flanders M, and Soechting JF. Parcellation of sensorimotor transformations for arm movements. *J Neurosci* 10: 2420-2427, 1990.

Flash T, and Hochner B. Motor primitives in vertebrates and invertebrates. *Curr Opin Neurobiol* 15: 660-666, 2005.

Fung J, and Macpherson JM. Determinants of Postural Orientation in Quadrupedal Stance. *J Neurosci* 15: 1121-1131, 1995.

Gentner R, and Classen J. Modular organization of finger movements by the human central nervous system. *Neuron* 52: 731-742, 2006.

Georgopoulos AP, Ashe J, Smyrnis N, and Taira M. The motor cortex and the coding of force. *Science* 256: 1692-1695, 1992.

Georgopoulos AP, Kalaska JF, Caminiti R, and Massey JT. On the Relations between the Direction of Two-Dimensional Arm Movements and Cell Discharge in Primate Motor Cortex. *J Neurosci* 2: 1527-1537, 1982.

Georgopoulos AP, Schwartz AB, and Kettner RE. Neuronal population coding of movement direction. *Science* 233: 1416-1419, 1986.

Gollhofer A, Horstmann GA, Berger W, and Dietz V. Compensation of translational and rotational perturbations in human posture: stabilization of the centre of gravity. *Neurosci Lett* 105: 73-78, 1989.

Gottlieb GL. Muscle activation patterns during two types of voluntary single-joint movement. *J Neurophysiol* 80: 1860-1867, 1998.

Gottlieb GL. On the voluntary movement of compliant (inertial-viscoelastic) loads by parcellated control mechanisms. *J Neurophysiol* 76: 3207-3229, 1996.

Grasso R, Bianchi L, and Lacquaniti F. Motor Patterns for Human Gait: Backward Versus Forward Locomotion. *J Neurophysiol* 80: 1868-1885, 1998.

Grillner S, and Shik M. On the descending control of the lumbosacral spinal cord from the" mesencephalic locomotor region". *Acta Physiol Scand* 87: 320, 1973.

Gruben KG, Lopez-Ortiz C, and Schmidt MW. The control of foot force during pushing efforts against a moving pedal. *Experimental Brain Research* 148: 50-61, 2003.

Harris CM, and Wolpert DM. Signal-dependent noise determines motor planning. *Nature* 394: 780-784, 1998.

He JP, Levine WS, and Loeb GE. Feedback gains for correcting small perturbations to standing posture. *IEEE Trans Autom Control* 36: 322-332, 1991.

Helms-Tillery SI, Ebner TJ, and Soechting JF. Task dependence of primate arm postures. *Exp Brain Res* V104: 1-11, 1995.

Henry SM, Fung J, and Horak FB. Effect of stance width on multidirectional postural responses. *J Neurophysiol* 85: 559-570, 2001.

Herzog W, and Leonard TR. Validation of optimization models that estimate the forces exerted by synergistic muscles. *J Biomech* 24: 31-39, 1991.

Hof AL. The force resulting from the action of mono- and biarticular muscles in a limb. *J Biomech* 34: 1085-1089, 2001.

Holdefer RN, and Miller LE. Primary motor cortical neurons encode functional muscle synergies. *Experimental Brain Research* 146: 233-243, 2002.

Holmes P, Full R, Koditschek DE, and Guckenheimer J. The dynamics of legged locomotion: models, analyses, and challenges. *SIAM Review* 48: 207-304, 2006.

Honeycutt CF, Gottschall JS, and Nichols TR. Electromyographic Responses From the Hindlimb Muscles of the Decerebrate Cat to Horizontal Support Surface Perturbations. *J Neurophysiol* 101: 2751-2761, 2009.

Honeycutt CF, and Nichols TR. The decerebrate cat generates the essential features of the force constraint strategy. *J Neurophysiol* 00764.02009, 2010.

Horak FB, and Diener HC. Cerebellar control of postural scaling and central set in stance. *J Neurophysiol* 72: 479-493, 1994.

Horak FB, and Macpherson JM. Postural orientation and equilibrium. In: *Handbook of Physiology, Section 12*. New York: American Physiological Society, 1996, p. 255-292.

Hoyt DF, and Taylor CR. Gait and the energetics of locomotion in horses. *Nature* 292: 239-240, 1981.

Inglis JT, Horak FB, Shupert CL, and Jones-Rycewicz C. The importance of somatosensory information in triggering and scaling automatic postural responses in humans. *Exp Brain Res* 101: 159-164, 1994.

Inglis JT, and Macpherson JM. Bilateral labyrinthectomy in the cat: effects on the postural response to translation. *J Neurophysiol* 73: 1181-1191, 1995.

Ivanenko YP, Cappellini G, Dominici N, Poppele RE, and Lacquaniti F. Coordination of locomotion with voluntary movements in humans. *J Neurosci* 25: 7238-7253, 2005.

Ivanenko YP, d'Avella A, Poppele RE, and Lacquaniti F. On the Origin of Planar Covariation of Elevation Angles During Human Locomotion. *J Neurophysiol* 99: 1890-1898, 2008.

Ivanenko YP, Grasso R, Zago M, Molinari M, Scivoletto G, Castellano V, Macellari V, and Lacquaniti F. Temporal components of the motor patterns expressed by the human spinal cord reflect foot kinematics. *J Neurophysiol* 90: 3555-3565, 2003.

Ivanenko YP, Poppele RE, and Lacquaniti E. Five basic muscle activation patterns account for muscle activity during human locomotion. *Journal of Physiology-London* 556: 267-282, 2004.

Jacobs JV, and Horak FB. Cortical control of postural responses. *J Neural Transm* 114: 1339-1348, 2007.

Jacobs R, and Macpherson JM. Two functional muscle groupings during postural equilibrium tasks in standing cats. *J Neurophysiol* 76: 2402-2411, 1996.

Kargo WJ, and Giszter SF. Individual Premotor Drive Pulses, Not Time-Varying Synergies, Are the Units of Adjustment for Limb Trajectories Constructed in Spinal Cord. *J Neurosci* 28: 2409-2425, 2008.

Kargo WJ, Nelson F, and Rome LC. Jumping in frogs: assessing the design of the skeletal system by anatomically realistic modeling and forward dynamic simulation. *J Exp Biol* 205: 1683-1702, 2002.

Kargo WJ, Ramakrishnan A, Hart CB, Rome LC, and Giszter SF. A Simple Experimentally Based Model Using Proprioceptive Regulation of Motor Primitives Captures Adjusted Trajectory Formation in Spinal Frogs. *J Neurophysiol* 103: 573-590, 2010.

Kawato M. Internal models for motor control and trajectory planning. *Curr Opin Neurobiol* 9: 718-727, 1999.

Kaya M, Jinha A, Leonard TR, and Herzog W. Multi-functionality of the cat medical gastrocnemius during locomotion. *J Biomech* 38: 1291-1301, 2005.

Knyazev AV, and Argentati ME. Principal Angles between Subspaces in an A-Based Scalar Product: Algorithms and Perturbation Estimates. *SIAM Journal on Scientific Computing* 23: 2008-2040, 2002.

Krishnamoorthy V, Goodman S, Zatsiorsky V, and Latash ML. Muscle synergies during shifts of the center of pressure by standing persons: identification of muscle modes. *Biol Cybern* 89: 152-161, 2003.

Krishnamoorthy V, Latash ML, Scholz JP, and Zatsiorsky VM. Muscle modes during shifts of the center of pressure by standing persons: effect of instability and additional support. *Exp Brain Res* 157: 18-31, 2004.

Krouchev N, Kalaska JF, and Drew T. Sequential Activation of Muscle Synergies During Locomotion in the Intact Cat as Revealed by Cluster Analysis and Direct Decomposition. *J Neurophysiol* 96: 1991-2010, 2006.

Kubow TM, and Full RJ. The role of the mechanical system in control: a hypothesis of self-stabilization in hexapedal runners. *Philosophical Transactions of the Royal Society B: Biological Sciences* 354: 849-861, 1999.

Kuo AD. An optimal state estimation model of sensory integration in human postural balance. *J Neural Eng* 2: S235-249, 2005.

Kuo AD, and Zajac FE. A biomechanical analysis of muscle strength as a limiting factor in standing posture. *J Biomech* 26 Suppl 1: 137-150, 1993.

Kurtzer I, Pruszynski JA, Herter TM, and Scott SH. Primate Upper Limb Muscles Exhibit Activity Patterns That Differ From Their Anatomical Action During a Postural Task. *J Neurophysiol* 95: 493-504, 2006.

Kuxhaus L, Roach SS, and Valero-Cuevas FJ. Quantifying deficits in the 3D force capabilities of a digit caused by selective paralysis: application to the thumb with simulated low ulnar nerve palsy. *J Biomech* 38: 725-736, 2005.

Latash ML, and Anson JG. Synergies in health and disease: relations to adaptive changes in motor coordination. *Phys Ther* 86: 1151-1160, 2006.

Lawrence JH, 3rd, Nichols TR, and English AW. Cat hindlimb muscles exert substantial torques outside the sagittal plane. *J Neurophysiol* 69: 282-285, 1993.

Lee DD, and Seung HS. Algorithms for non-negative matrix factorization. *Adv Neural Info Proc Syst* 13: 556-562, 2001.

Lee DD, and Seung HS. Learning the parts of objects by non-negative matrix factorization. *Nature* 401: 788-791, 1999.

Lehman SL, and Stark LW. Three algorithms for interpreting models consisting of ordinary differential equations: Sensitivity coefficients, sensitivity functions, global optimization. *Math Biosci* 62: 107-122, 1982.

Lloyd DG, and Besier TF. An EMG-driven musculoskeletal model to estimate muscle forces and knee joint moments in vivo. *J Biomech* 36: 765-776, 2003.

Lockhart DB, and Ting LH. Optimal sensorimotor transformations for balance. *Nat Neurosci* 10: 1329-1336, 2007.

Loeb EP, Giszter SF, Saltiel P, Bizzi E, and Mussa-Ivaldi FA. Output units of motor behavior: an experimental and modeling study. *J Cognit Neurosci* 12: 78-97, 2000.

Lyalka VF, Zelenin PV, Karayannidou A, Orlovsky GN, Grillner S, and Deliagina TG. Impairment and recovery of postural control in rabbits with spinal cord lesions. *J Neurophysiol* 94: 3677-3690, 2005.

Macpherson JM. Changes in a postural strategy with inter-paw distance. *J Neurophysiol* 71: 931-940, 1994.

Macpherson JM. How flexible are muscle synergies? In: *Motor Control: Concepts and Issues*, edited by Humphrey DR, and Freund H-J. New York: Wiley Press, 1991, p. 33-47.

Macpherson JM. Strategies that simplify the control of quadrupedal stance. I. Forces at the ground. *J Neurophysiol* 60: 204-217, 1988a.

Macpherson JM. Strategies that simplify the control of quadrupedal stance. II. Electromyographic activity. *J Neurophysiol* 60: 218-231, 1988b.

Macpherson JM, and Fung J. Weight support and balance during perturbed stance in the chronic spinal cat. *J Neurophysiol* 82: 3066-3081, 1999.

Macpherson JM, Horak FB, Dunbar DC, and Dow RS. Stance dependence of automatic postural adjustments in humans. *Exp Brain Res* 78: 557-566, 1989.

Macpherson JM, Lywood DW, and Van Eyken A. A system for the analysis of posture and stance in quadrupeds. *J Neurosci Methods* 20: 73-82, 1987.

McGeer T. Passive Dynamic Walking. *The International Journal of Robotics Research* 9: 62-82, 1990.

McKay JL, Burkholder TJ, and Ting LH. Biomechanical capabilities influence postural control strategies in the cat hindlimb. *J Biomech* 40: 2254-2260, 2007.

McKay JL, and Ting LH. Functional muscle synergies constrain force production during postural tasks. *J Biomech* 41: 299-306, 2008.

Muceli S, Boye AT, d'Avella A, and Farina D. Identifying representative synergy matrices for describing muscular activation patterns during multi-directional reaching in the horizontal plane. *J Neurophysiol* 00559.02009, 2010.

Müller H, and Sternad D. Motor learning: changes in the structure of variability in a redundant task. *Adv Exp Med Biol* 629: 439-456, 2009.

Mushahwar VK, Aoyagi Y, Stein RB, and Prochazka A. Movements generated by intraspinal microstimulation in the intermediate gray matter of the anesthetized, decerebrate, and spinal cat. *Can J Physiol Pharmacol* 82: 702-714, 2004.

Nashner LM. Adapting reflexes controlling the human posture. *Experimental Brain Research* 26: 59-72, 1976.

Nashner LM. Fixed patterns of rapid postural responses among leg muscles during stance. *Experimental Brain Research* 30: 13-24, 1977.

Neptune RR, Clark DJ, and Kautz SA. Modular control of human walking: A simulation study. *J Biomech* 42: 1282-1287, 2009.

Nichols TR. Musculoskeletal mechanics: A foundation of motor physiology. In: *Sensorimotor Control of Movement and Posture*2002, p. 473-479.

Nichols TR, Lawrence JH, 3rd, and Bonasera SJ. Control of torque direction by spinal pathways at the cat ankle joint. *Experimental Brain Research* 97: 366-371, 1993.

O'Sullivan I, Burdet E, and Diedrichsen Jr. Dissociating Variability and Effort as Determinants of Coordination. *PLoS Comput Biol* 5: e1000345, 2009.

Olshausen BA, and Field DJ. Sparse coding of sensory inputs. *Curr Opin Neurobiol* 14: 481-487, 2004.

Pandy MG, Zajac FE, Sim E, and Levine WS. An optimal control model for maximum-height human jumping. *J Biomech* 23: 1185-1198, 1990.

Peterka RJ. Sensorimotor integration in human postural control. *J Neurophysiol* 88: 1097-1118, 2002.

Poppele R, and Bosco G. Sophisticated spinal contributions to motor control. *Trends Neurosci* 26: 269-276, 2003.

Poppele RE, Bosco G, and Rankin AM. Independent representations of limb axis length and orientation in spinocerebellar response components. *J Neurophysiol* 87: 409-422, 2002.

Pratt CA, Fung J, and Macpherson JM. Stance Control in the Chronic Spinal Cat. *J Neurophysiol* 71: 1981-1985, 1994.

Prilutsky BI, Herzog W, and Allinger TL. Forces of individual cat ankle extensor muscles during locomotion predicted using static optimization. *J Biomech* 30: 1025-1033, 1997.

Raasch CC, and Zajac FE. Locomotor strategy for pedaling: Muscle groups and biomechanical functions. *J Neurophysiol* 82: 515-525, 1999.

Raikova RT, and Prilutsky BI. Sensitivity of predicted muscle forces to parameters of the optimization-based human leg model revealed by analytical and numerical analyses. *J Biomech* 34: 1243-1255, 2001.

Rossignol S, BarriËre G, Frigon A, BarthÈlemy D, Bouyer L, Provencher J, Leblond H, and Bernard G. Plasticity of locomotor sensorimotor interactions after peripheral and/or spinal lesions. *Brain Res Rev* 57: 228-240, 2008.

Roweis ST, and Saul LK. Nonlinear Dimensionality Reduction by Locally Linear Embedding. *Science* 290: 2323-2326, 2000.

Runge CF, Shupert CL, Horak FB, and Zajac FE. Role of vestibular information in initiation of rapid postural responses. *Experimental Brain Research* 122: 403-412, 1998.

Saltiel P, Wyler-Duda K, d'Avella A, Ajemian RJ, and Bizzi E. Localization and connectivity in spinal interneuronal networks: the adduction-caudal extension-flexion rhythm in the frog. *J Neurophysiol* 2005.

Saltiel P, Wyler-Duda K, D'Avella A, Tresch MC, and Bizzi E. Muscle synergies encoded within the spinal cord: evidence from focal intraspinal NMDA iontophoresis in the frog. *J Neurophysiol* 85: 605-619, 2001.

Sanger T. Optimal unsupervised motor learning for dimensionality reduction ofnonlinear control systems. *IEEE Trans Neural Networks* 5: 965-973, 1994.

Sanger TD. Human Arm Movements Described by a Low-Dimensional Superposition of Principal Components. *J Neurosci* 20: 1066-1072, 2000.

Schieber MH, and Santello M. Hand function: peripheral and central constraints on performance. *J Appl Physiol* 96: 2293-2300, 2004.

Schmidt MW, Lopez-Ortiz C, Barrett PS, Rogers LM, and Gruben KG. Foot force direction in an isometric pushing task: prediction by kinematic and musculoskeletal models. *Exp Brain Res* 150: 245-254, 2003.

Scholz J, Schöner G, Hsu W, Jeka J, Horak F, and Martin V. Motor equivalent control of the center of mass in response to support surface perturbations. *Exp Brain Res* 180: 163-179, 2007.

Scholz JP, and Schöner G. The uncontrolled manifold concept: identifying control variables for a functional task. *Experimental Brain Research* 126: 289-306, 1999.

Scott SH. Optimal feedback control and the neural basis of volitional motor control. *Nat Rev Neuro* 5: 534-546, 2004.

Scott SH, and Kalaska JF. Reaching movements with similar hand paths but different arm orientations. I. Activity of individual cells in motor cortex. *J Neurophysiol* 77: 826-852, 1997.

Scovil CY, and Ronsky JL. Sensitivity of a Hill-based muscle model to perturbations in model parameters. *J Biomech* 39: 2055-2063, 2006.

Shadmehr R, and Mussa-Ivaldi FA. Adaptive representation of dynamics during learning of a motor task. *J Neurosci* 14: 3208-3224, 1994.

Shah A, Fagg AH, and Barto AG. Cortical Involvement in the Recruitment of Wrist Muscles. *J Neurophysiol* 91: 2445-2456, 2004.

Siegel SG, Nichols TR, and Cope TC. Reflex activation patterns in relation to multidirectional ankle torque in decerebrate cats. *Motor Control* 3: 135-150, 1999.

Stapley PJ, Ting LH, Hulliger M, and Macpherson JM. Automatic postural responses are delayed by pyridoxine-induced somatosensory loss. *J Neurosci* 22: 5803-5807, 2002.

Stevens JA. Falls among older adults--risk factors and prevention strategies. *J Saf Res* 36: 409-411, 2005.

Stevens JA, Mack KA, Paulozzi LJ, and Ballesteros MF. Self-Reported Falls and Fall-Related Injuries Among Persons Aged >=†65 Years-United States, 2006. *J Saf Res* 39: 345-349, 2008.

Sumbre G, Fiorito G, Flash T, and Hochner B. Octopuses use a human-like strategy to control precise point-to-point arm movements. *Curr Biol* 16: 767-772, 2006.

Szentesi P, Zaremba R, van Mechelen W, and Stienen GJM. ATP utilization for calcium uptake and force production in different types of human skeletal muscle fibres. *The Journal of physiology* 531: 393-403, 2001.

Tenenbaum JB, Silva Vd, and Langford JC. A Global Geometric Framework for Nonlinear Dimensionality Reduction. *Science* 290: 2319-2323, 2000.

Ting LH, Kautz SA, Brown DA, and Zajac FE. Phase reversal of biomechanical functions and muscle activity in backward pedaling. *J Neurophysiol* 81: 544-551, 1999.

Ting LH, and Macpherson JM. A limited set of muscle synergies for force control during a postural task. *J Neurophysiol* 93: 609-613, 2005.

Ting LH, and Macpherson JM. Ratio of shear to load ground-reaction force may underlie the directional tuning of the automatic postural response to rotation and translation. *J Neurophysiol* 92: 808-823, 2004.

Ting LH, and McKay JL. Neuromechanics of muscle synergies for posture and movement. *Curr Opin Neurobiol* 17: 622-628, 2007.

Todorov E. Optimality principles in sensorimotor control. *Nat Neurosci* 7: 907-915, 2004.

Todorov E, and Jordan MI. Optimal feedback control as a theory of motor coordination. *Nat Neurosci* 5: 1226-1235, 2002.

Torres-Oviedo G, Macpherson JM, and Ting LH. Muscle synergy organization is robust across a variety of postural perturbations. *J Neurophysiol* 96: 1530-1546, 2006.

Torres-Oviedo G, and Ting LH. Muscle synergies characterizing human postural responses. *J Neurophysiol* 2007.

Tresch MC, Saltiel P, and Bizzi E. The construction of movement by the spinal cord. *Nat Neurosci* 2: 162-167, 1999.

Tseng Y, Scholz JP, and Schöner G. Goal-equivalent joint coordination in pointing: affect of vision and arm dominance. *Motor Control* 6: 183-207, 2002.

Tseng YW, and Scholz JP. The effect of workspace on the use of motor abundance. *Motor Control* 9: 75-100, 2005.

Valero-Cuevas FJ. A mathematical approach to the mechanical capabilities of limbs and fingers. In: *Progress in Motor Control V*. State College, Pennsylvania: 2006.

Valero-Cuevas FJ. Predictive modulation of muscle coordination pattern magnitude scales fingertip force magnitude over the voluntary range. *J Neurophysiol* 83: 1469-1479, 2000.

Valero-Cuevas FJ, Yi JW, Brown D, McNamara RV, 3rd, Paul C, and Lipson H. The tendon network of the fingers performs anatomical computation at a macroscopic scale. *IEEE Trans Biomed Eng* 54: 1161-1166, 2007.

Valero-Cuevas FJ, Zajac FE, and Burgar CG. Large index-fingertip forces are produced by subject-independent patterns of muscle excitation. *J Biomech* 31: 693-703, 1998.

van Antwerp KW, Burkholder TJ, and Ting LH. Inter-joint coupling effects on muscle contributions to endpoint force and acceleration in a musculoskeletal model of the cat hindlimb. *J Biomech* 40: 3570-3579, 2007.

van Bolhuis BM, and Gielen CC. A comparison of models explaining muscle activation patterns for isometric contractions. *Biol Cybern* 81: 249-261, 1999.

Weber DJ, Stein RB, Everaert DG, and Prochazka A. Limb-state feedback from ensembles of simultaneously recorded dorsal root ganglion neurons. *J Neur Eng* 4: S168-S180, 2007.

Welch TDJ. A feedback model for the evaluation of the adaptive changes to temporal muscle activation patterns following postural disturbance. In: *The Wallace H Coulter Department of Biomedical Engineering*. Atlanta, Georgia: Emory University and Georgia Tech, 2008.

Welch TDJ, and Ting LH. A Feedback Model Explains the Differential Scaling of Human Postural Responses to Perturbation Acceleration and Velocity. *J Neurophysiol* 101: 3294-3309, 2009.

Welch TDJ, and Ting LH. A Feedback Model Reproduces Muscle Activity During Human Postural Responses to Support-Surface Translations. *J Neurophysiol* 99: 1032-1038, 2008.

Widmer CG, Carrasco DI, and English AW. Differential activation of neuromuscular compartments in the rabbit masseter muscle during different oral behaviors. *Exp Brain Res* 150: 297-307, 2003.

Winter DA. Human balance and posture control during standing and walking. *Gait & posture* 3: 193-214, 1995.

Yamaguchi GT. *Dynamic Modeling of Musculoskeletal Motion*. Kluwer, 2001.

Yang JF, Scholz JP, and Latash ML. The role of kinematic redundancy in adaptation of reaching. *Exp Brain Res* 176: 54-69, 2007.

Zajac FE. Muscle and tendon: properties, models, scaling, and application to biomechanics and motor control. *Crit Rev Biomed Eng* 17: 359-411, 1989.

Zajac FE. Understanding muscle coordination of the human leg with dynamical simulations. *J Biomech* 35: 1011-1018, 2002.

Zajac FE, Neptune RR, and Kautz SA. Biomechanics and muscle coordination of human walking: Part I: Introduction to concepts, power transfer, dynamics and simulations. *Gait & posture* 16: 215-232, 2002.

Zatsiorsky VM, Gao F, and Latash ML. Prehension synergies: Effects of object geometry and prescribed torques. *Exp Brain Res* 148: 77-87, 2003.

VITA

J. Lucas McKay grew up in Key Biscayne, Florida. Before coming to Georgia Tech to study neuromechanics, he studied electrical engineering at Brown University in Providence, Rhode Island. His Master's thesis work was in the design of analog circuits for brain-computer interfaces.